

University of Kentucky

UKnowledge

---

Theses and Dissertations--Molecular and Cellular Biochemistry

Molecular and Cellular Biochemistry

---


2023

## THE DEVELOPMENT AND CHARACTERIZATION OF NANOBODIES SPECIFIC TO PROTEIN TYROSINE PHOSPHATASE 4A3 (PTP4A3/PRL-3) TO DISSECT AND TARGET ITS ROLE IN CANCER.

Caroline Smith

University of Kentucky, [cns229@uky.edu](mailto:cns229@uky.edu)

Author ORCID Identifier:

 <https://orcid.org/0000-0002-1876-7790>

Digital Object Identifier: <https://doi.org/10.13023/etd.2023.159>

[Right click to open a feedback form in a new tab to let us know how this document benefits you.](#)

### Recommended Citation

Smith, Caroline, "THE DEVELOPMENT AND CHARACTERIZATION OF NANOBODIES SPECIFIC TO PROTEIN TYROSINE PHOSPHATASE 4A3 (PTP4A3/PRL-3) TO DISSECT AND TARGET ITS ROLE IN CANCER." (2023). *Theses and Dissertations--Molecular and Cellular Biochemistry*. 63.  
[https://uknowledge.uky.edu/biochem\\_etds/63](https://uknowledge.uky.edu/biochem_etds/63)

This Doctoral Dissertation is brought to you for free and open access by the Molecular and Cellular Biochemistry at UKnowledge. It has been accepted for inclusion in Theses and Dissertations--Molecular and Cellular Biochemistry by an authorized administrator of UKnowledge. For more information, please contact [UKnowledge@lsv.uky.edu](mailto:UKnowledge@lsv.uky.edu).

## **STUDENT AGREEMENT:**

I represent that my thesis or dissertation and abstract are my original work. Proper attribution has been given to all outside sources. I understand that I am solely responsible for obtaining any needed copyright permissions. I have obtained needed written permission statement(s) from the owner(s) of each third-party copyrighted matter to be included in my work, allowing electronic distribution (if such use is not permitted by the fair use doctrine) which will be submitted to UKnowledge as Additional File.

I hereby grant to The University of Kentucky and its agents the irrevocable, non-exclusive, and royalty-free license to archive and make accessible my work in whole or in part in all forms of media, now or hereafter known. I agree that the document mentioned above may be made available immediately for worldwide access unless an embargo applies.

I retain all other ownership rights to the copyright of my work. I also retain the right to use in future works (such as articles or books) all or part of my work. I understand that I am free to register the copyright to my work.

## **REVIEW, APPROVAL AND ACCEPTANCE**

The document mentioned above has been reviewed and accepted by the student's advisor, on behalf of the advisory committee, and by the Director of Graduate Studies (DGS), on behalf of the program; we verify that this is the final, approved version of the student's thesis including all changes required by the advisory committee. The undersigned agree to abide by the statements above.

Caroline Smith, Student

Dr. Jessica Blackburn, Major Professor

Trevor Creamer, Director of Graduate Studies

THE DEVELOPMENT AND CHARACTERIZATION OF NANOBODIES SPECIFIC  
TO PROTEIN TYROSINE PHOSPHATASE 4A3 (PTP4A3/PRL-3) TO DISSECT AND  
TARGET ITS ROLE IN CANCER.

---

DISSERTATION

---

A dissertation submitted in partial fulfillment of the  
requirements for the degree of Doctor of Philosophy  
in the College of Medicine  
at the University of Kentucky

By  
Caroline N. Smith

Lexington, Kentucky

Director: Dr. Jessica Blackburn, Associate Professor of  
Molecular and Cellular Biochemistry

Lexington, Kentucky

2023

Copyright © Caroline N. Smith 2023  
<https://orcid.org/0000-0002-1876-7790>

## ABSTRACT OF DISSERTATION

### THE DEVELOPMENT AND CHARACTERIZATION OF NANOBODIES SPECIFIC TO PROTEIN TYROSINE PHOSPHATASE 4A3 (PTP4A3/PRL-3) TO DISSECT AND TARGET ITS ROLE IN CANCER

Protein Tyrosine Phosphatase 4A3 (PTP4A3 or PRL-3) is an oncogenic dual-specificity phosphatase that drives tumor metastasis, promotes cancer cell survival, and is correlated with poor patient prognosis in a variety of solid tumors and leukemias. The mechanisms that drive PRL-3's oncogenic functions are not well understood, in part due to a lack of research tools available to study this protein. The development of such tools has proven difficult, as the PRL family is ~80% homologous and the PRL catalytic binding pocket is shallow and hydrophobic. Currently available small molecules do not exhibit binding specificity for PRL-3 over PRL family members, and the only new antibody specific for PRL-3, PRL-3-zumab, is inaccessible to the research community while in clinical trial.

To address the lack of tools available to study PRL-3, I have developed alpaca-derived single-domain antibodies, or nanobodies, targeting PRL-3. Nanobodies have emerged as a valuable research tool and show promise as cancer therapeutics. Their advantages include their small size and lack of light chains, allowing them to reach cavities within active sites that conventional antibodies cannot access. Nanobodies also have high specificity and affinity for their antigens. I hypothesized that PRL-3 nanobodies may be able to differentiate between the PRL family and provide new insights into the role of PRL-3 in cancer progression.

Following synthesis, sequencing, and purification, I identified seven unique nanobodies that bind to PRL-3 with little to no activity towards PRL-1 and PRL-2, making them one of the first tools to selectively target and bind directly to PRL-3 in its native conformation. The nanobodies can be used in immunoprecipitation and immunofluorescence assays. Interestingly, I found that N-terminal tags on PRL-3, such as 3XFLAG or GFP, enhanced PRL-3 localization to the membrane, while untagged PRL-3 is widely distributed throughout the cell. These data may have important implications for previous PRL-3 functional studies that necessarily relied on tagged-PRL-3.

The nanobody binding affinity for PRL-3 is within a  $K_D$  of 30 - 300 nM, similar to that of commercially available antibodies. Hydrogen-deuterium exchange mass spectrometry showed nanobodies bind near the PRL-3 active site and could reduce PRL-3 phosphatase activity against a generic substrate. The interaction between PRL-3 and the nanobody also showed overlap with the binding site of a known PRL-3 interacting partner,

the magnesium transport protein CNNM3. A competition assay showed that the nanobody and CNNM3 can bind PRL-3 simultaneously, but the nanobody partially outcompetes the CNNM3 binding.

The nanobodies can be used immediately as a PRL-3 specific research tool and can be further developed as an inhibitor. They also have a great deal of potential in additional applications. First, we are using these nanobodies to stabilize PRL-3 in X-ray crystallography to develop higher-resolution structures to establish exactly where the nanobodies bind PRL-3. Determining the location of these binding pockets would allow us to better contribute to substrate identification and drug design. Secondly, we are using a fluorescently labeled nanobody to examine the PRL-3:CNNM complex, PRL-3 trafficking and function during cancer processes, such as proliferation, invasion, and stress. Our ultimate goal is to provide new insight into how PRL-3 contributes to cancer progression with the use of this exciting tool.

KEYWORDS: camelid, phage display, antibody engineering, protein purification, confocal microscopy, hydrogen-deuterium exchange

Caroline N. Smith

*(name of student)*

03/28/2023

Date

THE DEVELOPMENT AND CHARACTERIZATION OF NANOBODIES SPECIFIC  
TO PROTEIN TYROSINE PHOSPHATASE 4A3 (PTP4A3/PRL-3) TO DISSECT AND  
TARGET ITS ROLE IN CANCER

By

Caroline N. Smith

Dr. Jessica Blackburn

Director of Dissertation

Trevor Creamer

Director of Graduate Studies

03/28/2023

Date

DEDICATION

*To my family, for their unwavering support.*

## Acknowledgements

The work presented in this dissertation would not have been possible without the encouragement and support of numerous people. I would initially like to express my immense gratitude to my mentor, Dr. Jessica Blackburn. Not only for her outstanding mentorship and guidance throughout the course of my graduate work, but also for her continual support of my goals and for encouraging me to be the best scientist, teammate, and person I can be. This would not have been possible without her patience, kindness, leadership, and trust, and for that, I am so grateful.

I would like to thank my dissertation committee: Dr. Rebecca Dutch, Dr. Doug Andres, and Dr. Michael Kilgore. Throughout my PhD training, they have each provided me with valuable guidance and feedback. I would also like to thank my outside examiner, Dr. Sanda Despa, for her time and effort in reviewing my dissertation. I would like to thank the faculty, my fellow trainees, and the staff in the Biochemistry department for creating a community and space where I have been fortunate to learn and grow. I would like to thank Dr. Trevor Creamer for being a wonderful support for graduate students as both the DGS and Interim Chair in the department. I am also incredibly thankful to the administrative staff in the department; Rachel Putty, Brenda Woods, Tonya Knox, and Jonathan Oepping, for their efforts in ensuring that the department runs smoothly.

To the members of the Blackburn Lab, I would like to thank all of you for creating a truly amazing environment in which I could develop as a scientist and lab mate. I am so thankful for the support and mentorship from Dr. Min Wei and Dr. Meghan Haney who provided me immeasurable training at the bench and most importantly friendship. I am grateful for the kindness and encouragement from all of our previous lab members. Thank you to our current lab members: Dr. Yelena Chernyavskaya, Dr. Shilpa Sampathi, Viral Oza, Trace Jolly, Majd Al-Hamaly, and Izzy Snyder. They have each made the lab a wonderful place to learn. You each contribute to an environment that is infectious, enthusiastic, and supportive. Thank you all and all previous Blackburn Lab members for making this an incredible place to learn.

To the Markey Cancer Center Office of Cancer Education and Mentoring, thank you for supporting my training. Dr. Kathy O'Connor and Dr. Erin Oakley have continued to invest their time into my future, and I cannot thank them enough for their support.

I would like to thank my family and friends; this journey would not have been possible without their love and support. Thank you to all my friends that I have made through the IBS program at UK, and I look forward to our friendship for years to come. To my Bellarmine friends, thank you for ten years of unconditional love, support, and encouragement. Thank you to my grandmother, aunts, uncles, and cousins for always cheering me on from afar. Thank you to the Williamson family for welcoming me into your family with open arms and for your continual love and support. Thank you to my brother, Isaac and sister-in-law, Maria, for continually supporting me. To my parents, Pat and Donya, thank you for always believing in me and for all of the sacrifices you have made to ensure that I could pursue my passions and dreams.

Lastly, I would like to thank my husband, Zach. Thank you for your endless support and for always encouraging me to reach for the stars. I am beyond lucky to have such an incredible partner in life.



## Table of Contents

Acknowledgments	iii
List of Tables	vii
List of Figures	viii
List of Additional Files	x
Chapter 1. The Oncogenic Phosphatase, PRL-3.	11
1.1. The Phosphatase of Regenerating Liver (PRL) Family of Proteins.	11
1.1.1. Phosphatases regulate cellular signaling.	11
1.1.2. Discovery of the PRL phosphatases.	12
1.2. The PRLs as oncogenes.	13
1.2.1. PRLs in normal physiology.	13
1.2.2. The discovery of PRLs as oncogenes.	14
1.3. Proposed PRL-3 mechanisms of action in cancer.	15
1.3.1. PRL-3 associated with signaling mechanisms in cancer.	15
1.3.2. The CNNM membrane transport proteins as regulators of PRL-3 function.	16
1.4. Studying and targeting PRL-3 function in cancer to date.	18
1.4.1. Anti-PRL-3 antibodies in the literature: advancements and pitfalls.	18
1.4.2. PRL-3 small molecule inhibitors in the literature.	20
1.4.3. Current methods for defining PRL-3 substrates and cellular localization.	22
Chapter 2. Introduction to Nanobodies	29
2.1. Discovery and advantages of camelid-derived nanobodies.	29
2.2. The potential of nanobodies as a scientific research tool.	31
2.2.1. Fluorescent nanobodies for cellular imaging.	31
2.2.2. Using nanobodies to identify protein substrates and DNA binding partners.	33
2.2.3. Nanobody-directed protein degradation.	34
2.2.4. Nanobodies enhance x-ray crystallography.	35
2.3. Nanobody use in cancer.	35
2.3.1. Nanobodies for cancer diagnosis.	35
2.3.2. Nanobodies for cancer treatment.	37
Chapter 3. Materials and Methods	42
3.1. Bacterial and mammalian expression vectors.	42
3.1.1. Bacterial expression vectors.	42
3.1.2. Mammalian expression vectors.	42
3.2. Production, bacteriophage display, and sequencing of nanobodies.	43
3.3. Cell lines and culture conditions.	44
3.4. Expression and purification of recombinant proteins.	44
3.4.1. PRL-1, -2, and -3 purification.	44
3.4.2. Anti-PRL-3 nanobody purification.	45
3.4.3. 3XFLAG-PRL-3 and CBS-HA purification.	46
3.5. Nanobody specificity analysis for PRL-3 using an in-house ELISA approach.	46

3.6. Immunoprecipitation (IP) of PRL-3 with nanobody or commercially available PRL antibodies.	47
3.6.1. IP of PRL-3 with nanobody coupled Dynabeads.	47
3.6.2. IP of PRL-3 with commercially available PRL antibodies.	48
3.7. Fixed immunofluorescence of HCT116 cells using anti-PRL-3 nanobodies to detect PRL-3 expression and cellular localization.	49
3.7.1. Nanobody specificity for GFP-PRL-3 over GFP-PRL-1 and GFP-PRL-2.	49
3.7.2. Co-staining of commercially available PRL-3 antibodies with nanobody.	49
3.7.3. Cellular localization of tagged PRL-3 compared to wildtype PRL-3.	50
3.8. Biolayer Interferometry (BLItz) analysis to determine the binding affinity of nanobodies for PRL-3.	51
3.9. Phosphatase assay.	52
3.10. Hydrogen deuterium exchange mass spectrometry (HDX-MS).	52
3.11. Co-immunoprecipitation of CBS-HA and nanobodies with 3XFLAG-PRL-3.	54
3.12. Western blot analysis.	54
Chapter 4. Alpaca-derived anti-PRL-3 nanobodies show specificity for their antigen and can be utilized to study PRL-3 biology in cancer	65
4.1. Introduction.	65
4.2. Results.	65
4.2.1. Nanobody variability resides in Complimentary Determining Region 3.	65
4.2.2. Nanobodies show specificity for PRL-3 over other family members in indirect ELISA analysis.	67
4.2.3. Nanobodies maintain specificity for PRL-3 over other family members in cell-based assays.	68
4.2.4. Comparison of anti-PRL-3 nanobodies to commercially available PRL antibodies.	70
4.2.5. N-terminal tags alter PRL-3 localization.	72
Chapter 5. Anti-PRL-3 nanobodies block the CNNM/PRL-3 interaction that contributes to tumorigenesis.	88
5.1. Introduction.	88
5.2. Results.	88
5.2.1. Nanobody affinity for PRL-3 is comparable to the affinity of FDA-approved antibodies for their targets and partially inhibits PRL-3 activity.	88
5.2.2. Nanobodies partially bind the PRL-3 active site.	90
5.2.3. Nanobodies disrupt interaction with known PRL-3 binding partner, CNNM3.	91
Chapter 6. Discussion	102
6.1. Strengths and weaknesses of anti-PRL-3 nanobodies in their current iteration.	102
6.2. Impact on the field – understanding PRL-3 function.	103
6.3. Impact on the field – new ways to target PRL-3.	105
6.4. Future Directions.	106
6.4.1. Analysis of PRL-3 trafficking.	106
6.4.2. Targeted degradation of PRL-3.	107
6.4.3. Advancing PRL-3 crystal structures.	108
6.4.4. Other PRL nanobodies.	109

6.5. Final conclusions.	109
References	111
Vita	123

## List of Tables

Table 2.1. Comparison of conventional antibodies and nanobodies, adapted from (147).	39
Table 2.2. Nanobodies currently in clinical trial, adapted from (5).	40
Table 4.1. PRL-3 antibodies in the literature.	74
Table 5.1. Local $K_D$ of nanobodies binding to six concentrations of PRL-3.	94
Table 5.2. Global $K_D$ of nanobodies binding to PRL-3.	95

## List of Figures

Figure 1.1. Sequence homology of human PRLs. ....	24
Figure 1.2. Over-expression of the PRL genes in cancer. ....	25
Figure 1.3. Published structures of CNM CBS-domain/PRL interactions, determined by x-ray crystallography. ....	26
Figure 1.4. Off-target binding of Anti-PTP4A3/PRL-R antibody (ab50276) in western blot. ....	27
Figure 1.5. R&D Biosystems antibody MAB3219 is specific for PRL-3. ....	28
Figure 2.1. Size and domains of immunoglobulin proteins. ....	41
Figure 3.1. Plasmid map of pskb3-PRL-3. ....	56
.....	57
Figure 3.2. Plasmid map of plenti-CMV-puro-3XFLAG-PRL-3. ....	57
.....	58
Figure 3.3. Plasmid map of pcDNA3.1 GFP-PRL-3. ....	58
Figure 3.4. Colony PCR yields VHH-positive clones. ....	59
Figure 3.5. Purification of PRL family of proteins from BL21 DE3 E.coli. ....	60
Figure 3.6. Ni-NTA purification of Nanobody 91 from BL21 DE3 E.coli. ....	61
Figure 3.7. Protein purification of 3XFLAG-PRL-3 and CBS-HA.....	62
Figure 3.8. Tagged versions of PRL-3 were equally expressed across immunofluorescence experiments. ....	63
Figure 3.9. Sequence coverage map of apo-PRL-3 in HDX-MS. ....	64
Figure 4.1. Anti-PRL-3 nanobody sequences from bacteriophage display yielded 16 nanobodies with varying frequencies and complementary determining regions.....	75
Figure 4.2. Nanobodies are specific for PRL-3 over the other PRL family members.....	76
Figure 4.3. Nanobodies selectively immunoprecipitate PRL-3 from HEK293T cell lysate. ....	78
.....	78
Figure 4.4. Nanobody 91 is specific to PRL-3 in immunofluorescence assays.....	79
Figure 4.5. Nanobody 19 is specific to PRL-3 in immunofluorescence assays.....	80
Figure 4.6. Nanobody 26 is specific to PRL-3 in immunofluorescence assays.....	81
Figure 4.7. Nanobody 84 is specific to PRL-3 in immunofluorescence assays.....	82
Figure 4.8. Nanobody 19 binds more specifically to PRL-3 than commercial antibodies, MAB3219, and sc-130355.....	83
Figure 4.9. Commercial antibodies MAB3219, and sc-130355 bind GFP-PRL-3 while ab20576 and GTX100600 do not.....	84
Figure 4.10. Commercial antibodies MAB3219 and sc-130355 are specific for PRL-3 over PRL-1 and PRL-2. ....	86
Figure 4.11. PRL-3 localization assessed by Nanobody 26 and 19 is altered by N-terminal 3XFLAG and GFP tags.....	87
Figure 5.1. Biolayer Interferometry Analysis (BLItz) to denote KD of Nanobody 26 for PRL-3.....	96
Figure 5.2. Anti-PRL-3 nanobodies inhibit PRL-3 phosphatase activity in a dose-dependent manner. ....	97
Figure 5.3. Hydrogen Deuterium Exchange Mass Spectrometry (HDX-MS) defines Nanobody 19 binding sites with PRL-3.....	98
Figure 5.4. Hydrogen Deuterium Exchange Mass Spectrometry (HDX-MS) defines Nanobody 26 binding sites with PRL-3.....	99

Figure 5.5. Hydrogen Deuterium Exchange Mass Spectrometry (HDX-MS) defines Nanobody 91 binding sites with PRL-3.....	100
Figure 5.6. Anti-PRL-3 nanobodies partially interact with the PRL-3 active site and site of CNNM3 CBS-domain binding. ....	101

## List of Additional Files

[Supplemental Table 1. Raw values for calculating local and global  $K_D$ ]. [XLSX 1.3 MB]

## Chapter 1. The Oncogenic Phosphatase, PRL-3.

### 1.1. The Phosphatase of Regenerating Liver (PRL) Family of Proteins.

#### 1.1.1. *Phosphatases regulate cellular signaling.*

Protein tyrosine phosphorylation is a critical regulatory mechanism in eukaryotic cell physiology. Protein phosphorylation is catalyzed by protein kinases (PTKs) and regulated by protein phosphatases (PTPs). Protein phosphorylation is necessary for many cellular processes, including communication between and within cells, metabolism, motility, trafficking and transport, proliferation, apoptosis, and other critical physiological processes (1). Over the last approximately 45 years, the uncontrolled activation of kinases has been frequently observed in cancer (2). As a result, PTKs have been studied extensively in order to develop PTK inhibitors for the prevention and treatment of cancer. However, 20 years after the discovery of oncogenic kinases, the discovery of the phosphatase PTEN demonstrated that suppression of phosphatases contributes to cancer as well (2, 3). PTEN is now known to be a tumor suppressor, often losing its function in a variety of tumors (3) leading to advanced disease, chemotherapy resistance, and poor survival in patients (4).

With the discovery of phosphatases involved in cancer came the knowledge that failure to balance kinase and phosphatase activity leads to tumorigenesis in many types of tumors (5). Since the discovery of PTEN, loss and gain of function of other phosphatases have continued to be discovered in cancer. Two of the most notable are SHP2 and PTP1B. SHP2 is an oncogene that is mutated in several types of leukemia and hyperactivated by other mechanisms in some solid tumors (6). PTP1B promotes oncogenesis in many tumor types (pancreatic, glioblastoma, colorectal, ovarian, and breast), yet it has also been shown to be tumor suppressive in fibroblasts and endothelial cells (7). This dual role makes targeting PTP1B in cancer challenging. The roles of SHP2 and PTP1B have been extensively studied in cancer, and there are several other phosphatases that have been shown to be involved with cancer, but their overall function has yet to be defined, one of which is the Phosphatase of Regenerative Liver (PRL) family of proteins.



### 1.1.2. Discovery of the PRL phosphatases.

PRL-1 was the first identified PRL, discovered in 1991 as an up-regulated gene in regenerating rat liver after partial hepatectomy (8, 9). Following sequence analysis, Diamond et al. found that PRL-1 contained an eight amino acid long signature PTP motif in its active site (10). This motif is formally known as the VCH(X)<sub>5</sub>R motif, encompassing valine-histidine-cysteine-(up to any five amino acids)-arginine. However, PRL-1 showed no homology to other PTPs outside of this phosphatase domain; therefore, they tested the protein in an *in vitro* assay and demonstrated that it had phosphatase activity on a generic substrate (10), creating a new class of phosphatases known as the PRLs. The final two phosphatase family members, PRL-2 and PRL-3, were discovered through database searches using the PRL-1 sequence seven years later in 1998 (11).

Following the discovery of the three PRL proteins, Zeng et al. began assessing the similarities and differences between the PRLs structurally by comparing the murine phosphatase sequences. Later, identification of the human PRL sequence designated a high level of sequence homology between the PRLs (PRL-1/PRL-2: 86%); (PRL-1/PRL-3: 78%); (PRL-2/PRL-3: 75%), represented in Figure 1.1 (12). With the discovery of PRL-2 and PRL-3 also came the discovery of unique features of this protein family. Phosphatase catalysis is a conserved, two-step nucleophilic reaction that is facilitated by a number of conserved loops that form the active site (13). Like PRL-1, PRL-2 and -3 exhibit this classical active site which includes a phosphatase binding loop (P-loop) that contains the catalytic cysteine that attacks the phosphate on the substrate (9, 13). The second conserved loop of the PRL active site is the WFPDD-loop that contains the catalytic aspartate that donates a proton to the leaving group of the substrate, therefore the dephosphorylated substrate can be released (9, 13). For step two, the aspartate in the WFPDD-loop activates a water molecule to hydrolyze the phosphatase-phosphate complex to release the phosphate group (13).

In addition, all three proteins contain a C-terminal consensus sequence for prenylation (11), making the PRLs the only prenylated phosphatase family (14). The presence of the CAAX motif leads the field to hypothesize that this motif anchors the PRLs to the plasma membrane and early endosomes (15). Furthermore, the PRLs have a

polybasic region upstream of the CAAX motif that facilitates interactions with negatively charged phospholipids, thought to enhance this potential membrane anchoring.

Sequence analysis also revealed that the PRL proteins exhibited significant sequence homology to the newly identified phosphatase that is a tumor suppressor, PTEN (11). Structural studies have also exemplified that the PRLs exhibit similar overall folding compared to PTEN (9, 16). Furthermore, the PRLs have a shallow binding pocket (9, 16, 17), similar to that of PTEN, while also exhibiting similarities to PTEN outside the active site. Thus began an intense exploration into the normal function of the PRL proteins and how they may contribute to cancer.

## 1.2. The PRLs as oncogenes.

### 1.2.1. *PRLs in normal physiology.*

The original studies that began trying to outline PRL function in animals were with knock-out mice. There have been several studies conducted examining phenotypes following PRL knock-out. Most notably, PRL-1 and PRL-2 were found to be critical requirements for both in mouse embryonic development, as double knock-out mice were not viable (18). To investigate which stage the embryos were dead, Bai et al. carried out time mating to harvest embryos at E17.5, E14.5, E11.5 and E9.5 days. They could not identify any viable double knockout mice at any of these staging, indicating early embryonic lethality and necessity of both PRL genes for survival. However, individual knock-outs were viable and showed subtle phenotypic changes (18), suggesting that the PRLs may be able to compensate for one another functionally. The PRLs are known to regulate cellular magnesium concentrations (see below 1.3.2.), and following PRL-2 knock-out, serum magnesium levels were up-regulated (18).

Two independent groups have developed conditional PRL-3 knock-out mice; unfortunately, resulting phenotypes confound one another. In the first study in 2011, PRL-3 knock-out mice showed no significant differences in body weights, blood glucose, or lipid metabolism (19). However, John Lazo's group showed that knock-out in males exhibited a 10% lower body weight and a 7% decrease in BMI compared to wild-type

littermates (20). Individual knock-outs of PRL-3 were embryonically viable, but post-natal lethality was higher in males than females, consistent with the phenotypes observed (20). These conflicting results leave the mechanisms of action of PRL-3 relatively unknown.

Elizabeth Patton's group has generated PRL-3 knock-out models in zebrafish to study melanocyte regeneration. Zebrafish have two PRL genes, *prl3a* and *prl3b*. This group decided to knock them out individually, as PRL-3A is most similar to the human PRL-3 protein (21). They showed that a TALEN, zinc-finger nucleases, *prl3a* mutant had no embryonic melanocyte phenotype, but had increased melanocyte regeneration in a stem cell background model (21). *Prl3b* deletion through CRISPR, along with *prl3a* and *prl3b* morpholino double knock-out showed no detectable embryonic or stem cell regeneration, indicating that *prl3b* does not have a unique role in zebrafish melanocyte regeneration (21). Due to the lack of *prl3b*'s role, the rest of their studies focused on *prl3a*. While these models are interesting, future research should still focus on and examine the use of double-knockout zebrafish depending on the nature of the study. PRL3b may not have a role in melanocyte regeneration, but it may play roles in oncogenesis and other disease states.

### 1.2.2. *The discovery of PRLs as oncogenes.*

As mentioned, PRL-1 was determined initially to be an immediate early gene expressed in liver regeneration. In that same study, cells stably transfected with PRL-1 were transformed and displayed altered cell growth and morphology (10). This study was the first to show that the PRLs potentially contribute to tumorigenesis. Ten years later, Vogelstein's group showed evidence that PRL-3 acted as an oncogene in colorectal cancer (22). Specifically, they compared the global gene expression profiles of the normal colorectal epithelium to benign tumors, primary cancers, and metastatic lesions in the colon. PRL-3 expression was at high levels in 18 metastatic tissue samples studied but at low levels in primary, benign, and normal tissue (22). Soon after, in 2002, high expression of PRL-2 was linked to prostate cancer (23). Since these pioneering studies, many research groups have validated Vogelstein's findings, showing that over-expression of PRL-3 correlates to poor survival in a variety of models, including colorectal cancer cell lines

(24), immunohistochemistry of tumor sections (25), and mouse xenograft models (26). Figure 1.2 describes each of the tumor types that each PRL influences.

Following their discovery as oncogenes, many groups show that all PRLs are up-regulated in numerous solid tumors. PRL-3 is the only family member overexpressed in a wide variety of cancers (14). Overall, research groups show that over-expression of PRL-3 acts as a potential biomarker of cancer progression and metastasis in colorectal (22, 27), gastric (28), ovarian (29), kidney (30), bladder (31), lung (32), breast (33), brain (34), and prostate (35) cancers, as well as melanoma (21, 36), and leukemias (37, 38). Experimental evidence indicates that PRL-3 expression increases cancer cell proliferation, migration, and invasion *in vitro* (39-41) and enhances tumor growth and metastasis in mouse models (11, 22). In contrast, PRL-3 knock-down significantly suppresses tumor formation and spread *in vivo* (20). PRL-3 is well-established in inhibiting apoptosis, promoting epithelial-to-mesenchymal transition (EMT), and inducing migration in cancer cells. With all of the research surrounding PRL-3 and its role as an oncogene, thus far, conclusions drawn about its role in promoting cancer are widely varied.

### 1.3. Proposed PRL-3 mechanisms of action in cancer.

#### 1.3.1. *PRL-3 associated with signaling mechanisms in cancer.*

While PRL-3 is associated with many types of cancer, PRL-3's direct substrates have not been identified. However, many studies have suggested their impact on cellular signaling pathways. The currently suggested substrates are phosphatidylinositol (4,5) bisphosphate (42), ezrin (43), Keratin 8 (44), Integrin $\alpha$ 1 (45), Elongation factor 2 (46) and nucleolin (47). However, these are not validated extensively as direct binding partners. For example, the influence of PRL-3 over-expression on ezrin phosphorylation states has yet to be confirmed (44). Nucleolin and Keratin 8 were co-immunoprecipitated with inactive PRL-3 (44, 47) but there is no evidence of direct effects on phosphorylation. Over-expression of PRL-3 has demonstrated an impact on the phosphorylation state of PI (4,5)P<sub>2</sub> (42); unfortunately, validation using *in vivo* models does not exist. While the potential substrates demonstrate progress and effort toward discovering a PRL-3 substrate in cancer,

searching for direct substrates of this protein is necessary for the field to define it as a biomarker.

With the search for PRL-3 substrates, the list of mechanisms that PRL-3 is involved in or contributes to in cancer progression continues to grow. In a review article in 2018, Hardy et al. outlined those mechanisms assessed by multiple research groups (14). First, the PI3K-Akt pathway is activated by PRL-3 in hematologic malignancies, yet the mechanism is still unclear (14). The primary regulator of the PI3K-Akt pathway is the tumor suppressor PTEN. Groups reported that PTEN is down-regulated following the over-expression of PRL-3 in colon (48) and gastric (49) cancer cells. While these findings suggest that PTEN downregulation could be an essential factor in PRL-3/PI3K-Akt signaling, there have yet to be findings that better explain this relationship.

Several research groups, including the Blackburn lab, have linked PRL-3 to Src activation, yet the direct effect on Src still needs clarification. Liang et al. began telling this story by demonstrating that PRL-3 promotes cell invasion and proliferation by downregulating Csk, a negative regulator of Src, leading to Src activation (50). More recently, the Blackburn lab confirmed that the SRC pathway is associated with PRL-3 expression at both the mRNA and protein level through Gene Set Enrichment Analysis (GSEA) and Reverse-Phase Protein Array (RPPA), respectively (37) in a T-cell leukemia model. We also confirmed that PRL-3 downregulated CSK expression by examining the Src Y527 phosphorylation site regulated by CSK. When PRL-3 is overexpressed, phosphorylation at this site decreases; PRL-3 is knock-down, resulting in phosphorylation increases, confirming Liang et al. findings (37). Unfortunately, Src did not co-immunoprecipitate with PRL-3, indicating that Src is not a direct substrate of PRL-3 in this model (37). PRLs also regulate p53, Rho family GTPases, E-Cadherin, and matrix metalloproteases (9), with no direct targeting mechanisms discovered. The search for direct substrates of PRL-3 phosphorylation regulation is very much alive.

### *1.3.2. The CNNM membrane transport proteins as regulators of PRL-3 function.*

While no direct substrates of PRL-3's phosphatase activity are exclusively defined, one binding partner of PRL-3, the CNNM family of proteins, is the most extensively

researched class of PRL binding partners. Also known as the CBS-pair domain, divalent metal cation transport mediators (CNNMs) are a conserved family of integral membrane proteins that maintain cellular Mg<sup>2+</sup> influx and efflux for many physiologic functions (51). Hardy et al. showed that PRL-2 forms a heterodimer with CNNM3 and that CNNM3 is not a phosphorylated substrate of PRL-2 (52). Specifically, this interaction occurs between the active site of PRL-2 and a loop unique to the CBS domains in the CNNM proteins. Furthermore, they demonstrate that the knock-down of PRL-2 decreases cellular magnesium influx both in vitro and in vivo (52). These results indicated a clear relationship between the PRL proteins and magnesium regulation. They even show that in xenograft tumor assays, the PRL-2/CNNM3 interaction promotes cellular transformation (52). Since this discovery, many groups have solved the structure for many of the PRL/CNNM CBS-domain using x-ray crystallography approaches. Thus far interactions have been shown for PRL-1/CNNM2 (PDB: 5MMZ, 5LXQ (53)), PRL-2/CNNM3 (PDB: 5K22 (54)), 5K23 (55), 5K24 (55)), and PRL-3/CNNM3 (PDB: 5TSR (55)) (Fig 1.3).

The original link between PRL-3 and the CNNM proteins was established in 2014 when Funato et al. demonstrated the tumorigenic effects in colorectal cancer (56). They determined that when PRL-3 binds CNNM4, it prevents CNNM-dependent magnesium efflux, which has roles linked to cell metabolism and AMK/mTOR signaling (56). The Gehring group has determined that the formation of a phosphocysteine in the active site regulated the PRL/CNNM complex; cysteine phosphorylation blocks binding to the CNNM proteins and prevents magnesium regulation (54). They have since characterized the binding sites of CNNM proteins on PRL-3 and how interrupting each site affects magnesium regulation and cancer phenotypes (57). They have also characterized PRL-3 as a pseudo-phosphatase, demonstrating that PRL-3 catalytic activity is not required in a mouse metastasis model, but CNNM4 binding is necessary (57). However, as outlined in 1.1.2., the PRL proteins have classical phosphatase characteristics and catalytic activity. Therefore, this group hypothesizes that phosphatase activity leads to the formation of this phosphocysteine that blocks CNNM activity. In the future, when designing new PRL inhibitors, researchers should consider the proteins' ability to block CNNM binding. Deeming this protein as a pseudo-phosphatase seems premature when examining the literature surrounding PRL-3 catalytic activity.

Ultimately, PRL-3 expression is highly elevated in various cancers and leads to poor survival in vitro and in vivo, and this data correlates to poor patient prognosis (37). Nevertheless, no one has identified a direct substrate of PRL-3. Furthermore, while PRL-3/CNNM interactions alter magnesium regulation, how these changes lead to downstream effects contributing to cancer progression and metastasis is poorly understood. This lack of clarity is mainly due to the fact that outside of over-expression, knock-out, and point mutation studies, few tools allow researchers to differentiate between the PRLs and study their function.

#### 1.4. Studying and targeting PRL-3 function in cancer to date.

##### *1.4.1. Anti-PRL-3 antibodies in the literature: advancements and pitfalls.*

Developing antibodies specific for PRL-3 has also proven difficult, with most antibodies lacking specificity towards PRL-3 over other PRL proteins. Four PRL antibodies have primarily been used in the literature to demonstrate PRL-3 protein expression and cellular localization. We have continued to test these antibodies in our research.

Many groups, including ours, have published findings over the last ten years using the Abcam antibody, Anti-PTP4A3/PRL-R antibody (ab50276). Abcam claims this tool can be used for western blot and immunohistochemistry studies to examine PRL-3 protein expression. Many groups have taken advantage of this tool to look at PRL-3 expression in cell lines (37, 58), tumor tissue samples (59), and even protein expression in tumor microarrays using immunofluorescence (60). However, one of the pitfalls we began to notice when examining PRL-3 expression in leukemia cell lines in our lab was that, when blotting for endogenous PRL-3, we often saw many off-target band patterns (Fig 1.4). Secondly, this antibody seems only useful when studying PRL-3 expression; it has never been used to determine PRL-3 binding partners, cellular localization, or any other characteristics that may aid in its contribution to tumorigenesis. While all of this work has contributed to specifying all of the tumor types PRL-3 is over-expressed in (35, 59-61) the advancements are halted here based on the limitations of this antibody.

Next is the Genetex antibody, PTP4A3 antibody [N1C3]. This tool is interesting, as the designated immunogen is a “Recombinant protein encompassing a sequence within the center region of human PTP4A3.” Yet, its reactivity is with zebrafish, with predicted reactivity with human, mouse, rat, bovine, xenopus tropicalis, and rhesus monkey. PRL-3 is highly conserved between humans, mice (14), and zebrafish (62), and the Blackburn lab has confirmed that this antibody can detect zebrafish PRL-3 protein expression (63). Yet, no other publications have referenced this antibody for research use. The Blackburn lab is the only zebrafish lab studying PRL-3 currently, and while this tool has advantages in detecting PRL-3 expression in our model, it has yet to do much to advance the PRL field as a whole.

The antibody that the Blackburn lab currently uses for PRL-3 protein expression studies is the R&D Systems antibody, Human/Mouse/Rat PRL-3 Antibody (MAB3219). Like the Abcam antibody, R&D Systems recommends using their antibody to define PRL-3 protein expression in multiple tumor types using western blot (64-66) along with immunohistochemistry staining approaches (65, 67). Our lab demonstrated that this antibody is specific for PRL-3 over PRL-1 and PRL-2 in a dot blot using purified protein (Fig 1.5). We recently published a manuscript using this antibody to confirm PRL-3 overexpression in manufactured cell lines (68). However, no publications have used this antibody in immunofluorescence studies to examine cellular localization or immunoprecipitation assays to assess PRL-3 substrates.

The final commercially available antibody widely used in the literature is the Santa Cruz Biotechnology antibody, PRL-3 Antibody (318) (sc-130355). This antibody is the one commercial antibody licensed for applications other than PRL-3 protein expression. It is also the only antibody that claims to differentiate PRL-3 from PRL-1 and PRL-2. The company recommends using it in western blot, immunohistochemistry, immunofluorescence, immunoprecipitation, and flow cytometry. Many assumed that following the development of this tool, it would open up the PRL field, allowing researchers to develop assays studying PRL-3 biology in normal and cancer cells. Yet, most of this tool's research still focuses on protein expression data surrounding western blotting (69-78) and immunohistochemistry (74, 79). One group in particular, Hjort et al., expanded the use of this antibody in their research. They detected PRL-3 expression in



flow cytometry and showed punctate localization of PRL-3 in the cytoplasm of B-cell leukemia cells (80). They also examined PRL-3 expression in Hodgkin's lymphoma using immunohistochemistry and immunofluorescence (79). Yet, other groups are not utilizing this antibody for PRL-3 biology research and are utilizing protein tagging mechanisms, further discussed in 1.4.3. Furthermore, while the use of this antibody is more widespread than others, only one group has examined its specificity for PRL-3. Shi et al. transfected DLD-1 colorectal cancer cells with GST-PRL-1, -2, and -3, and western blot with sc-130355 only detected a signal on PRL-3 overexpressing cell lysates (70). Furthermore, while research groups are utilizing this antibody in the various assays described, no one has tested its specificity for PRL-3 outside of western blotting.

Finally, a few groups have developed in-house anti-PRL-3 antibodies to complete their research studies (81). Unfortunately, these are not often made available to the research community. The most recently in-house antibody in the literature was a humanized monoclonal antibody, PRL-3-zumab, that binds to PRL-3 specifically over PRL-1 and PRL-2 and has anti-cancer effects *in vivo* (82, 83). The authors of this work predicted that PRL-3 is presented on the cell surface via exosomal secretion to allow binding by PRL-3-zumab. This event stimulates Fc-receptor-dependent interactions between PRL-3 positive cells and host immune effectors, activating classical antibody-mediated tumor clearance pathways leading to tumor cell death (83). While PRL-3-zumab is currently in phase 2 clinical trial in Singapore (NCT04118114) for gastric and hepatocellular carcinomas and in the United States (NCT04452955) for solid tumors, this antibody is not currently commercially available, which limits its research use.

#### *1.4.2. PRL-3 small molecule inhibitors in the literature.*

The literature demonstrates that the over-expression of PRL-3 in tumor cells correlates to poor patient outcomes; therefore, there has been significant interest in designing inhibitors of PRL-3. Unfortunately, similar to antibody design, developing inhibitors of PRL-3 has proven difficult due to PRL's conservative active site with other phosphatases, like PTEN, and the high degree of homology within the PRL family. Due to

the challenges faced when developing a PRL-3 inhibitor, many of the PRL inhibitors discovered thus far were found by screening drug libraries.

Some PRL inhibitors are already used in the clinic to treat other diseases. For example, pentamidine is a well-known PRL inhibitor that inhibits the growth of cancer cell lines with high PRL-3 expression (84). However, pentamidine has also been shown to inhibit PTP1B, showing that it is not selective for the PRLs (84). Furthermore, our collaborators have shown that pentamidine does not bind to PRL-3 in NMR. Another example is curcumin, a compound extracted from turmeric previously known to induce apoptosis of cancer cells. Curcumin inhibits mRNA expression of PRL-2 and PRL-3 (85). We also completed a screen of 1443 FDA-approved drugs for activity against each of the PRLs. We identified two potent, non-toxic broad PRL inhibitors, Salirasib and Candesartan (68). While *in silico* modeling revealed allosteric binding of both drugs to PRL-3 and potential inhibition of substrate binding, each of these drugs binds all three PRLs, lacking specificity for PRL-3.

The other most common practice for identifying PRL inhibitors has been using a technique known as structural-activity-relationship (SAR), which examines drug properties to find relationships between its chemical structure and chemical activity that may stabilize the compound and limit off-target effects. SAR was used to identify rhodanine (86), Analog 3 (87), and thienopyridone (66) as PRL inhibitors. Rhodanine inhibits PRL-3 in phosphatase assays (66). Rhodanine lacked specificity for PRL-3 (86); however, many groups have continued to design and develop derivatives of rhodanine to target PRL-3 (88). Unfortunately, neither rhodanine nor its derivatives have proven to target PRL-3 over other phosphatases specifically and do not interact directly with PRL-3. The story is similar for Analog 3, which inhibits the activity of the entire PRL family and has an IC<sub>50</sub> of 31  $\mu$ M (87), which is outside the range of a physiologically relevant dose one would consider administering to a patient.

Thienopyridone has been the most studied PRL inhibitor, showing selectivity for the PRL proteins over eleven other phosphatases (66). Again, thienopyridone inhibited the activity of all PRL family members. To improve the selectivity of this compound, John Lazo's group performed a SAR study of thienopyridone to try to stabilize the compound and limit off-target effects (89). This experiment resulted in the development of JMS-053,

a thienopyridone derivative that demonstrated a 10-fold increase in potency in inhibiting the PRL proteins (89). JMS-053 has shown anti-cancer effects in ovarian (89), colorectal (90), and breast (89) tumors. Thienopyridone binds PRL-3 in computational docking models, but these findings have not been validated in molecular or in vivo models (89, 91). Unfortunately, Zhang et al. performed in vitro phosphatase assays along with NMR and showed that both thienopyridone and JMS-053, also known as iminothienopyridone, are redox active compounds and inhibit the PRLs and other phosphatases through oxidation (92). While they both effectively inhibit PRL activity, these data make their use for studying cellular function problematic due to the likelihood of off-target effects (92). There has yet to be a small molecule inhibitor specific for PRL-3, reduces protein activity, and binds directly to the protein.

#### *1.4.3. Current methods for defining PRL-3 substrates and cellular localization.*

Due to the lack of tools available to specifically study PRL-3, localization and substrate identification studies were primarily performed with over-expressed PRL-3 with different protein tags to examine the characteristics of PRL-3. These types of experiments are how each of the substrates discussed in section 1.3.1. were discovered. For example, the interactions of phosphatidylinositol (4,5) bisphosphate and ezrin with PRL-3 were shown using FLAG-PRL-3 and FLAG beads for immunoprecipitation (42, 43). Keratin and nucleolin studies utilized eGFP-PRL-3 both in immunoprecipitation assays along with co-localization studies to show protein interaction (44, 47). Similarly, scientists found the interactions between Integrin $\alpha$ 1 and PRL-3 using a GST-PRL-3 (45). None of these substrates bind to endogenous PRL-3, only these forms of overexpressed PRL-3.

The same tools have been used in most research focusing on PRL-3 localization. It is often GFP-PRL-3, as it doesn't require an antibody to visualize in immunofluorescence studies. Most research examining PRL-3 localization has used either eGFP-PRL-3 (93, 94) or Myc-PRL-3 (15, 57, 95). Studies using both tags have demonstrated that PRL-3 predominantly localizes to the cell membrane (15, 57). This hypothesis is influenced by the presence of the prenylation motif at the C-terminus of the protein (15), along with its interactions with the CNNM proteins (57). PRL-3 also localizes in punctate structures in

the cytoplasm (95). However, the functional outcomes of this localization have yet to be determined. Mutants of PRL-3 that are not prenylated can localize to the nucleus (93, 96); nuclear localization correlates to telomere deprotection and chromosomal instability. Researchers often assume that N- and C-terminal tags have little influence on the secondary and tertiary structures and localization of fused proteins (44). However, several reports have demonstrated that using GFP may impact the biological activity of fusion proteins (19, 45, 46), including cellular localization. Therefore, it is necessary to have a tool in the field that can detect wild-type PRL-3 rather than tagged versions of the protein to study its localization.

```

hPRL-3      MARMNRPAPVEVSYKHMRFLITHNPTNATLSTFIEDLKKYGATTVVRVCEVTYDKTPLEK      60
hPRL-1      MARMNRPAPVEVTYKNMRFLITHNPTNATLNKFIEELKYGVTTIVRVCEATYDTTLVEK      60
hPRL-2      ---MNRPAPVEISYENMRFLITHNPTNATLNKFIEELKYGVTTLVRVCDATYDKAPVEK      57
          *****: * : ***** . * * : ***** . ** : ***** : . *** . : **

hPRL-3      DGITVVDWPFDDGAPPPGKVVEDWLSLVKAKFCEAPGSCVAVHCVAGLGRAPVLVALALI      120
hPRL-1      EGIHVLDWPFDDGAPPSNQIVDDWLSLVKIKFFREEPGCCIAVHCVAGLGRAPVLVALALI      120
hPRL-2      EGIHVLDWPFDDGAPPPNQIVDDWLNLLKTKFREEPGCCVAVHCVAGLGRAPVLVALALI      117
          : ** * : ***** . : : * : *** . * : * * * * * . : *****

hPRL-3      ESGMKYEDAIQFIRQKRRGAINSKQLTYLEKYRPKQRLRFKDPHTHKTRCCVM      173
hPRL-1      EGGMKYEDAVQFIRQKRRGAFNSKQLLYLEKYRPKMRLRFKDSNGHRNNCCIQ      173
hPRL-2      ECGMKYEDAVQFIRQKRRGAFNSKQLLYLEKYRPKMRLRFRDTNGH---CCVQ      167
          * *****: ***** . ***** ***** ***** * : * ** :

```

**Figure 1.1. Sequence homology of human PRLs.** Human PRL protein sequences aligned using Clustal Omega Multiple Sequence Alignment.

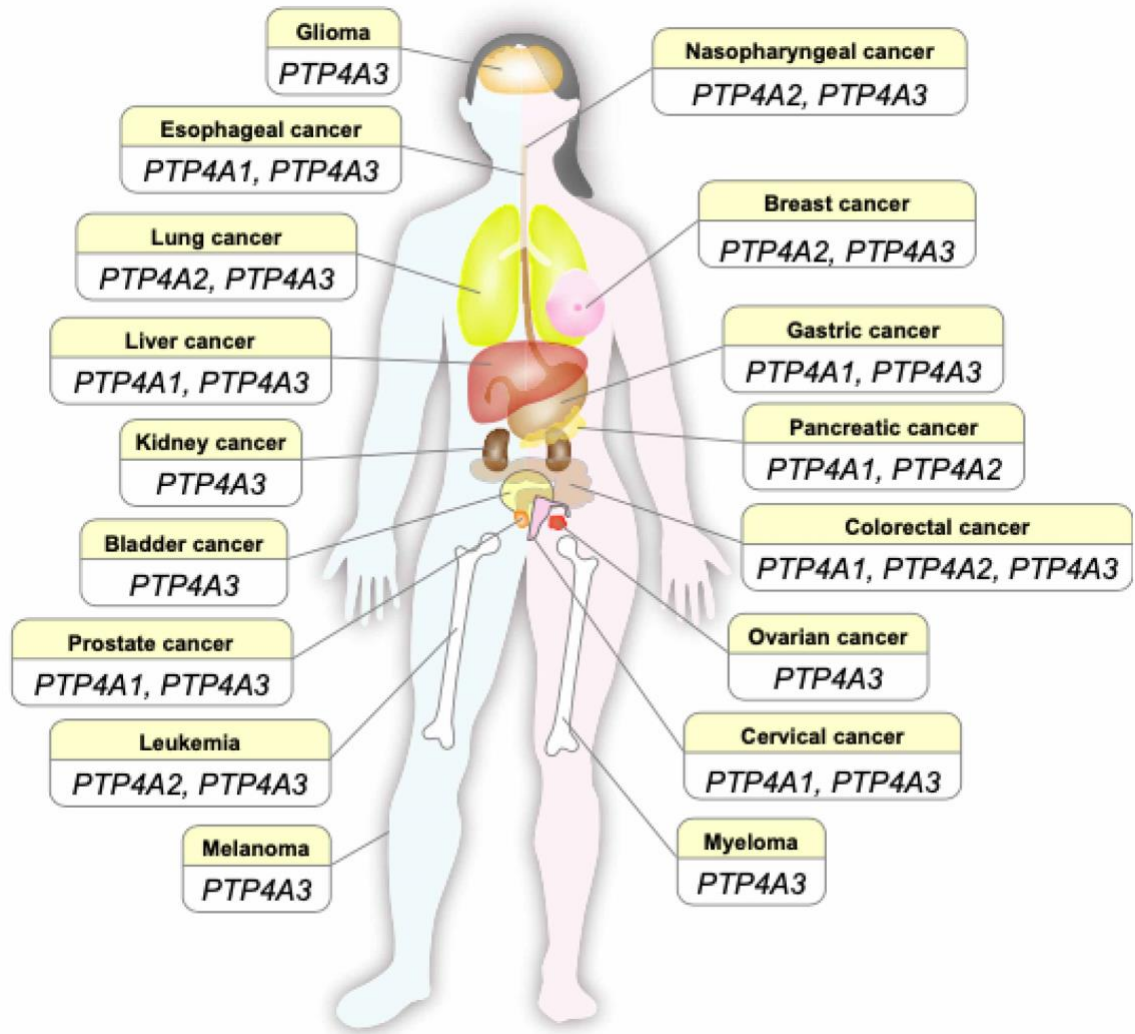


**Figure 1.2. Over-expression of the PRL genes in cancer.** This figure is reprinted from (14) with permission. Representation by gene name (PTP4A1/PRL-1; PTP4A2/PRL-2; PTP4A3/PRL-3) showing over-expression of the proteins at the mRNA or protein level by cancer type.

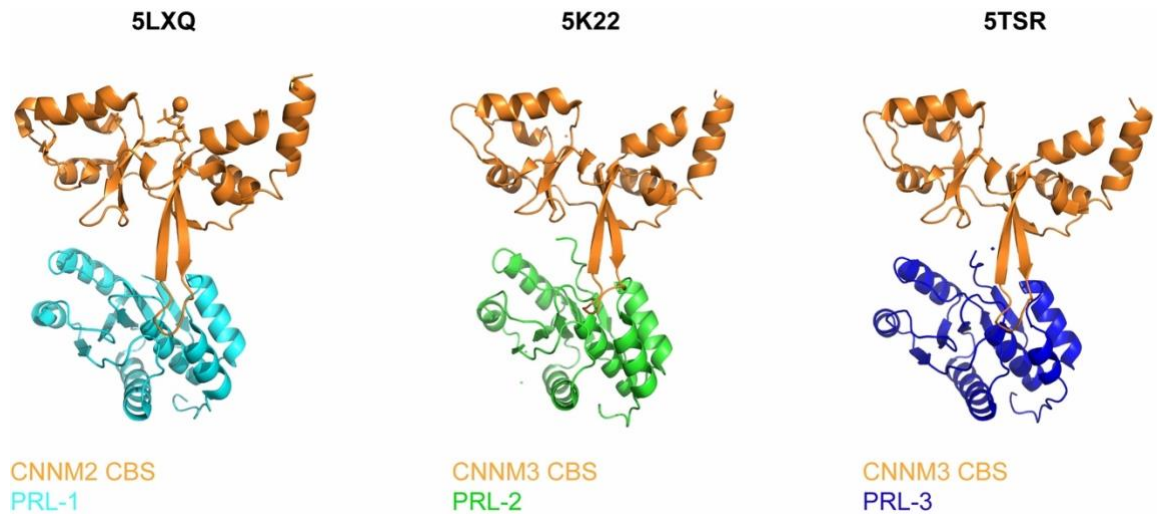


**Figure 1.3. Published structures of CNNM CBS-domain/PRL interactions, determined by x-ray crystallography.** 5LXQ (PRL-1/CNNM2) both are made based on mouse protein sequence, structure derived by x-ray diffraction at 3.33 Å; 5K22 (PRL-2/CNNM3) both are made based on human protein sequence, PRL-2 is in the reduced state, and structure was derived by x-ray diffraction at 3.00 Å; 5TSR (PRL-3/CNNM3) both are made based on human protein sequence and structure was derived by x-ray diffraction at 3.19 Å. Each of these renderings was made in Pymol after downloading their associated PDB files, available on the Protein Data Bank.

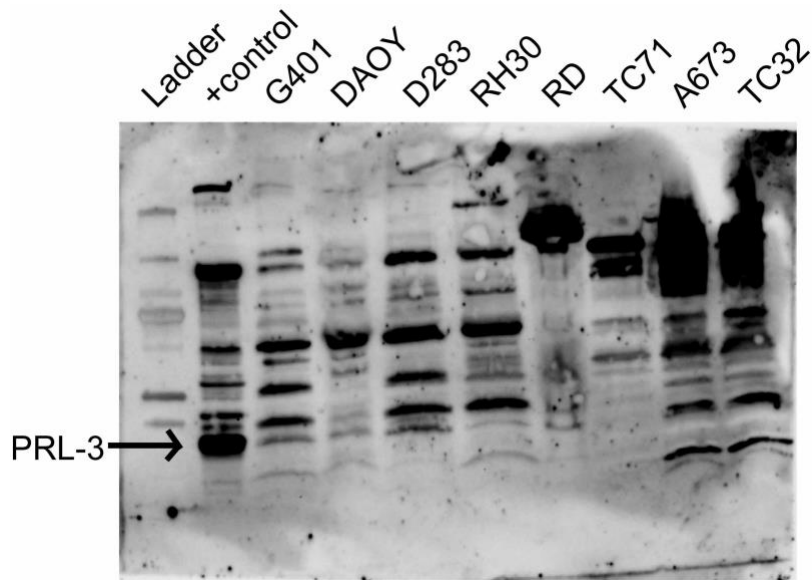


**Figure 1.4. Off-target binding of Anti-PTP4A3/PRL-R antibody (ab50276) in western blot.** Western blot of solid tumor cell lines for PRL-3. Primary antibody Anti-PTP4A3/PRL-R antibody (ab50276) 1:1000, secondary rabbit-HRP 1:5000. Cell lines include G401 (rhabdoid tumor), DAOY (medulloblastoma), D283 (medulloblastoma), RH30 (rhabdomyosarcoma), RD (rhabdomyosarcoma), TC71, A673, and TC32 (Ewing sarcomas). Positive control is HEK293T cells transfected with plenti-CMV-PRL-3 construct.



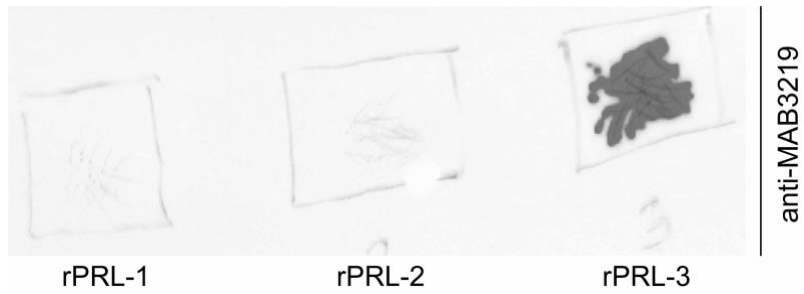


**Figure 1.5. R&D Biosystems antibody MAB3219 is specific for PRL-3.** Dot blot of recombinant PRL-1, PRL-2, and PRL-3 absorbed by PVDF membrane. Membrane was blocked for 1 hour at room temperature with 5% milk, incubated with MAB3219 1:1000 for 1 hour followed by TBST washes and 1 hour of incubation with anti-mouse-HRP secondary 1:2500 for 1 hour, and imaged with ECL substrate.

## Chapter 2. Introduction to Nanobodies

### 2.1. Discovery and advantages of camelid-derived nanobodies.

Nanobodies were discovered serendipitously 30 years ago, in 1993 (97). Serge Muyldermans' group noticed that camel, dromedary, and llama serum contain conventional antibodies. However, about half of the IgG populations included a unique type of antibody devoid of light chains (97). Since their discovery, cartilaginous fish have been the only other animals found to produce these types of antibodies (98). These "heavy chain only" antibodies have heavy chains with a lower molecular weight than conventional antibodies due to the absence of a CH1 domain (Fig 2.1). With the lack of light chains, these antibodies bind their antigen solely with the variable domain of the heavy chain, referred to as the VHH domain (99). These antibodies comprise the VHH domain and a hinge region connecting the CH2 and CH3 domains (Fig 2.1). The antigen binding domain, or VHH, derived from these antibodies is only 15 kDa (99). The lack of light chains causes the formation of a longer complementary determining region-(CDR)3 with a secondary disulfide bond to stabilize the structure of the VHH domain. Thus far, no one has determined why camelids and cartilaginous fish produce these antibodies and other animals do not. A complete comparison of conventional antibodies and VHH domains is displayed in Table 2.1.

Five years after the discovery of heavy chain-only antibodies, Lauwereys et al. found that isolated VHH from these antibodies can act as a potent inhibitor of their antigen (100). First, they immunized dromedaries with  $\alpha$ -amylase and harvested both heavy chain-only antibodies and conventional antibodies, where only the heavy chain-only antibodies acted as inhibitors of the protein (100). Secondly, they cloned the VHH domains out of the heavy chain-only antibodies using phage-display technology and produced the VHH domains as a recombinant protein in *E.coli*. They demonstrated that these small VHH proteins also act as competitive inhibitors against their substrate (100). They were among the first to exhibit that these small antibody fragments would be valuable in designing small synthetic inhibitors.

Cloning the repertoire of antigen-binding fragments in an immunized phage display vector and selection by phage display became a routine method at this time (101). Researchers quickly adapted the approach for the isolation of VHH. VHH antigen binding sites are encoded in a single gene fragment (102). By isolating peripheral blood lymphocytes, cDNA libraries are prepared following PCR of potential VHH regions. Isolating the VHH domain of heavy chain-only antibodies has led to the discovery of many advantages for using these small antibodies.

Along with being a single gene and easily cloned, VHH domains offer a variety of advantages compared to conventional antibodies. They exude high expression yields and are easily purified from *E. coli*. (103). Recombinant VHH are most commonly purified from bacterial expression systems that direct the protein to the periplasm (103). These periplasm's oxidizing environment stimulates disulfide bond formation, which is crucial in producing a functional VHH. Further purification using Immobilized Metal Affinity Chromatography and size exclusion chromatography is standard if cDNA libraries clone C-terminal His-tags fused to the VHH sequences.

VHH domains are also highly stable and naturally soluble due to substitutions of hydrophobic by hydrophilic residues in their framework regions (102). Ghahroudi et al. tested VHH stability by examining activity after incubation at 37°C for 200 hours, and VHHs retained 100-80% of binding activity to their antigens (104). The presence or absence of the critical CDR3 secondary disulfide bond caused variation in binding activity (104). Furthermore, their small size (15 kDa), ten times smaller than conventional antibodies, permits binding in grooves and cavities in active sites (100). Specifically, VHH domains can form convex shapes, allowing VHH regions to reach narrow, concave binding and activation sites on proteins that normal antibodies cannot bind to (100), establishing high specificity and affinity for their antigens. VHH regions also are stable under stringent conditions, lack immunogenicity, and show affinities for their antigens in the nanomolar range (105, 106), establishing their potential as therapeutic agents. These single antigen binding domains of heavy chain-only antibodies were trademarked by Ablynx as nanobodies (107), based on their size (4 nm in length, 2.5 nm in width) (108), which is what they will be referred to as for the remainder of this dissertation.

## 2.2. The potential of nanobodies as a scientific research tool.

### 2.2.1. *Fluorescent nanobodies for cellular imaging.*

Monoclonal antibodies have continued to be invaluable tools for studying proteins for many decades, both in research and clinical settings. While they will continue to remain indispensable, the development of nanobodies offered an exciting new research tool for applications that antibodies were less than a desirable tool. For example, the large size of antibodies has caused them to mainly target extracellular proteins *in vivo*, as they cannot readily penetrate cellular membranes (109). For this same reason, they are primarily used to examine protein expression only in fixed tissue samples (109). Finally, for proteins like the PRLs, current antibodies, other than PRL-3-zumab, do not offer the specificity to differentiate between these phosphatase family members (see Chapter 1). Since their discovery, research groups have continued to manipulate the advantages nanobodies offer for further use in scientific research to study protein biology.

First and foremost, nanobodies made against proteins that do not currently have antibodies to study them are immediately helpful in fixed immunofluorescence assays. In addition, nanobodies improve penetration during these fixed analyses, as shown by de Beer and Giepmans when anti-GFP nanobodies demonstrate improved nuclear labeling of Histone 2B-GFP compared to conventional GFP antibodies (110). Conducting traditional immunolabeling applications occurs using one of two procedures. First, nanobodies can act as primary antibodies in immunofluorescence thanks to companies like Jackson ImmunoResearch, which have developed fluorescently linked VHH secondary antibodies ([www.jacksonimmuno.com](http://www.jacksonimmuno.com)). This tool detects alpaca nanobodies and delineates their localization through fluorescent labeling.

Secondly, chromobodies, which are nanobodies genetically or chemically fused to a fluorescent protein, are helpful in similar approaches. Nanobodies are also linked to fluorescent probes following purification by chemical modifications (111) or using company-manufactured kits, such as the Biotium mix-n-Stain nanobody labeling protocol. These can be useful for real-time visualization of endogenous proteins in the cell (111).

Due to the stability of nanobodies, following fusion to fluorescent proteins or probes, they retain their dynamic folds and functional antigen binding (112).

Chromobodies set themselves apart from conventional immunolabeling tools because they can serve as tracers for intracellular target localization and trafficking studies, avoiding the need for modifying proteins with fluorescent tags (112). The field had to overcome the hurdle of getting these nanobodies into cells to label their specific antigens when looking at intracellular targets. The plasma membrane is a physical barrier for nanobodies; therefore, the discovery of custom delivery methods was necessary to target endogenous proteins (110). Delivery of fluorescent nanobodies to cells occurs through engineered endocytosis (113) or lipid-based protein transfection (114, 115). There is a second obstacle these nanobodies face, which is escaping endosomal degradation upon cellular delivery. Unfortunately, endosomal escape is often low (116). Therefore, alternative methods were necessary so nanobodies could reach their targets.

To prevent endocytic uptake, researchers developed cell-penetrating peptide-linked (CPP) nanobodies. CPPs are arginine-rich peptides that facilitate direct penetration of the plasma membrane for dispense into the cytoplasm, independent of endocytosis (110). For example, Herce et al. attached intracellularly stable cyclic arginine-rich cell-penetrating peptides (CPPs) to nanobodies (117). CPPs increase the size of cargo that can be delivered efficiently into living cells (118). This strategy was successful in delivering nanobodies targeted against GFP (27.5 kD), GFP-PCNA (63 kD), and the therapeutically relevant Mecp2- GFP fusion protein (83 kD) into HeLa cells to study protein interactions (117). Delivering nanobodies to cells via chromobodies has advantages, primarily if controlling the amount of nanobody is necessary. But, the disadvantage is the necessity of these complex delivery mechanisms to visualize outcomes.

Another form of fluorescent nanobodies created to combat these delivery challenges are intrabodies. Intrabodies express the cDNA of the nanobody sequence fused to the cDNA of a fluorescent probe, which is then expressed by cellular machinery. The nanobody directs the fluorescent protein to its antigen (119). The benefit of using cDNA encoding intrabodies over chromobodies is the ease of switching between probes fused to the nanobody and the ease of delivery to cells through basic DNA transfection methods (110). Many groups have developed intrabodies against disease-related targets, including

HIF-1 $\alpha$  (120), HPV16 E6 (121), Ras (122), and many others. The primary challenge in intrabody development is that the reducing environment of the cytosol can impact the formation of the disulfide bonds needed for nanobody folding, which can negatively impact nanobody-reporter gene folding and the ability of the intrabody to recognize its target (123). Most nanobodies yielded from conventional screening methods are not readily functional in living cells. Therefore, many groups have employed different selection methods to acquire functional intracellular binders, reviewed by Wagner and Rothbauer (119). One strategy is to remove conserved cysteine residues, and test if nanobodies are functional; if they are then the reducing environment is no longer a disadvantage. However, this usually contributes to a loss in nanobody stability. Rather than mutating nanobodies after phage display, there are also methods such as yeast-two-hybrid systems, that lend themselves to initial nanobody identification (124). In yeast-two-hybrid the nanobody and antigen are fused to a DNA binding domain and growth on selection media following binding serves as a reporter. The advantage of this method is the potential for cytosol and nuclear expression when fused to a DNA binding domain (119). However, there is potential for numerous false positives with this method and such methods are continually being optimized to improve intrabody screening. Overall, chromobodies and intrabodies have distinct advantages when used for fixed and live-cell imaging, depending on the project's research goal.

### *2.2.2. Using nanobodies to identify protein substrates and DNA binding partners.*

Conventional antibodies will continue to be useful for co-immunoprecipitation studies to identify protein substrates and protein-protein interactions. Again, there are proteins like PRL-3 where protein-specific conventional antibodies still need to be developed. Fortunately, following purification, nanobodies have been evaluated for co-immunoprecipitation purposes (112, 125) and can be used to study specific protein-protein interactions. In the current research climate surrounding genomic and proteomic analyses, identifying signaling mechanisms involved in these protein and DNA interactions is a challenge. Nanobodies are now being used in chromatin immunoprecipitation (ChIP) to identify protein-DNA interactions, as well as being followed up with DNA microarray

hybridization (ChIP-on-chip) to assess genome-wide identification for protein-DNA interactions (126). Nguyen-Duc et al. developed a proof of principal ChIP-on-chip assay to demonstrate that nanobodies are useful. They created Ss-LrpB-specific nanobodies, a well-studied transcription factor of the hyperthermophilic archaeon *Sulfolobus solfataricus* (126). Genome-wide ChIP-on-chip with this nanobody identified known Ss-LrpB binding sites and revealed several unknown target sequences. These findings are likely due to the unique specificity that nanobodies offer. Nanobodies will continue to be an excellent resource for identifying protein-protein and protein-DNA interactions.

### *2.2.3. Nanobody-directed protein degradation.*

One of the most common approaches to studying protein function is removing it from the cell to study molecular and phenotypic changes in its absence. Many studies have been done through genetic approaches with CRISPR-Cas9 and silencing RNA approaches, even to the point of conditional and tissue-specific knock-outs. However, a new approach that is becoming common is removing expression at the protein level rather than the RNA level by hijacking the proteasome. One way to achieve this is by fusing a nanobody of interest to a subunit of an E3 ubiquitin ligase complex, often the F-box subunit. The F-box stimulates the recruitment of the nanobody antigen to the complex, leading to polyubiquitination of the antigen and degradation by the proteasome (109). Caussinus et al. were the first to streamline this process by using an anti-GFP nanobody in *Drosophila*, a system now termed deGradFP, designed for the degradation of fluorescently labeled proteins (127). deGradFP has been used to degrade several *Drosophila* proteins and successfully degraded proteins in mammalian cell lines (128). However, research groups had to redesign this approach to target proteins in zebrafish by swapping in the zebrafish F-box protein rather than the homologous *Drosophila* protein (129), which is controlled conditionally under a heat-shock promoter, directed by the water temperature of zebrafish housing. Direct protein degradation has advantages over classical genetic approaches, including tissue-specific knock-out using specific E3 systems. Thus far, no one has taken this approach and replaced the GFP nanobody in these systems with a nanobody of interest.

Doing so would allow for the study of endogenous protein removal rather than tagged-over-expressed proteins.

#### *2.2.4. Nanobodies enhance x-ray crystallography.*

The fact that nanobodies are small and have high stability and specificity for their antigens lends them well to acting as chaperones in structural studies (130). Specifically, their specificity is for a single conformation of their antigen (131), so they can be applied in structural biology to freeze their dynamic antigens into single functional conformations (131). X-ray crystallography obtains three-dimensional molecular structures from a protein crystal. Groups have successfully crystallized a nanobody-antigen complex and get high-resolution structures because of the nanobody's highly specific nature (131). Zavrtnik et al. compared the binding characteristics of nanobodies to conventional antibodies by analyzing 105 nanobody-antigen crystal structures (132). This group demonstrated that while antibodies use six CDR loops for antigen binding, nanobodies only utilize three; nanobodies maintain an average 6 nM affinity for their antigen. Therefore, with fewer loops, they retain binding affinity for their antigen comparable to conventional antibodies (132). They also observed that nanobody recognition sites on their antigens are more similar to general protein-protein interactions than antibody-antigen interactions. Therefore, epitopes recognized by nanobodies may overlap with sites involved with protein-protein interactions (132). These discoveries are fascinating as they detail that nanobodies could act as potential inhibitors at these sites or aid in developing protein interaction inhibitors by mimicking the binding of protein substrates or binding partners.

### 2.3. Nanobody use in cancer.

#### *2.3.1. Nanobodies for cancer diagnosis.*

Tumors and their microenvironment are continuing to become more complex. Therefore, it is becoming increasingly important to detect tumor antigens and visualize the tumor microenvironment to effectively diagnose and treat patients, as it encompasses many



factors contributing to cancer growth and metastasis (133). For example, an anti-human epidermal growth factor nanobody, a kinase over-expressed in a variety of cancers, has been developed for single-photon emission computed tomography, or SPECT imaging (134). SPECT uses a variety of radionuclides to emit gamma-ray photons to visualize the body's organs, tissues, and bones (135). This anti-HER2 nanobody (<sup>68</sup>Ga-HER2 Nbs 2Rs15d) is radiolabeled with gallium-68 (134). Phase I clinical trial showed that 60 minutes post-injection, these nanobodies detected HER2-positive primary and metastatic tumors in breast cancer patients with no adverse effects (136). These positive results led to a phase II clinical trial that demonstrated these nanobodies could cross the blood-brain barrier and detect HER2-positive metastatic brain lesions in an orthotopic tumor-bearing athymic nude mouse model (137).

Furthermore, this nanobody's uptake and therapeutic efficacy were compared to the anti-HER2 monoclonal antibody, trastuzumab. Radiolabeled HER2 nanobody exhibited high and specific tumor uptake, while trastuzumab could not accumulate in these brain tumor models, and the nanobody increased the median survival of the model (137). This single example of nanobodies for cancer imaging displays their usefulness in diagnosis and their ability to treat lesions inaccessible to monoclonal antibodies potentially.

Beyond imaging tumor cells, the tumor microenvironment (TME) has become an essential topic in cancer research, as it directly contributes to cancer cell support and survival. Many factors comprise the TME, including immune cells, stromal cells, blood vessels, and the extracellular matrix (138). Multiple nanobodies have targeted aspects of the TME, mainly focusing on the structural components, such as fibronectin and vasculature. An example of this is an anti-VCAM nanobody that targets the vasculature cell adhesion molecule 1(VCAM-1), a protein involved in the adhesion of leukocytes to vascular endothelium (139). Anti-VCAM-1 nanobodies allow imaging of tumor vasculature through ultrasound only 10 minutes after uptake (140). Tools like these will enable cancer researchers to not only diagnose the expression profile of tumor cells but also assess the makeup of the TME to prepare a better treatment plan that will eliminate tumor resources and contribute to limiting cancer relapse.

One of the caveats to radiolabeled nanobodies is their clearance mechanisms. In the HER2-nanobody study, one-hour post-injection, less than 10% of the injected dose was

circulating in the blood (107, 141), which limits toxicity to healthy tissue. However, this rapid clearance is pushing a large percentage of the radiolabeled nanobody through the kidneys, potentially leading to unwanted radiation damage in the kidneys. Fortunately, Huyvetter et al. demonstrated reduced kidney retention when co-infusing radiolabeled nanobodies with Gelofusin, a volume expander often used as a plasma replacement (141). Reducing kidney retention should allow nanobody cancer diagnostic research to expand and improve early detection and patient treatment plans to improve patient outcomes and quality of life.

### 2.3.2. *Nanobodies for cancer treatment.*

In 2019, the first nanobody therapeutic, Caplacizumab or Cablivi, was approved by the FDA to aid in accelerating platelet aggregation in acquired thrombotic thrombocytopenic purpura (aTTP). This disease causes tiny blood clots throughout the body. Many nanobodies targeting cancer-associated proteins have shown promise in *in vitro* studies. However, in tumor models, they are cleared rapidly due to their lack of immunogenicity. It is hypothesized that while these nanobodies can target the tumor cells independently, the absence of the Fc domain causes cells to lack an immune response that triggers white blood cells to kill tumor cells (142).

For this reason and others, there are currently no FDA-approved nanobodies. However, there are ~20 nanobodies in various clinical trial stages, of which 11 are in trials related to treating multiple types of tumors (5). These nanobodies are displayed in Table 2.2. Despite the lack of approved cancer nanobodies, numerous groups continue to contribute to the field with nanobodies that have therapeutic potential (5), each utilized with different techniques.

For example, several researchers have exploited nanobodies as vehicles to deliver drugs or toxins to tumor sites to reduce off-target toxicity in normal cells, ultimately diminishing the side effects of treatment (143). Nanobody-reduced immunogenicity is advantageous here, as a triggered immune response would stop the delivery of the cargo, and small size improves penetration within solid tumors (144). One example is an immunotoxin, which is the conjugation of an antigen-specific nanobody to a specific toxin

(143). There are many versions of nanobodies fused to different toxins in the literature. One example is the conjugation of a VEGFR-specific nanobody to Pseudomonas exotoxin A (PE38) (145). PE38 kills VEGFR-expressing tumor cells by binding the receptor on the cell surface with the nanobody, entering the cell via endocytosis where PE38 binds the ADP-ribosylating elongation factor II where it halts protein synthesis and cell proliferation (145). Behdani et al. was the first group to report a bacterial protein-based immunotoxin that inhibits tumor cell growth of VEGFR-positive tumors (145).

The other platform using nanobodies for cancer treatment has nanobodies acting as vehicles for drug delivery. Specifically, they decorate the surface of nanoparticles such as liposomes, micelles, or albumin nanoparticles carrying targeted therapies (142). The first instance showing that these nanobody tools are internalized by target cells was an anti-EGFR nanobody, EGa1, decorating a liposome (146). Since this discovery, micelles decorated with EGa1 nanobodies encapsulating doxorubicin, a commonly used chemotherapy that stunts cell growth, were shown to inhibit tumor growth and prolong animal survival compared to non-specific nanobody targeting (146). Utilizing nanobodies as cargo carriers for targeted therapy is an impressive way to harness these tools when they may not have antagonistic potential on their own.

**Table 2.1. Comparison of conventional antibodies and nanobodies, adapted from (147).**

<b>CONVENTIONAL ANTIBODY</b>	<b>NANOBODY</b>
High immunogenicity	Low immunogenicity
150 kda	15 kda
Long half-life	Short half-life
Slow clearance	Fast clearance
Limited tumor penetration	Deep tumor penetration
Average CDR3 length	Long CDR3 length
Low stability	High stability
Prone to degradation with temperature and pH changes	Tolerant of temperature, pressure, and pH changes
Expensive, large-scale production	Inexpensive, large-scale production
Mammalian expression	Bacterial expression

**Table 2.2. Nanobodies currently in clinical trial, adapted from (5).**

Nanobody	Disease	Target	Phase of trial	Clinical Trial
ALX-0061	Rheumatoid arthritis	IL6R	Phase II	NCT0251862
ALX-0061	SIE	IL6R	Phase II	NCT02437890
ATN-103	Rheumatoid arthritis	TNF	Phase II	NCT01063803
ALX-0761	Psoriasis	IL17A/IL17F	Phase II	NCT03384745
M1095	Psoriasis	IL17A/IL17F	Phase II	NCT03384745
Caplacizumab	TTP	VWF	Approved	NCT02878603
ALX-0171	RSV	F-protein RSV	Phase II	NCT02979431
ALX-0651	Healthy volunteers	CXCR4	Phase I	NCT01374503
BI836880	Solid tumors	Angiopoietin/VEGF	Phase I	NCT02674152
KN046	Squamous Non small-cell lung cancer	PD-L1/TLA4	Phase III	NCT04474119
KN046	Advanced HCC	PD-L1/CTLA4	Phase I	NCT04601610
KN035	Hepatocellular carcinoma	PD-L1	Phase I	NCT03101488
BCMA nanobody CAR-T cells	Relapsed/ Refractory Myeloma	CD8/4-1BB	Phase I	NCT03664661
CD7 CAR-T cells infusion	T-lymphoblastic Lymphoma	CD7	Phase I	NCT04004637
CD22 CAR-T cells	B-cell Lymphoma	CD22	Phase I	NCT03999697
$\gamma\delta$ T Cell infusion agent	B-cell Leukemia	CD22	Early Phase I	NCT04439721
CD19/CD20 CAR-T cells	B-cell Lymphoma	CD19/CD20	Phase I	NCT03881761
$\alpha$ PD1-MSLN CAR-T cells	Non small-cell Lung cancer	PD-1	Early Phase I	NCT04489862
$\alpha$ PD1-MSLN CAR-T cells	Mesothelioma	PD-1	Early Phase I	NCT04489862
$\alpha$ PD1-MSLN CAR-T cells	Colorectal Cancer	PD-1	Phase I	NCT05089266
M6495	Symptomatic Knee Osteoarthritis	ADAMTS-5	Phase II	NCT03583346

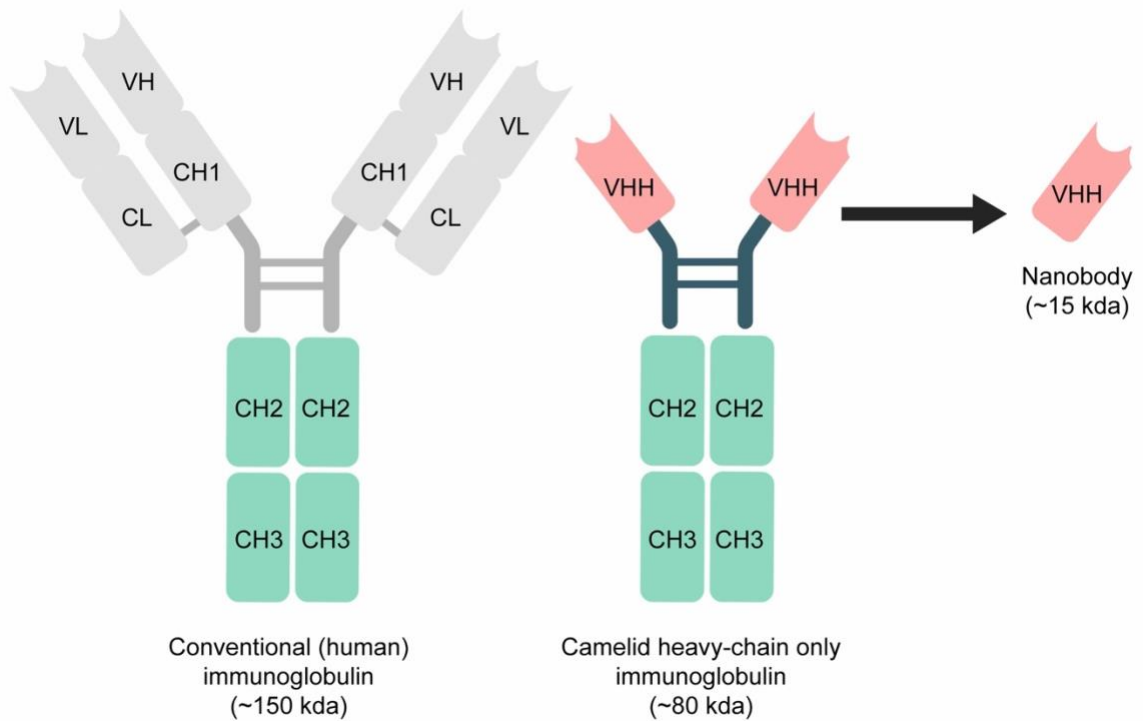


**Figure 2.1. Size and domains of immunoglobulin proteins.** Conventional antibodies found in humans and partially in camelid serum are 150 kda. Camelid heavy-chain only antibodies are 80 kda. Nanobodies are the antigen binding regions of heavy-chain only antibodies, at 15 kda. Abbreviations represent the following: VL – variable light chain; VH – variable heavy chain; CL – constant light chain; CH# - constant heavy chains 1-3; VHH – variable heavy chain of camelid antibodies.

## Chapter 3. Materials and Methods

### 3.1. Bacterial and mammalian expression vectors.

#### 3.1.1. Bacterial expression vectors.

To generate recombinant protein for alpaca immunization, human PRL-1, -2, and -3 cDNA was amplified with gene-specific primers and cloned into the bacterial expression vector, pSKB3. pSKB3 is a modified pET-28b vector. A TEV protease cleavage site replaced the original thrombin cleavage site in the vector initially constructed by Dr. Steve Burley, Rutgers, The State University of New Jersey. We used pSKB3 to clone PRL-1, -2, and -3 cDNA at NheI and XhoI restriction sites using T4 ligase. A representative plasmid map for pskb3-PRL-3 is shown in Figure 3.1.

The 3XFLAG-tagged PRL-3 protein expression vector was generated by amplifying 3XFLAG-PRL-3 from a plenti-CMV-3XFLAG-PRL-3 vector via PCR and cloned into pSKB3 utilizing NheI and XhoI restriction sites using T4 ligase. The CBS-HA protein expression vector was made by cloning full-length CNNM3 CBS-HA domain gBlocks™ Gene Fragments (IDT) into pSKB3 using NheI and XhoI restriction enzyme sites and T4 ligase.

#### 3.1.2. Mammalian expression vectors.

The 3XFLAG-tagged PRL mammalian expression plasmids were made by cloning full-length PRL-1, -2, or -3 human cDNA into a p3XFLAG-CMV-14 expression vector (Sigma, E7908). Then 3XFLAG-PRLs were cloned into pLenti-CMV-puro (Addgene 17452) to make plenti-CMV-3XFLAG-PRL-puro constructs. A representative map of the final plenti-CMV-puro-3XFLAG-PRL-3 is shown in Figure 3.2.

The GFP-tagged and untagged PRL mammalian expression plasmids were made by cloning full-length PRL-1, -2, or -3 gBlocks™ Gene Fragments (IDT) into the pcDNA™3.1 (-) (Invitrogen V79520) at BamHI and HindIII restriction sites. In addition, a GFP gBlock was cloned into the pcDNA3.1-PRL plasmids to generate CMV:GFP-PRL

fusion constructs at NotI and BamHI restriction sites. A representative pcDNA3.1 GFP-PRL-3 map is shown in Figure 3.3.

The HA-tagged PRL-3 mammalian expression plasmid was made by cloning a full-length HA-PRL-3 gBlocks™ Gene Fragments (IDT) into a pENTR middle entry vector. Invitrogen LR Clonase II (Life Technologies 11791020) allowed gateway cloning into pLenti-CMV-puro (Addgene 17452) to make a plenti-CMV-HA-PRL-3-puro construct.

### 3.2. Production, bacteriophage display, and sequencing of nanobodies.

Nanobodies were produced by the University of Kentucky Protein Core, as previously described in Chow et al. (130). All procedures with the alpacas were performed following protocols (2017-2627 and 2018-2925) approved by the University of Kentucky's Institutional Animal Care and Use Committee (IACUC) (130). In summary, 100 µg of recombinant PRL-3 antigen (See Section 3.4.1) was subcutaneously injected into alpacas once per week for six weeks to boost nanobody presence in the immune system. 3-5 days following the final injection, 50 mL of alpaca blood was harvested to isolate peripheral blood lymphocytes by density gradient centrifugation. RNA was isolated from these lymphocytes, and cDNA was synthesized using reverse transcriptase. A bacteriophage display cDNA library was made by cloning potential VHH regions, with restriction enzymes, into the phage display vector pMES4. pMES4 phage was expressed with the VHH insert fused to gene III of the filamentous phage to produce the phage solution. Two rounds of phage display against PRL-3, as described by Chow et al. (130), utilizing this cDNA library yielded 96 clones that were analyzed in multiple rounds of colony PCR by VHH specific primers (F: AGCGCCCAATACGCAAACCGCCT; R: GACAGCCCTCATAGTTAGCGTAACG). Figure 3.4 shows representative colony PCR, which yielded 32 potentially VHH-positive clones (~400 bp band). These clones were confirmed by sequencing using a VHH-specific primer, pEX-Rev (CAGGCTTTACTTTATGCTTCCGGC), by Eurofins Genomics. DNA sequences were translated using the ExPASy Bioinformatics Resource Portal Translate Tool (<https://web.expasy.org/translate/>), where they were analyzed for nanobody components, including pelB sequence and 6XHis-tag followed by a stop codon. 16 of 32 clones



embodied these components, represented in Figure 4.1, and were analyzed for specificity toward PRL-3 in ELISA experiments.

### 3.3. Cell lines and culture conditions.

Two human cell lines were utilized in this study (HEK293T, HCT116) and were authenticated by short tandem repeat (STR) profiling and tested for mycoplasma contamination before experiments using the LookOut® Mycoplasma PCR Detection Kit (Sigma, MP0035-1KT). HEK293T (ATCC CRL-3216) and HCT116 (ATCC CCL-247) cells were grown in 1X DMEM (Thermofisher, 11965092). For both cell lines, media was supplemented with 10% heat-inactivated fetal bovine serum (R&D Systems, S11150H, Lot. H19109). Cells were cultured at 37 °C with 5% CO<sub>2</sub>. To overexpress the CMV:PRL-3, CMV:GFP-PRL, CMV:3XFLAG-PRL, and CMV:HA-PRL-3 plasmids, cells were transfected using Lipofectamine 3000 (Thermofisher, L3000-015) following the manufacturer's protocol. HEK293T stably expressing PRL cell lines were selected with 1 µg/mL puromycin (Thermofisher, A1113803).

### 3.4. Expression and purification of recombinant proteins.

#### 3.4.1. PRL-1, -2, and -3 purification.

pskb3-PRL bacterial expression plasmids described in Section 3.1.1 were transformed into and expressed using the One-Shot BL21 Star DE3 bacterial cell line (Invitrogen, C601003) by stimulating induction with 0.5 mM IPTG (Fisher Scientific, BP175510) for 16 hours at 16°C following a culture O.D.<sub>600</sub> of 0.6. Cells were pelleted at 5,000 rpm for 15 minutes at 4°C and resuspended in 10 mL of lysis buffer [300 mM NaCl (VWR BDH9286), 20mM Tris pH 7.5, 10 mM Imidazole pH 8.0 (Sigma-Aldrich I2399), 1:1000 protease inhibitor cocktail (Sigma-Aldrich P8465)] per gram of cell pellet and lysed using a microfluidizer (Avestin, EmulsiFlex-C5). The soluble lysate was separated from the insoluble lysate by centrifugation at 18,000 rpm for 50 minutes at 4°C. The soluble

lysate was run over 1 mL columns (Biorad, 7321010) packed with Ni-NTA Resin (VWR, 786-940). Before elution, the resin is washed with 10 mL of lysis buffer.

The PRL proteins were eluted with 2 mL of elution buffer (300 mM NaCl, 20 mM Tris pH 7.5, and 250 mM Imidazole pH 8.0).

For the second purification step, the N-terminal 6XHis-tag on recombinant PRLs was cleaved using TEV protease (gift from Dr. Konstantin Korotkov), as the pSKB3 plasmid contains a TEV cleavage site. This cleavage is performed through dialysis against Wash Buffer [300 mM NaCl 20 mM Tris pH 7.5]. The cleaved recombinant PRLs were then reapplied to the Ni-NTA column to remove uncleaved protein. The resin was washed five times with 10 mL of wash buffer. Samples from the first and second purification steps were analyzed by SDS-PAGE gels using 4-20% Mini-PROTEAN TGX Stain-Free Gels (Biorad 4568094) for cleavage of the 6XHis-tag and homogeneity of samples from the second step. A representative gel of PRL-3 Ni-NTA purification and His-tag cleavage is shown in Figure 3.5A. Homogeneous flowthrough and wash fractions from the second step were pooled and concentrated for the third purification step.

The pooled PRLs were further purified using a Superdex 200 Increase 10/300 GL column (G.E., 28990944) on an ÄKTA purification system in buffer containing 100 mM NaCl and 20 mM HEPES (Fisher Scientific, BP310-100) pH 7.5. Purification was verified by running samples on 4-20% Mini-PROTEAN TGX Stain-Free Gels. The purest fractions were pooled, concentrated, flash-frozen on dry ice, and stored at -80°C. A representative gel of purified fractions is shown in Figure 3.5B.

#### *3.4.2. Anti-PRL-3 nanobody purification.*

pMES4-nanobody plasmids, as described in section 3.2, are also bacterial expression vectors, which were transformed into BL21 Star DE3 bacterial cells, as described in section 3.4.1. Bacteria were induced, harvested, and lysed in the same manner as 3.4.1. Following lysis, separation from the insoluble proteins, and running over the 1 mL Ni-NTA column, nanobodies underwent a stepwise elution. The first step was elution with 6 mL of 30 mM Imidazole elution buffer to remove as many non-specific proteins as possible. The second elution step was with 2 mL of 250 mM Imidazole elution buffer

containing the purified sample. A representative gel of nanobody 91's Ni-NTA purification is shown in Figure 3.6. Recombinant nanobodies remained with their C-terminal 6XHis-tag intact, as the pMES4 vector does not contain a protease cleavage site. All samples underwent buffer exchange and concentration by centrifugation with ~25 mL of wash buffer to remove imidazole. Nanobodies were further purified using a Superdex 200 Increase 10/300 GL column, verified through gel electrophoresis, and stored as described in 3.4.1.

#### *3.4.3. 3XFLAG-PRL-3 and CBS-HA purification.*

The protocol outlined in 3.4.1 was followed to express and purify pSKB3-3XFLAG-PRL-3 and pSKB3-CBS-HA (Section 3.1.1). Purification was completed following protease cleavage of the 6X-His-tag and reapplication to the Ni-NTA column (Section 3.4.1). Further purification was unnecessary for competition studies, and purification was confirmed using gel electrophoresis outlined in 3.4.1 for the 3XFLAG-PRL-3, shown in Figure 3.7A. A western blot was necessary to confirm CBS-HA purification. This protein does not contain any tryptophan residues, which are required to see total protein on Biorad Mini-PROTEAN TGX Stain-Free Precast Gels. A western blot showing the purification of the CBS-HA protein is shown in Figure 3.7B.

### 3.5. Nanobody specificity analysis for PRL-3 using an in-house ELISA approach.

Recombinant, purified, PRL-1, -2, and -3 (Section 3.4.1) proteins were plated at 1  $\mu\text{g/mL}$  (100  $\mu\text{l}$ ) in sodium bicarbonate buffer [0.42g sodium bicarbonate (Fisher Scientific, BP328-500) in 50 mL  $\text{dH}_2\text{O}$ ] in Corning® 96 Well EIA/RIA Assay Microplates (Sigma, CLS3590) and incubated for 16-20 hours at 4°C. Plates were washed three times with 0.05% PBST and loaded with a blocking solution of 0.5% BSA (Fisher Scientific, BP9706100) in 0.1% PBST for 1 hour at room temperature. The blocking buffer was removed, and nanobodies were diluted to 1  $\mu\text{g/mL}$ , or designated pMol concentration for dosing experiments, and incubated in wells for 1 hour at room temperature. Wells were washed three times in PBS and incubated with 1:1000 anti-His HRP antibody (GenScript,

A00612, Lot. 19K001984) for 1 hour at room temperature. Plates were washed three times with PBS and developed with TMB 2-Component Microwell Peroxidase Substrate Kit (Seracare, 5120-0053). Reactions were stopped after 90 seconds with 0.1 N HCl (Fisher Scientific, A144500) and read on a Biotek Synergy Multi-mode Plate Reader at 450 nm. Controls included PRL-only wells to specify the lack of a 6X-His-tagged nanobody, secondary-only wells to establish the necessity of PRL presence for binding and buffer only to provide evidence that sodium bicarbonate and BSA did not elucidate a colorimetric change. Raw data from all control wells were pooled for each plate, and experimental wells were normalized to controls by dividing individual wells by average control wells. Individual well readouts were placed in GraphPad Prism 9 in a Grouped format Table. Values for two replicate experiments were graphed for relative absorbance at 450 nm compared to the average of control wells. A two-way ANOVA analyzed statistics using Sidak's multiple comparisons tests where ns = not significant, \* $p < 0.05$ , \*\*\* $p < 0.001$ .

3.6. Immunoprecipitation (IP) of PRL-3 with nanobody or commercially available PRL antibodies.

*3.6.1. IP of PRL-3 with nanobody coupled Dynabeads.*

PRL-3 nanobodies were coupled to Dynabeads (Life Technologies, 14311D) for 3XFLAG-PRL immunoprecipitation following the manufacturer's instructions. Briefly, 150  $\mu\text{g}$  of nanobody protein supplemented with C1 buffer to 250  $\mu\text{L}$  was added to 5 mg of Dynabeads® M-270 Epoxy beads after the beads were washed with 1 mL of C1 buffer. Then, 250  $\mu\text{L}$  of C2 buffer was added to the beads and nanobody mixture to incubate on a rotator at room temperature overnight (16–24 hours). After removing the supernatant, the nanobody-coupled beads were washed with H.B. (0.05% Tween 20), L.B. (0.05% Tween 20) buffer once, S.B. buffer shortly twice, and S.B. buffer for 15 minutes once. Finally, the resulting beads covalently linked to the nanobody were resuspended in 500  $\mu\text{L}$  S.B. buffer and stored at 4°C before experimentation. Before conducting all experiments, 30  $\mu\text{L}$  of beads were heated at 95°C for 5 minutes with 50  $\mu\text{L}$  2x Laemmli Sample Buffer (Biorad,

161-0737) with 2-Mercaptoethanol (Fisher Scientific, 03446I-100) and the supernatant was run on an SDS-PAGE gel to confirm coupling.

HEK293T (~20 million) stably expressing pLenti-CMV-puro (Addgene 17452) empty vector, 3XFLAG-PRL-1/-2, or -3 under 1 µg/mL puromycin selection were lysed for 30 minutes with intermittent vortexing in Pierce IP lysis buffer (Thermo 87788) supplemented with 1% protease inhibitor cocktail (I.P. buffer) at 500 µl per 10 million cells. Following lysis, cells supplemented with I.P. buffer were spun at 12,000 rpm for 10 minutes at 4°C to pellet cell debris. Protein concentration was quantified using the QuickStart Bradford 1X Dye Reagent (Biorad, 5000205). 150 µL of nanobody-coupled beads were washed in 1 mL of PBS for 5 minutes, then equilibrated in 500 µL of I.P. buffer for 5 minutes. 2.5 mg of total extracted protein was added to the equilibrated nanobody-beads complex overnight for incubation at 4°C with rocking. After washing the beads-protein complex in cold I.P. buffer four times, 50 µL 2x Laemmli Sample Buffer with 2-Mercaptoethanol was added to the beads for elution. The mixture was boiled at 95°C for 10 minutes to denature immunoprecipitated proteins and coupled nanobodies, and the supernatant was collected for western blot analysis.

### *3.6.2. IP of PRL-3 with commercially available PRL antibodies.*

HCT116 cells were transfected with CMV-HA-PRL-3, as described in Section 3.1.2. 48 hours post-transfection, cells were lysed as described in 3.1.7. PRL-3 nanobodies were coupled to Dynabeads for HA-PRL-3 immunoprecipitation following the manufacturer's instructions, as outlined in Section 3.6.1.

For commercial antibodies (Abcam, ab50276; GeneTex, GTX100600; R&D Systems, MAB3219; and Santa Cruz Biotechnology, sc-130355), 3 µg of each antibody was incubated with 400 µg of HCT116/CMV-HA-PRL-3 cell lysate at 4°C overnight with rocking. Lysate/antibody complexes were then incubated with 25 µl of Protein A (Cell Signaling Technologies 70024) and 25 µl of Protein G (Cell Signaling Technologies 73778) beads for 2 hours at 4°C with rocking. Washing, elution, and western blot analysis were carried out identically to methods outlined in 3.6.1.

3.7. Fixed immunofluorescence of HCT116 cells using anti-PRL-3 nanobodies to detect PRL-3 expression and cellular localization.

*3.7.1. Nanobody specificity for GFP-PRL-3 over GFP-PRL-1 and GFP-PRL-2.*

HCT116 colorectal cancer cells were plated at 5,000 cells per well in 96-well black glass-bottomed plates (Cellvis, P96-1.5H-N) and transfected with either CMV:GFP-PRL-1/-2/-3, as described in section 3.1.2. All solution exchanges and imaging occurred in the 96-well plate. 24 hours post-transfection, cells were washed once with 100  $\mu$ l of PBS, fixed with 50  $\mu$ l 4% paraformaldehyde (VWR, AAJ61899-AK) for 15 minutes, washed once with 100  $\mu$ l of PBS, permeabilized for 10 minutes in 50  $\mu$ l of 1% Triton X-100 (Sigma, X100-100), and washed three times again with 100  $\mu$ l of PBS. A blocking solution of 2% BSA in PBS was applied to all wells for 1 hour. Acting as primaries, all nanobodies were diluted to 1 mg/ml in blocking solution, further diluted 1:100 in blocking solution, and incubated with the fixed cells for 1 hour at room temperature, followed by five 100  $\mu$ l PBS washes. The secondary antibody used to detect nanobody staining was an anti-alpaca IgG VHH conjugated to Alexa Fluor-594 (Jackson ImmunoResearch, 128-585-232) diluted 1:400 in blocking solution and counterstained with Hoechst, 1:1000 dilution (ThermoFisher, H3570). Images were acquired at the University of Kentucky Light Microscopy Core using a Nikon A1R confocal microscope using a 40X water objective. To detect Hoescht counterstain, images were obtained using the DAPI (405nm) laser at gain 150, power 6.00. To detect GFP-PRLs, images were acquired using the FITC (488) laser at gain 30, power 2.00. To detect nanobody staining, images were obtained using the TRITC (561 nm) laser at gain 60, power 2.00. Images were processed in Adobe Photoshop 2022 to both increase image brightness and overlay the 405 (Hoescht), 488 (GFP-PRL-3), and 561 (Nanobodies) channels. Channels were pseudocolored by RGB channels.

*3.7.2. Co-staining of commercially available PRL-3 antibodies with nanobody.*

HCT116 colorectal cancer cells were plated at 5,000 cells per well in 96-well black glass-bottomed plates (Cellvis, P96-1.5H-N) and transfected with either CMV:PRL-3, as

described in section 3.1.2. Cells were fixed and permeabilized according to the protocol outlined in section 3.7.1. To act as primary antibodies, nanobody 19 was diluted to 1 mg/ml in blocking solution and further diluted 1:100 in blocking solution. For commercial antibodies R&D Systems, MAB3219 was diluted to 1:500, and Santa Cruz Biotechnology, sc-130355 was diluted to 1:500, each in blocking solution. Primary antibodies were incubated with the fixed cells for 1 hour at room temperature, followed by five 100  $\mu$ l PBS washes. The secondary antibody used to detect nanobody staining was the anti-alpaca IgG VHH (3.7.1) conjugated to Alexa Fluor-594 diluted 1:400 in blocking solution. The secondary antibody to detect the commercial primaries was a goat anti-mouse IgG conjugated to Alexa Fluor-647 (ThermoFisher, A21235). All samples were counterstained with Hoechst, 1:1000 dilution (ThermoFisher, H3570). Images were acquired at the University of Kentucky Light Microscopy Core using a Nikon A1R confocal microscope using a 40X water objective. To detect Hoescht counterstain, images were acquired using the DAPI (405nm) laser at gain 150, power 6.00. To detect nanobody staining, images were acquired using the TRITC (561 nm) laser at gain 60, power 2.00. To detect MAB3219 and sc-130355 staining, images were acquired using the Far red (640 nm) laser at gain 60, power 2.00. Images were processed in Adobe Photoshop 2022 to both increase image brightness and overlay the 405 (Hoescht), 488 (GFP-PRL-3), and 561 (Nanobodies) channels. Channels were pseudocolored by RGB channels.

### *3.7.3. Cellular localization of tagged PRL-3 compared to wildtype PRL-3.*

HCT116 colorectal cancer cells were plated at 5,000 cells per well in 96-well black glass-bottomed plates (Cellvis, P96-1.5H-N) and transfected with either pcDNA3.1-PRL-3, CMV:GFP-PRL-3, plenti-HA-PRL-3, or pLV-3XFLAG-PRL-3 (Addgene 123223) as previously described in section 3.1.2. Equal expression of all constructs was measured via western blot, shown in Figure 3.8. Cells were fixed, permeabilized, and stained according to the protocol outlined in section 3.7.1. Images were again acquired on a Nikon A1R confocal microscope using a 40X water objective. To detect Hoescht counterstain, images were acquired using the DAPI (405nm) laser at gain 150, power 6.00. To detect GFP-PRL-3, images were acquired using the FITC (488 nm) laser at gain 30, power 2.00. To detect

nanobody staining of tagged PRL-3, images were acquired using the TRITC (561nm) laser at gain 60, power 2.00.

Image J was used to quantify the average grey area of the TRITC channel for the tagged-PRL-3 in three cellular compartments (membrane, cytoplasm, and nucleus). Briefly, Nikon files (.nd2) were converted to .tif files, and images from Channel 3 (561 nm) were opened in Adobe Photoshop 2022, where brightness and contrast were adjusted to match the three different tags. Adobe Photoshop 2022 images were saved as .tif files and opened in ImageJ. The Straight tool, or the line tool, was selected from the toolbar to draw and measure a line across a single cell. Five 120-pixel rectangles were drawn on a single cell and placed on the two points on the line that showed the plasma membrane, two sides of the cytoplasm, and one to denote the nucleus. The average grey value for each rectangle was measured, and the plasma membrane and cytoplasm results were averaged for each cell. Ten cells were measured for each condition (3XFLAG, GFP, or W.T.). The Analyze menu was selected from the toolbar, and then Plot Profile was selected. Average grey value quantifications were exported to Microsoft Excel as .xls files and graphed using GraphPad Prism 9. Statistical analysis was done using a two-way ANOVA with multiple comparisons to examine the localization of three different types of PRL-3 to three separate cellular compartments.

### 3.8. Biolayer Interferometry (BLItz) analysis to determine the binding affinity of nanobodies for PRL-3.

Anti-Penta-HIS (HIS1K) Biosensors (ForteBio, 18-5120) were hydrated for 10 minutes in 1X kinetics buffer (ForteBio, 18-1105, Lot. 20070082) in a 96-well black bottom plate. Following hydration, the biosensor was secured to the biosensor mount. The Advanced Kinetics Assay protocol on BLItzPro1.3 software was used, with five steps in the following order: (1) Initial Baseline 30 seconds, 250  $\mu$ l 1X kinetics buffer (ForteBio, 18-1105) in a 500  $\mu$ l black microcentrifuge tube; (2) Loading 30 seconds, 4  $\mu$ l of ligand (626.57 nM nanobody) in the drop holder; (3) Baseline 30 seconds, 250 $\mu$ l 1X kinetics buffer in a 500  $\mu$ l black microcentrifuge tube; (4) Association 5 minutes, 4  $\mu$ l analyte (PRL-3) in the drop holder; Dissociation 2 minutes, 250  $\mu$ l 1X kinetics buffer in a 500  $\mu$ l black



microcentrifuge tube. An exchange between the tube holder and drop holder was manually performed between each step. A new biosensor was hydrated and used for each concentration of PRL-3 and each nanobody. Global K.D. for each nanobody was analyzed with BLItzPro 1.3 software using baseline correction for the association and dissociation steps.

### 3.9. Phosphatase assay.

2.5  $\mu\text{M}$  recombinant PRL-1, -2, or -3 (6.25  $\mu\text{l}$ ) was mixed with 2.5  $\mu\text{M}$  of each nanobody (6.25  $\mu\text{l}$ ) in black 384-well plates (Thermo Scientific, 164564) and incubated at room temperature for 1 hour in Reaction Buffer (20 mM Tris, 150 mM NaCl). Following incubation, the recombinant protein mixtures were combined with 12.5  $\mu\text{l}$  of 12.5  $\mu\text{M}$  6,8-Difluoro-4-Methylumbelliferyl Phosphate (DiFMUP) (Life Technologies, E12020) or 12.5  $\mu\text{l}$  of reaction buffer, added to 384-well plates, and incubated for 20 minutes in the dark at room temperature. Reactions without DiFMUP substrate act as the negative control for background fluorescence, and PRL-3 alone wells act as the baseline and positive control. Fluorescence intensities were measured on a Biotek Synergy Multi-mode Plate Reader at 360 nm/460 nm excitation and emission wavelengths, respectively. Assays were completed with six technical replicates and repeated in two biological replicates. Raw values for non-substrate-containing controls were averaged and subtracted from values of wells incubated with the substrate to remove background fluorescence and then normalized to fluorescence of PRL-3 alone. Normalized values were transferred to Prism 7 software in a Grouped format, where one-way ANOVA with Dunnett's multiple comparisons test was performed with ns = not significant, \*\* $p < 0.01$ , \*\*\* $p < 0.001$  \*\*\*\* $p < 0.0001$ .

### 3.10. Hydrogen deuterium exchange mass spectrometry (HDX-MS).

The coverage map for PRL-3, shown in Figure 3.9, was performed by the Deredge Lab at the University of Maryland School of Pharmacy. The result in Figure 3.9 was obtained from undeuterated controls as follows: 3  $\mu\text{L}$  of 20  $\mu\text{M}$  apo-PRL-3 in 20 mM HEPES pH 7.5, 100 mM NaCl was added to 9  $\mu\text{L}$  of buffer (20 mM HEPES, pH 7.5, 100

mM NaCl). The reaction was quenched with 14  $\mu$ L of ice-cold quench (100 mM glycine, pH 2.5, 7 M Guanidine HCl, 10 mM TCEP) and then diluted with 54  $\mu$ L of ice-cold dilution buffer (100 mM Glycine, pH 2.5, 10 mM TCEP). Next, 40  $\mu$ L of this solution was injected into a Waters HDX nanoAcquity UPLC (Waters, Milford, MA) with in-line protease XIII/pepsin digestion (NovaBioAssays). Peptic fragments were trapped on an Acquity UPLC BEH C18 peptide trap and separated on an Acquity UPLC BEH C18 column. A 7 min, 5–35% acetonitrile (0.1% formic acid) gradient was used to elute peptides directly into a Waters Synapt G2-Si mass spectrometer (Waters, Milford, MA). MSE data were acquired with a 20–30 V ramp trap C.E. for high energy acquisition of product ions and continuous lock mass (Leu-Enk) for mass accuracy correction. Peptides were identified using Waters's ProteinLynx Global Server 3.0.3 (PLGS). Further filtering of 0.3 fragments per residue was applied in DynamX 3.0.

For each complex and the apo-PRL-3, the H.D. exchange reactions and controls were acquired using a LEAP autosampler controlled by Chronos software. The reactions were performed as follows: 1.5  $\mu$ L of 40  $\mu$ M PRL-3 in buffer with 1.5  $\mu$ L 100  $\mu$ M of the given nanobody in buffer (or 1.5  $\mu$ L of buffer for the apo PRL-3 experiments) was labeled with 9  $\mu$ L of 20 mM HEPES, pD 7.5  $^2$ H<sub>2</sub>O based buffer with 100 mM NaCl, and quenched with 14  $\mu$ L of ice-cold quench (100 mM Glycine, pH 2.5, 7 M Guanidine HCl, 10 mM TCEP) then diluted with 54  $\mu$ L ice-cold dilution buffer (100 mM Glycine, pH 2.5, 10 mM TCEP). 40  $\mu$ L of this solution was used for analysis. All deuteration time points were acquired in triplicates. Back exchange correction was performed against fully deuterated controls. Fully deuterated controls were done by incubating 2  $\mu$ L of 40  $\mu$ M PRL-3 in 8  $\mu$ L of unfolding buffer (100 mM Glycine pH 2.5, 7 M Guanidine HCl, 10 mM TCEP) for two hours. Then 3  $\mu$ L of the unfolded solution was deuterated for 2 hours in 9  $\mu$ L of a deuterium-based buffer. This reaction was quenched with 14  $\mu$ L of ice-cold quench (100 mM Glycine, pH 2.5, 10 mM TCEP) and then diluted with 54  $\mu$ L ice-cold dilution buffer (100 mM Glycine, pH 2.5, 10 mM TCEP). 40  $\mu$ L of this solution was used for analysis. The deuterium uptake for all identified peptides with increasing deuteration time and for the fully deuterated control was determined using Water's DynamX 3.0 software. The normalized percentage of deuterium uptake (%D<sub>t</sub>) at an incubation time t for a given peptide is calculated as such:

$$\%D_t = \left( \frac{m_t - m_0}{m_f - m_0} \right) * 100\%$$

With  $m_t$  the centroid mass at incubation time  $t$ ,  $m_0$  the centroid mass of the undeuterated control, and  $m_f$  the centroid mass of the fully deuterated control. The percentage deuterium difference was calculated as  $\Delta\%D_t(\text{PRL-3} - \text{PRL-3 NB Complex})$ .  $\Delta\%D_t$  for each complex at each time point was mapped onto the PRL-3 structure. Kinetic uptake plots and corresponding heatmaps were generated using an in-house python script.

### 3.11. Co-immunoprecipitation of CBS-HA and nanobodies with 3XFLAG-PRL-3.

For each pulldown, 50  $\mu\text{l}$  of Anti-FLAG M2 magnetic beads (Sigma, M8823-5ML, Lot. SLCF4223) were prepared by washing in 500  $\mu\text{l}$  of Wash Buffer (300 mM NaCl, 20 mM Tris pH 7.5) twice. Initial complexing to beads occurred for 1 hour at 4°C, with secondary complexing occurring for a second hour at 4°C; complexing steps are outlined in Figure 5.6. CBS-HA, and Nanobody 26 were added in 1:1.1 molar ratios to 3XFLAG-PRL-3 complexed beads. Following the second complexing step, the supernatant was removed, and beads were washed four times with 900  $\mu\text{l}$  of Wash Buffer. Next, beads were eluted with 50  $\mu\text{l}$  2x Laemmli Sample Buffer with 2-Mercaptoethanol. The eluates were boiled at 95°C for 10 minutes to denature immunoprecipitated proteins, and the supernatant was collected for western blot analysis. The density of 3XFLAG-PRL-3, CBS-HA, and NB26-His pulldown in experimental lanes was determined by ImageLab band detection software. The amount of NB26-His and CBS-HA pulled down in each assay was normalized to the amount of 3XFLAG-PRL-3 immunoprecipitation in the respective lane.

### 3.12. Western blot analysis.

For western blots, 30  $\mu\text{g}$  of total protein for input or 45  $\mu\text{l}$  of pulldown supernatant was loaded into 4–20% Mini-PROTEAN® TGX Stain-Free™ Protein Gels. Total protein was assessed through stain-free imaging on a Biorad ChemiTouch Imaging System, which allows total protein loaded into the well to be used as the loading control. Protein was transferred onto the PVDF membrane (Biorad, 162-0255) using the Trans-Blot Turbo

Transfer System (Biorad 1704150). Membranes were blocked with 5% milk in 0.1% TBST for 1 hour and probed with one of the following antibodies at the designated dilution overnight at 4°C. 1:3000 Monoclonal ANTI-FLAG® M2 antibody (Sigma, F1804, Lot. SLBK1346V) (Sections 3.6.1 and 3.11), 1:1000 anti-His HRP antibody (GenScript, A00612, Lot. 19K001984) (Section 3.11), 1:1000 anti-HA-Tag (C29F4) Rabbit mAb (Cell Signaling, 37245, Lot. 8) (Section 3.4.3, 3.7.2, and 3.11), or 1:1000 anti-Human/Mouse/Rat PRL-3 Antibody (R&D Systems, MAB3219, Lot. WXH0419091) (Section 3.7.1). Following three 5-minute washes with 0.1% TBST, secondary HRP-conjugated 1:2500 anti-mouse IgG antibody (Cell Signaling, 7076S, Lot. 33) or 1:5000 anti-Rabbit IgG HRP Linked F(ab')<sub>2</sub> (Sigma, NA9340V, Lot. 17065618) was added for 1 hour. Membranes were again washed three times for 5 minutes with 0.1% TBST. Blots were imaged using Clarity Western ECL Substrate (Biorad, 1705061), a Biorad ChemiTouch Imaging System, using a Chemiluminescence filter.

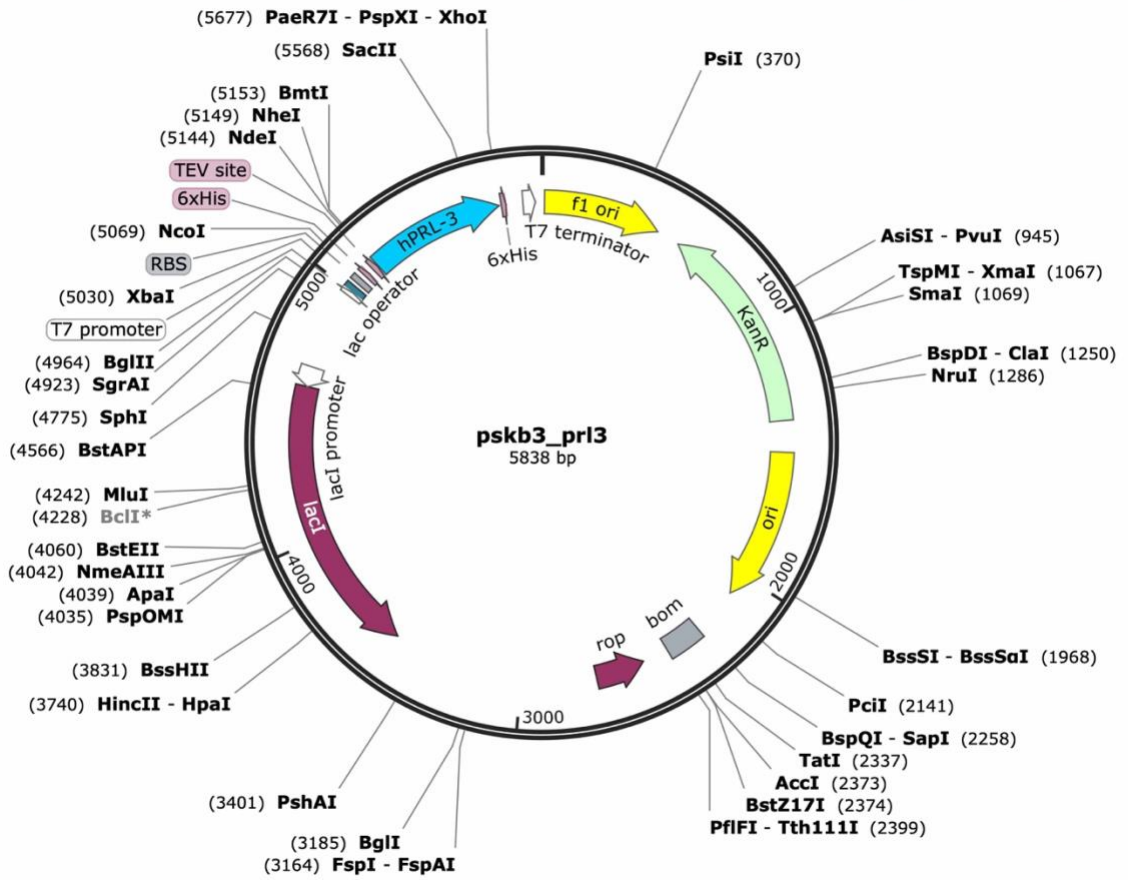


Figure 3.1. Plasmid map of pskb3-PRL-3.

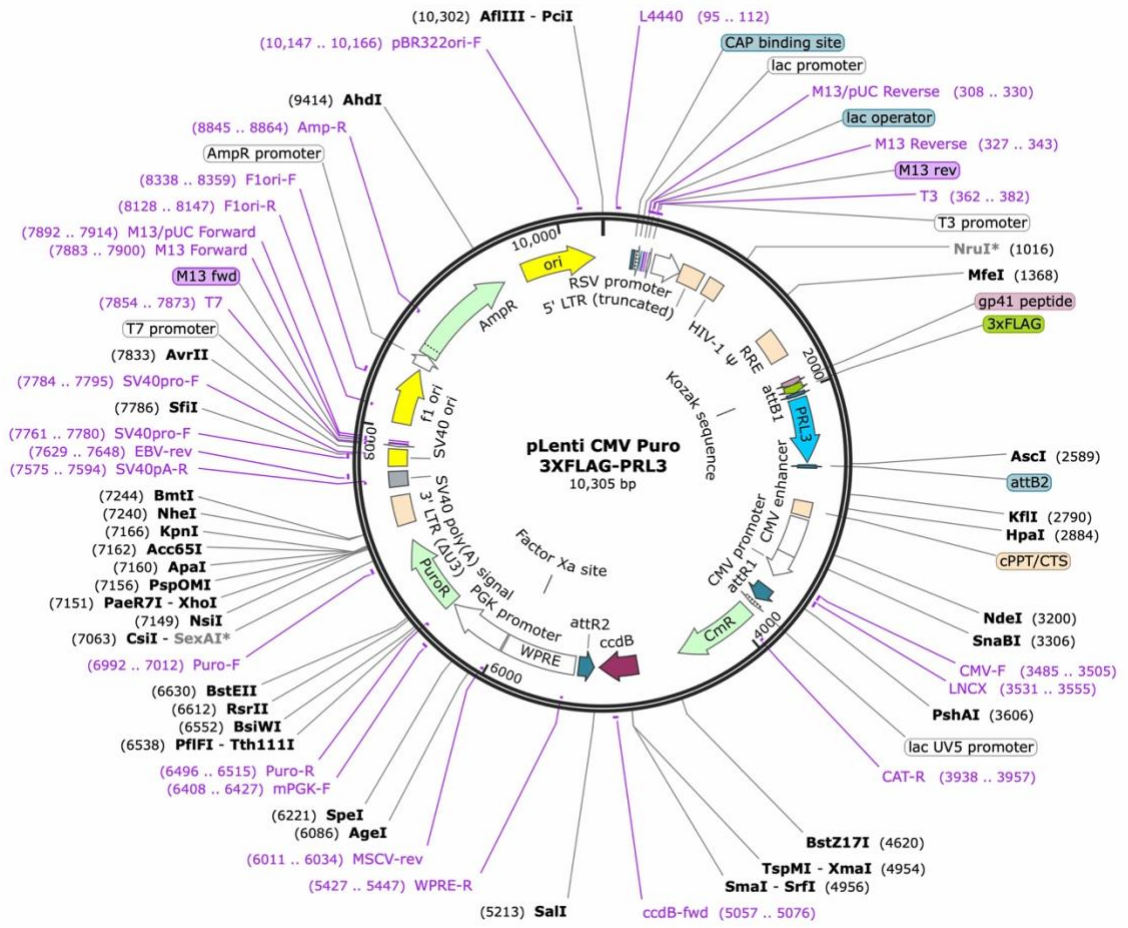


Figure 3.2. Plasmid map of plenti-CMV-puro-3XFLAG-PRL-3.

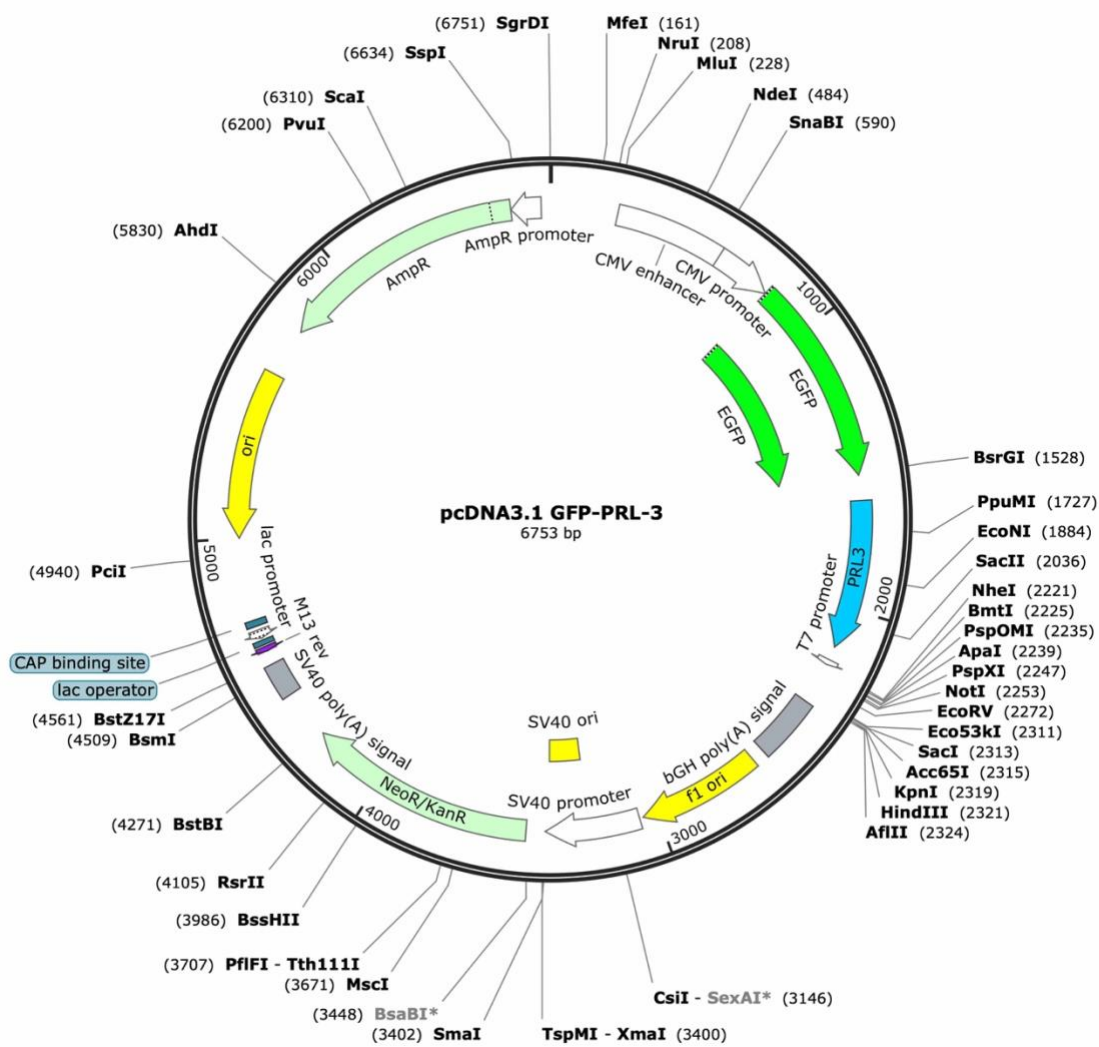
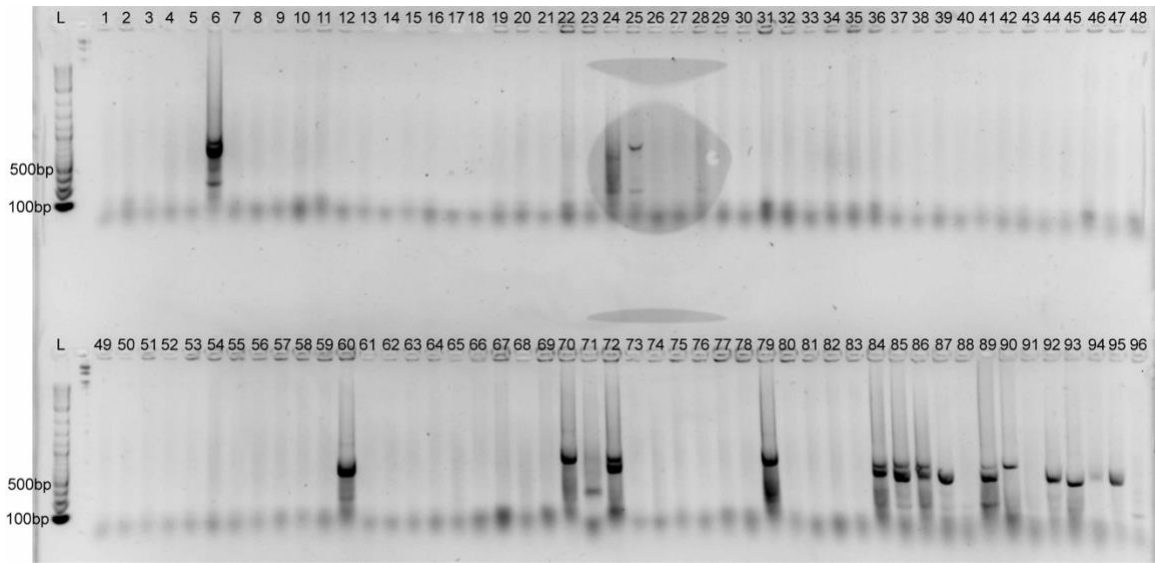
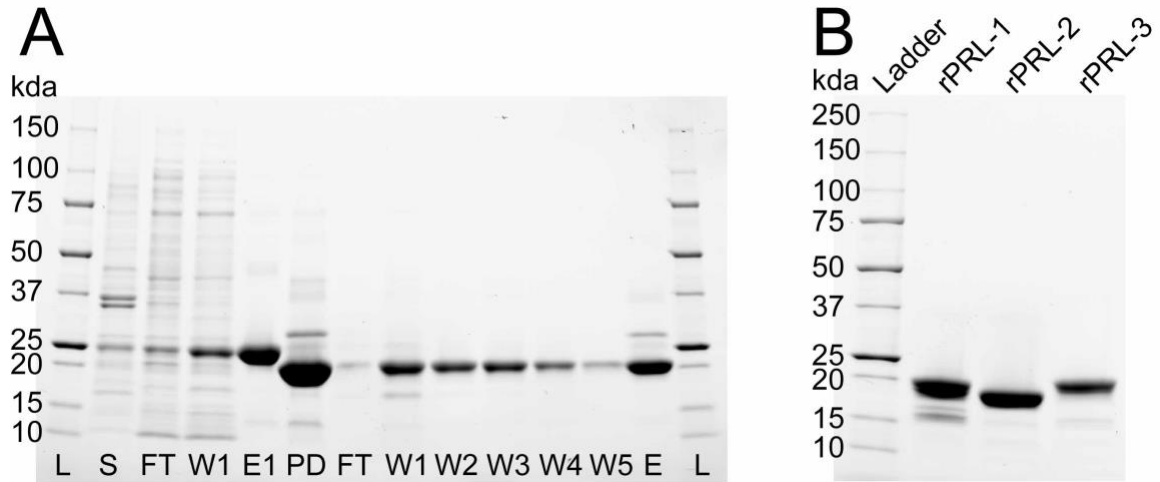


Figure 3.3. Plasmid map of pcDNA3.1 GFP-PRL-3.



**Figure 3.4. Colony PCR yields VHH-positive clones.** Glycerol stocks of 96 clones resulting from two rounds of bacteriophage display were thawed, and 2ul of cells were used for colony PCR utilizing the Q5 polymerase protocol (New England Biolabs M0491). PCR products were run on a 3% agarose gel for 1 hour at 120V. VHH-positive clones are represented by a PCR product of ~400 bp. L marks the 100 base pair DNA ladder, with 100 and 500 base pair markers denoted.





**Figure 3.5. Purification of PRL family of proteins from BL21 DE3 E.coli.** (A) Step 1 of PRL-3 purification using Ni-NTA Resin, including 6X-His-tag cleavage. Abbreviations denote the following: L – ladder, S – soluble protein fraction, F.T. – Flowthrough, W# - wash number, E# - elution, P.D. – post dialysis fraction. >1  $\mu$ g of protein sample loaded per lane. FT2, W1-W5 were concentrated together for size exclusion chromatography. (B) Final PRL purification product following Ni-NTA, size exclusion chromatography, and protein concentration. 10  $\mu$ g of protein was loaded per lane. All images were taken with the Stain Free Gel application on a Biorad ChemiTouch Imaging System.

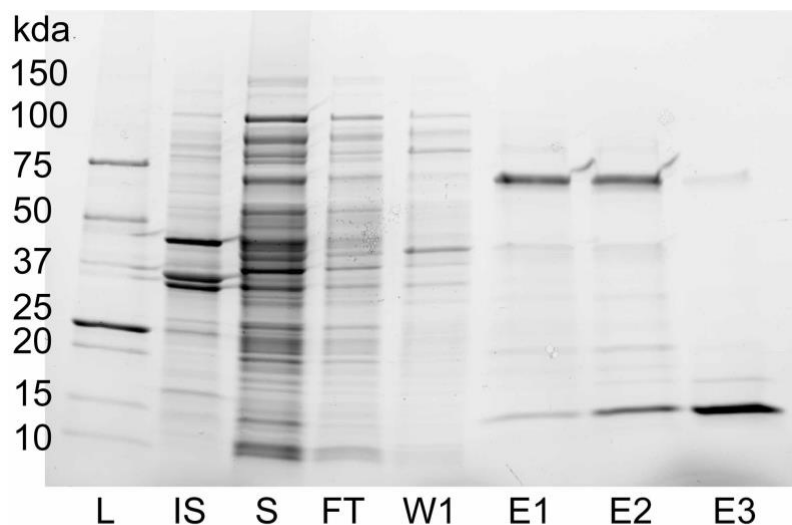


**Figure 3.6. Ni-NTA purification of Nanobody 91 from BL21 DE3 E.coli.** (A) Step 1 of Nanobody 91 purification using Ni-NTA Resin, 6X-His-tag was not cleaved. Abbreviations denote the following: L – ladder, I.S. – insoluble protein fraction, S – soluble protein fraction, F.T. – Flowthrough, W1 - wash, E1 and E2 – 30 mM imidazole elution, E3 – 250 mM imidazole elution. >1  $\mu\text{g}$  of protein sample loaded per lane. All images were taken with the Stain Free Gel application on a Biorad ChemiTouch Imaging System. All other nanobodies were purified using this protocol.

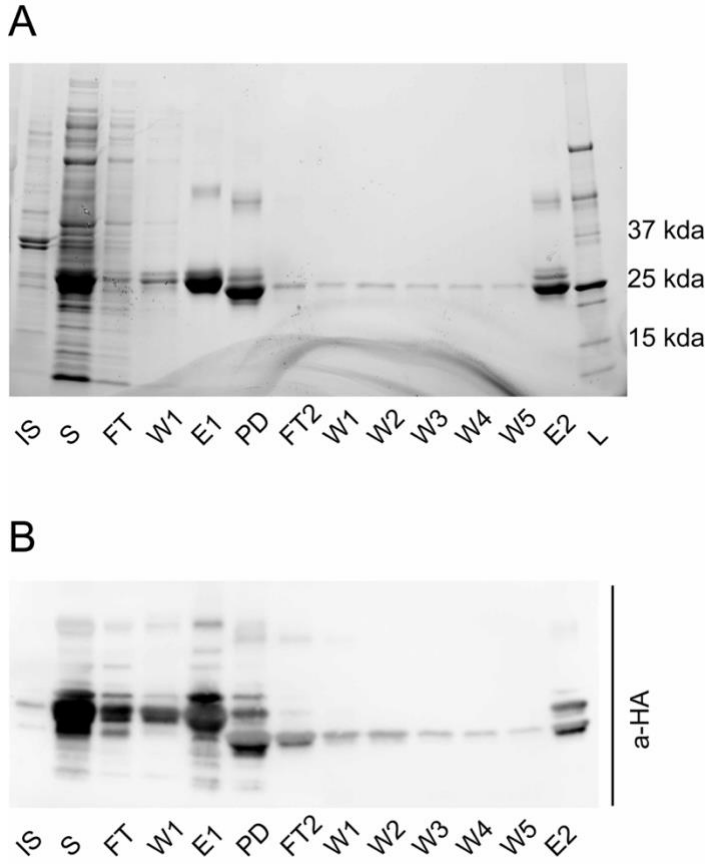


**Figure 3.7. Protein purification of 3XFLAG-PRL-3 and CBS-HA.** (A) Immobilized metal affinity chromatography purification of 3XFLAG-PRL-3, with an expected size of 25 kDa. FT2, W1-W5 were concentrated together for final protein amounts. (B) Immobilized metal affinity chromatography purification of CBS-HA was validated with an anti-HA western blot. FT2, W1-W5 were concentrated together for final protein amounts. Abbreviations denote the following: L – ladder, I.S. – insoluble protein fraction, S – soluble protein fraction, F.T. – Flowthrough, W# - wash, E1 – elution, P.D. – post dialysis. >1 ug of protein sample loaded per lane.

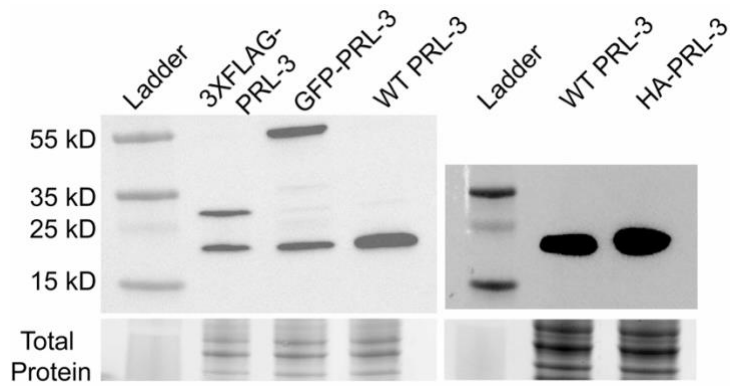


**Figure 3.8. Tagged versions of PRL-3 were equally expressed across immunofluorescence experiments.** PRL-3 western blots indicate a similar expression of exogenous proteins using the R&D Systems MAB3219 anti-PRL-3 antibody. 3XFLAG-PRL-3 can be seen at ~27 kD, and GFP-PRL-3 is shown at ~55 kD. HA-PRL-3, CMV-PRL-3, and endogenous PRL-3 are represented at 22 kD.



**Figure 3.9. Sequence coverage map of apo-PRL-3 in HDX-MS.** After mass spectrometry, all deuterated peptides were mapped back to the PRL-3 amino acid sequence. Each blue bar represents a detected peptide. The high coverage and redundancy of PRL-3 peptides indicated that epitope mapping experiments would yield high-quality data. 1  $\mu$ l of 40  $\mu$ M PRL-3 was used for deuterium exchange; the reaction was quenched with 200  $\mu$ l 1XQ (0.5 mM Guanidine HCl); 100  $\mu$ l was injected for mass spectrometry analysis. 87 peptides were detected with a redundancy score of 7.70. 89.6% of PRL-3 was mapped with these peptides.

## **Chapter 4. Alpaca-derived anti-PRL-3 nanobodies show specificity for their antigen and can be utilized to study PRL-3 biology in cancer**

### 4.1. Introduction.

With the challenges presented by anti-PRL antibodies currently on the market, nanobodies became a logical step when developing a tool specific for studying PRL-3. Following the production of anti-PRL-3 nanobodies in alpacas, bacteriophage display against PRL-3, and purification using an *E.coli* system, we needed to determine if these nanobodies could even bind to PRL-3. Furthermore, it was necessary to assess if this specificity is retained within a cell. Therefore, we utilized multiple approaches to assess the specificity of PRL-3 nanobodies using recombinant protein as well as PRL-3 expressed in cancer cell models.

### 4.2. Results.

#### *4.2.1. Nanobody variability resides in Complimentary Determining Region 3.*

To produce alpaca-derived anti-PRL-3 nanobodies, human recombinant PRL-3 protein was purified from the BL21 Star DE3 *E.coli* strain (3.4.1). The recombinant PRL-3 was injected into alpacas once per week, and B-lymphocytes expressing potential anti-PRL-3 nanobodies were harvested six weeks later. All possible anti-PRL-3 nanobody sequences were cloned into a pMES4 phage display vector to develop a cDNA library, as diagramed in Figure 4.1A. To pull out PRL-3-specific nanobodies, we performed two rounds of bacteriophage display panning of the library against recombinant PRL-3. The resulting pool of nanobody-expressing colonies was screened by colony PCR with nanobody or VHH-specific primers. Of 96 clones screened by colony PCR, 32 showed a 400 bp band designating a potential anti-PRL-3 nanobody (Fig 3.1). Those 32 clones were sent for sequencing with a nanobody-specific primer and analyzed for a complete N-terminal PelB sequence for packaging the protein in the bacterial periplasm for protein purification, a C-terminal 6XHis-tag for immobilized metal affinity chromatography

purification, and a stop codon. Of the 32 clones identified in colony PCR, only 16 nanobodies contained all three parameters (Fig 4.1B).

Sequence alignment demonstrated that nanobodies 91, 90, and 13 were 100% identical in their amino acid sequence. The fact that the alpacas continued to make this specific nanobody, which we will refer to as nanobody 91, illustrates that it may contain an evolutionary advantage in its structure or binding capacity to PRL-3. With the nanobody 91 sequence recurring most frequently, we utilized nanobody 91 as our standard anti-PRL-3 nanobody in all studies. The complementary determining regions of this nanobody were predicted using ABodyBuilder, an automated antibody modeling pipeline (148). Nanobody sequences were clustered based on the number of amino acid alterations or insertions compared to nanobody 91. These include four groups containing 0, 1-4, 10-20, and 25+ amino acid changes compared to nanobody 91 (Fig 4.1B).

Multiple unique aspects encompass these nanobodies. Throughout the development of nanobodies as research tools, it has been shown that binding specificity and diversity are primarily carried in the third complementary determining region (CDR3) (149) due to its unique development in B-lymphocytes. The amino acid differences that occur in the 1-4 group predominantly occur in CDR1 and CDR2, and there are no changes to CDR3 among these nine nanobodies compared to nanobody 91 (Fig 4.1B). Most of these amino acid changes occur within the same amino acid family or are very similar structurally. For example, nanobody 10 has an aspartic acid to asparagine change, which differ in its R group by the presence of a polar -OH. There are two phenylalanine to tyrosine changes, one in nanobody 4 and another in nanobody 29, which also differ by the presence of a polar -OH on their benzene ring. With nanobody 10, there is an isoleucine to leucine change, which varies faintly in their R-group structure. Overall, these small amino acid changes are unlikely to impact the structure, binding capacity, or specificity of the anti-PRL-3 nanobodies.

However, the 16-24 group and the 25+ group have various changes in all of the CDR regions along with the framework regions (Fig 4.1B). In the 16-24 group, the amino acid changes in nanobodies 19 and 84 are highly conserved, mainly occurring in all three CDR regions, with the largest number of alterations occurring in CDR3. In the 25+ amino acid change group, amino acid variability in CDR3 comes into play. Nanobodies 23 and

26 broadly differ from all other nanobodies in all three CDR regions, mainly in the framework regions. Nanobodies 28 and 68 are primarily conserved in CDR1 and CDR2, yet the CDR3 of these two nanobodies is entirely different. Examining the CDR regions of all 16 nanobodies allows us to hypothesize which nanobodies will have similar binding capacity and specificity to PRL-3. Throughout this work, we will compare findings to nanobody 91 as the standard and determine if those nanobodies with highly variable CDR3s differ from nanobody 91 in any structural or functional capacities.

#### *4.2.2. Nanobodies show specificity for PRL-3 over other family members in indirect ELISA analysis.*

Following the sequencing of potential nanobody sequences, the 16 nanobodies with proper sequence characteristics were purified using an *E. coli* system outlined in 3.4.2. Interestingly, the first purification step showed that three nanobodies were not highly expressed following induction with IPTG and resulted in a low protein yield; these were nanobodies 7, 68, and 92. Therefore, these nanobodies were utilized for specificity studies but were noted for producing a low protein yield.

The PRL-1 and PRL-2 proteins have 79% and 76% amino acid sequence homology to PRL-3, making identifying specific small molecules challenging. To determine if these 16 purified anti-PRL-3 nanobodies showed specificity for PRL-3 over PRL-1 and PRL-2, we constructed an indirect ELISA method with the help of Dr. Jaqueline Rivas and Dr. Martin Chow (Fig 4.2A). PRL-1/-2/ and -3 were purified from *E. coli* following a similar protocol to that of the nanobodies outlined in Section 3.4.1. I screened all 16 nanobodies against the PRL family by detecting nanobody binding by the presence of their 6X-His-tag.

We found 11 of the 16 nanobodies had a significantly greater affinity for PRL-3 over PRL-1 and PRL-2 (Fig 4.2B). Nanobodies 7, 68, and 92 were among the five with low specificity, most likely due to their inability to be purified in the *E. coli* system. However, this also included nanobodies 23 and 28, which make up the nanobodies with 25 or more amino acid changes when compared to nanobody 91. Yet, nanobody 26 and all others showed highly significant specificity for PRL-3 over other PRL family members.



This initial endpoint assay was completed in mild saturating conditions with a 1:1.25 ratio of PRL:nanobody. Therefore, it was necessary to determine if the nanobodies bind nonspecifically to other PRL family members in highly saturated conditions.

The same ELISA protocol was carried out with a range of nanobody concentrations, with a PRL:nanobody ratio ranging from 1:0.12 to 1:2.5, allowing us to observe both the lower and upper range of binding of these nanobodies to all PRL family members. Even under these saturating conditions, most anti-PRL-3 nanobodies lacked any binding to PRL-1 or PRL-2 protein (Fig 4.2C). Again, we observed that nanobodies 23 and 28 had a lower binding capacity for PRL-3 at all concentrations when compared to the other 12 nanobodies. Therefore, nanobodies 7, 68, 92, 23, and 28 were no longer pursued as potential research tools for studying PRL-3. As expected, nanobodies with similar amino acid sequences had comparable binding to PRL-3. For example, nanobodies 91, 90, and 13 show similar specificity for PRL-3 in both the endpoint and saturating experiments. To streamline this study, the remaining dissertation experiments focus on four nanobodies (19, 26, 84, and 91). Nanobody 91 represents our standard, nanobodies 19 and 84 illustrate a large amount of variability in CDR3, and nanobody 26 represents variability throughout all CDR regions and framework regions. These demonstrate strong specificity and affinity for PRL-3 as defined by this indirect ELISA approach.

#### *4.2.3. Nanobodies maintain specificity for PRL-3 over other family members in cell-based assays.*

Thus far, nanobody specificity for PRL-3 has only been demonstrated in *in vitro* assays against recombinant PRL-3 purified from *E. coli*. It is known that post-translational protein modifications occur in a relatively low number of bacterial proteins compared to eukaryotic proteins (150), and the number of modifying enzymes differs significantly among bacterial species compared to eukaryotes. Therefore, we needed to test if our nanobodies still bind to PRL-3 in human cancer cells and if they retain their specificity for PRL-3. We examined this both in immunofluorescence assays as well as in immunoprecipitation.

One antibody on the market is specific to PRL-3 only in western blot (R&D MAB3219). There are no commercially available antibodies specific to PRL-1 or PRL-2, only MAB32191 (R&D Biosystems) that simultaneously detects PRL-1 and PRL-2, but not PRL-3. We tested the ability of the anti-PRL-3 nanobodies to immunoprecipitate PRL-3 protein from HEK293T cells stably expressing FLAG-tagged PRL-1, PRL-2, or PRL-3. With this method, we could exploit the 3XFLAG tag to detect the pulldown of each PRL without worrying about non-specific or cross-reactive antibodies. Nanobodies 19, 26, 84, and 91 were covalently coupled to Dynabeads, as outlined in 3.6.1. 3XFLAG-PRL expressing HEK293T cells were lysed, and immunoprecipitation was set up with each nanobody coupled to beads, outlined in 3.6.1. and all four nanobodies selectively pulled-down 3X-FLAG-tagged PRL-3 over PRL-1 and PRL-2 (Fig 4.3A). Nanobodies 19 and 84 immunoprecipitated small amounts of 3XFLAG-PRL-1 and PRL-2, but these were not comparable to PRL-3 pulled down. Confirmation of nanobody coupling to beads was detected by the presence of their 6X-His-tag (Fig 4.3B). Beads-only controls did not immunoprecipitate 3XFLAG-PRL-3 (Fig 4.3C), indicating that all FLAG-PRL-3 pulldown was due to the presence of each nanobody. These data demonstrate that these nanobodies can immunoprecipitate PRL-3 independent of post-translational modifications that may occur in HCT116 cells compared to *E. coli*.

We also examined the ability of our nanobodies to retain PRL-3 specificity in immunofluorescence experiments for two reasons. First, this acts as an avenue to confirm the immunoprecipitation specificity of these nanobodies. Secondly, there is a great deal of speculation as to where PRL-3 is localized in cells normally and in cancer conditions, as shown in Chapter 1. If these nanobodies can specifically detect PRL-3 localization in cells, they offer great potential for better defining PRL-3 cellular localization and how that may contribute to cancer phenotypes when PRL-3 is upregulated.

The human colon cancer cell line HCT116 was used, as it is efficiently transfected, has a large cell body to visualize localization, and expresses endogenous PRL-3. Cells were transfected with CMV:GFP-PRL-1, -2, or -3 constructs to visualize the PRLs, as no commercially available antibodies distinguish PRL-1 and PRL-2 in immunofluorescence. Transfection, fixation, permeabilization, immunofluorescence, and imaging protocols are outlined in 3.6.1. Our goal was to determine the extent to which the anti-PRL-3 nanobodies

co-localize with each of the GFP-PRLs. Nanobody 91 co-localized with GFP-PRL-3, found mainly at the plasma membrane and rarely in the nucleus (Fig 4.4), which are previously described sites of PRL-3 localization (15, 93, 96). The anti-PRL-3 nanobody did not stain cells expressing GFP-PRL-1, GFP-PRL-2, or the GFP vector control. Similar results were seen when staining with nanobodies 19 (Fig 4.5), 26 (Fig 4.6), and 84 (Fig 4.7). The immunoprecipitation and immunofluorescence results demonstrate that these nanobodies are specific for PRL-3 and can detect PRL-3 in human cell lines.

#### *4.2.4. Comparison of anti-PRL-3 nanobodies to commercially available PRL antibodies.*

As indicated previously, some antibodies on the market are designed to have PRL or PRL-3 specificity. Yet, many of them have shown the ability to bind PRL-1 and PRL-2 or are only designated for use in western blot. As discussed in Chapter 2, nanobodies are useful in various experiments, including immunoprecipitation. Therefore, it was necessary to demonstrate that these alpaca-derived nanobodies perform equal to or better than those tools currently available on the market. To do so, we turned to nanobody 19, as previous results indicate that it maintains the same specificity for PRL-3 as nanobody 91 and immunoprecipitation materials were on hand. We examined nanobody 19's ability to immunoprecipitate HA-PRL-3 compared to four commercially available anti-PRL-3 antibodies. These included ab50276 (Abcam), GTX100600 (GeneTex), MAB3219 (R&D Systems), and sc-130355 (Santa Cruz Biotechnology). Each of these has been used in various publications to define PRL-3 localization and expression, described in Chapter 1 and Table 4.1.

For these experiments, we transfected cells with an HA-PRL-3 plasmid; using any of the PRL-3 antibodies in the pulldown for western blot would cause cross-reactivity with the IgG and IgH used in the IPs. HCT116 colorectal cancer cells were used as they are efficiently transfected. Following transfection, cells were lysed, and protein was harvested according to 3.6.2. Nanobody 19 was coupled to Dynabeads while commercial antibodies were coupled to Protein A and Protein G beads, as nanobodies only have a VHH region and could not bind to Protein A and G beads efficiently. As shown in Fig 4.8A, ab50276 and GTX100600 could not immunoprecipitate PRL-3 compared to beads. Nanobody 19

exhibited an equally efficient pulldown of HA-PRL-3 compared to MAB3219 and sc-130355 (Fig 4.8A). These data demonstrate that nanobody 19 can immunoprecipitate PRL-3 as efficiently as antibodies used to immunoprecipitate PRL-3 in the literature.

We repeated this in HCT116 immunofluorescence experiments, similar to those outlined in 4.2.3. First, we examined the ability of these antibodies to bind PRL-3 in immunofluorescence experiments by transfecting cells with GFP-PRL-3 and examined their ability to co-localize with the protein. ab20576 and GTX100600 displayed no fluorescence signal following IF (Fig 4.9), while MAB3219 and sc-130355 showed some co-localization with GFP-PRL-3 (Fig 4.9). Therefore, due to these results and the lack of binding shown in IP experiments (Fig 4.8A) we did not perform further IF experiments using either of these antibodies. Next, we tested the specificity of MAB3219 and sc-130355 as this research is lacking in the literature, described in Chapter 1. We transfected HCT116 cells with either GFP-PRL-1, PRL-2, or PRL-3 and examined staining with either MAB3219 (Fig 4.10A) or sc-130355 (Fig 4.10B). Staining with both antibodies showed specificity for PRL-3 over PRL-1 and PRL-2. Yet, the antibodies did not completely co-localize with the GFP-PRL-3, mainly exhibiting staining only at the membrane (Fig 4.10). Therefore, we examined the co-localization of nanobody 19 versus these nanobodies with PRL-3.

Cells were transfected with CMV-PRL-3 and followed the immunofluorescence protocol outlined in 3.6.1. However, the primary and secondary antibody steps were more complex. For the primary antibody, we added either MAB3219 (R&D Systems) or sc-130355 (Santa Cruz Biotechnology) along with nanobody 19. This allowed us to directly compare the ability of commercially available PRL-3 antibodies to our nanobody in detecting PRL-3 localization. This can be done as MAB3219 and sc-130355 were both raised in mice, whereas our nanobodies were raised in alpacas. Therefore, secondaries specific to each animal allow us to differentiate between the staining patterns of each primary. Nanobody 19 is shown in red while staining with the commercially available antibodies is shown in green. Fig 4.8B shows that staining with nanobodies is much more robust than either of the commercially available counterparts. Localization of MAB3219 is overall similar to that of nanobody 19. Yet, sc-130355 exhibited staining only at the cell membrane. Overall, neither commercially available antibodies showed cytoplasmic and

nuclear staining to the extent of nanobody 19 (Fig 4.8B). These data demonstrate that nanobody 19 can detect PRL-3 better and is more sensitive than commercially available antibodies used to study PRL-3 in the literature.

#### 4.2.5. *N-terminal tags alter PRL-3 localization.*

While exploring GFP-PRL-3 (Fig 4.4) along with wildtype PRL-3 (Fig 4.8B) localization in the cell, we observed that GFP-tagged PRL-3 localized mainly to the cell membrane, with occasional foci present at the nucleus (Fig 4.4). However, wildtype PRL-3 localized more heavily in the cytosol (Fig 4.8B). GFP is ~28 kD in size, doubling the size of the PRL-3 expressed in HCT116 cells. Researchers often assume that N- and C-terminal tags have little influence on the secondary and tertiary structures and localization of fused proteins. However, several reports have demonstrated that using GFP may impact the biological activity of fusion proteins, including cellular localization. Many past studies examining PRL-3 localization, which have primarily characterized PRL-3 as membrane exclusive due to a C-terminal prenylation motif, have utilized N-terminal tags such as Myc or EGFP. PRL-3 nanobodies finally allow us to detect wild-type, untagged PRL-3 in cells to determine if tagged versions of PRL-3 localize differently than untagged PRL-3.

We examined the localization of GFP-PRL-3, 3XFLAG-PRL-3, HA-PRL-3, and an untagged (WT) PRL-3 in HCT116, as outlined in section 3.6.2. These tags are 238, 22, and 9 amino acids in length, respectively. FLAG tags, often utilized in immunoprecipitation experiments, are made of primarily charged amino acids, while HA has an overall neutral charge. We expressed GFP-tagged, 3XFLAG-tagged, HA-tagged, and WT PRL-3 at equal levels in HCT116 cells (Fig 3.5). Probing with Nanobody 26 or 19 revealed that GFP and 3XFLAG tagged PRL-3 were strongly localized to the membrane, compared to the cytoplasm, with punctate staining at the nucleus (Fig 4.11A). In comparison, HA-tagged and WT PRL-3 are evenly distributed across the cytoplasm and cell membrane (Fig 4.11A). Localization was quantified based on the protocol outlined in 3.6.2 (Fig 4.11B). HA-tagged PRL-3 most likely localizes similarly to the wildtype tag as the tag is only 3 kDa and has a neutral charge, indicating that it would change PRL-3 structure and charge the least of the three tags. We recommend that all future studies utilizing human cell culture or *in vivo* models use these forms of PRL-3 rather than GFP

or 3XFLAG-tagged protein. The presence of these tags in much of the PRL-3 literature, mentioned in Chapter 1, may need to be clarified for their results.

**Table 4.1. PRL-3 antibodies in the literature.**

Antibody Name	Supplier/Catalog Number	Specificity	Applications	Cited works
Anti-PTP4A3/PRL-R antibody	Abcam / ab50276	PTP4A3/PRL-R	IHC, Western blot	(35, 37, 58-61)
PTP4A3 antibody [N1C3]	Genetex / GTX100600	PTP4A3	Western blot	(63)
Human/Mouse/Rat PRL-3 Antibody	R&D Systems / MAB3219	PTP4A3	Western blot	(64-68)
PRL-3 Antibody (318)	SantaCruz Biotechnology / sc-130355	PTP4A3	Western blot, IP, IF, IHC and ELISA	(69-80)

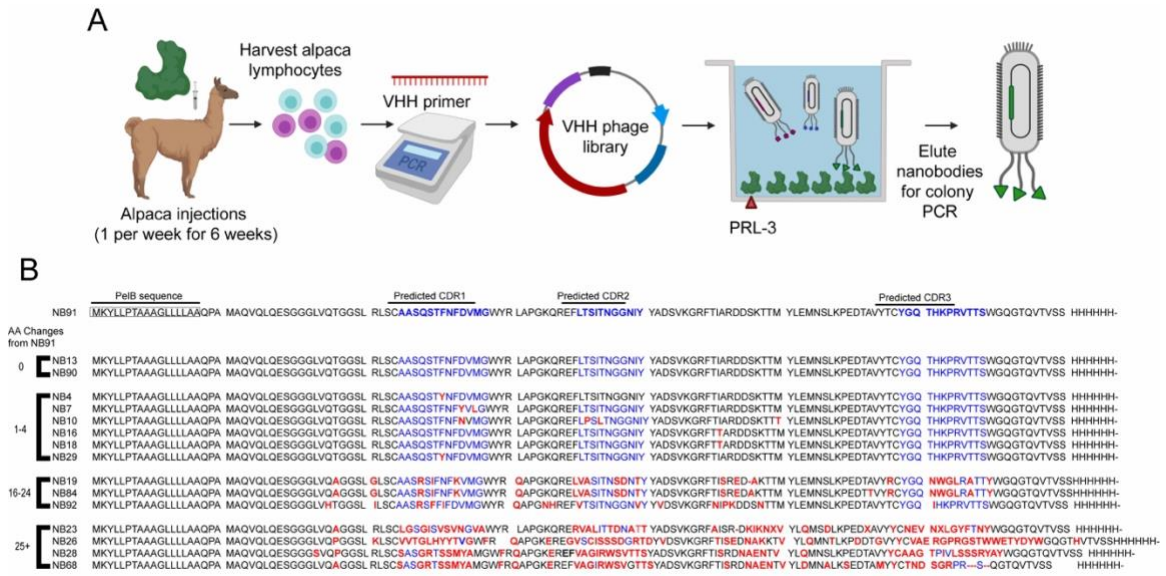


**Figure 4.1. Anti-PRL-3 nanobody sequences from bacteriophage display yielded 16 nanobodies with varying frequencies and complementary determining regions. (A)** Schematic of generating and isolating anti-PRL-3 nanobodies (Created with BioRender.com). **(B)** Amino acid sequence for 16 nanobodies (NB) used in this study. Nanobodies are grouped based on amino acid similarity to nanobody 91. Each group of nanobodies is either the same sequence as nanobody91, differs by 1-4, 10-25, or 25+ amino acids (red). Complimentary determining regions (CDs, blue) were predicted using ABodyBuilder.



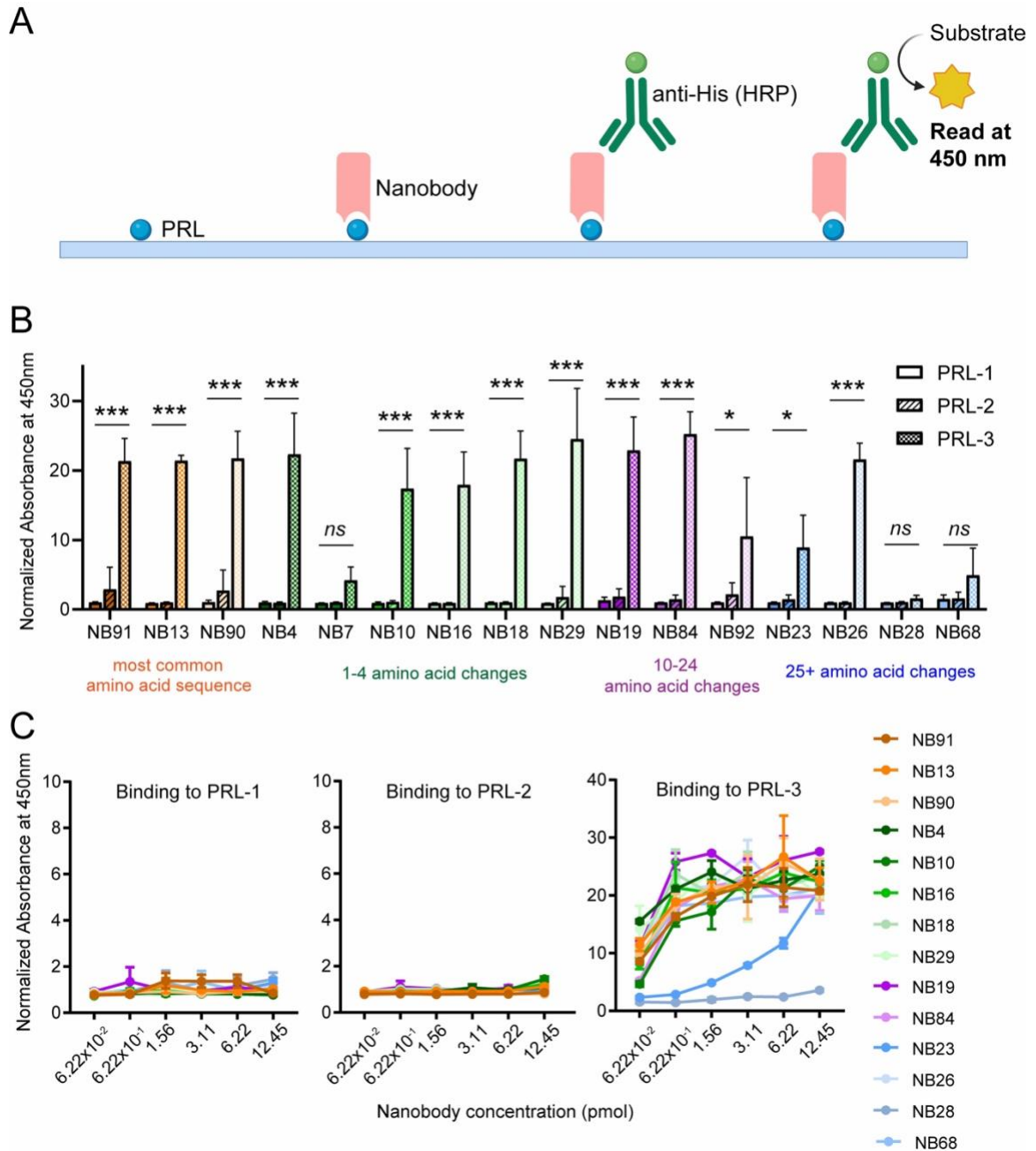


**Figure 4.2. Nanobodies are specific for PRL-3 over the other PRL family members.**

(A) Schematic indirect ELISA assay to test the specificity of nanobodies against PRL-1, -2, and -3 (Created with BioRender.com). (B) Binding of each histidine-tagged nanobody (NB, at a concentration of 6.22 pmol) to 5 pmol PRL-1, PRL-2, or PRL-3 in 96-well plates. (C) The binding of each nanobody at the concentrations indicated to 5 pmol of each PRL was measured by indirect ELISA. Data are the absorbance at 450 nm after NB/PRL wells

were washed and probed with His-HRP conjugated antibody. All assays were completed with two technical replicates and repeated in two biological replicates. Error bars represent standard deviation. ns = not significant, \* $p < 0.05$ , \*\*\* $p < 0.001$  by two-way ANOVA with Sidak's multiple comparisons tests. The number of amino acid changes compared to the most common anti-PRL-3 nanobody sequence is indicated by color coding.

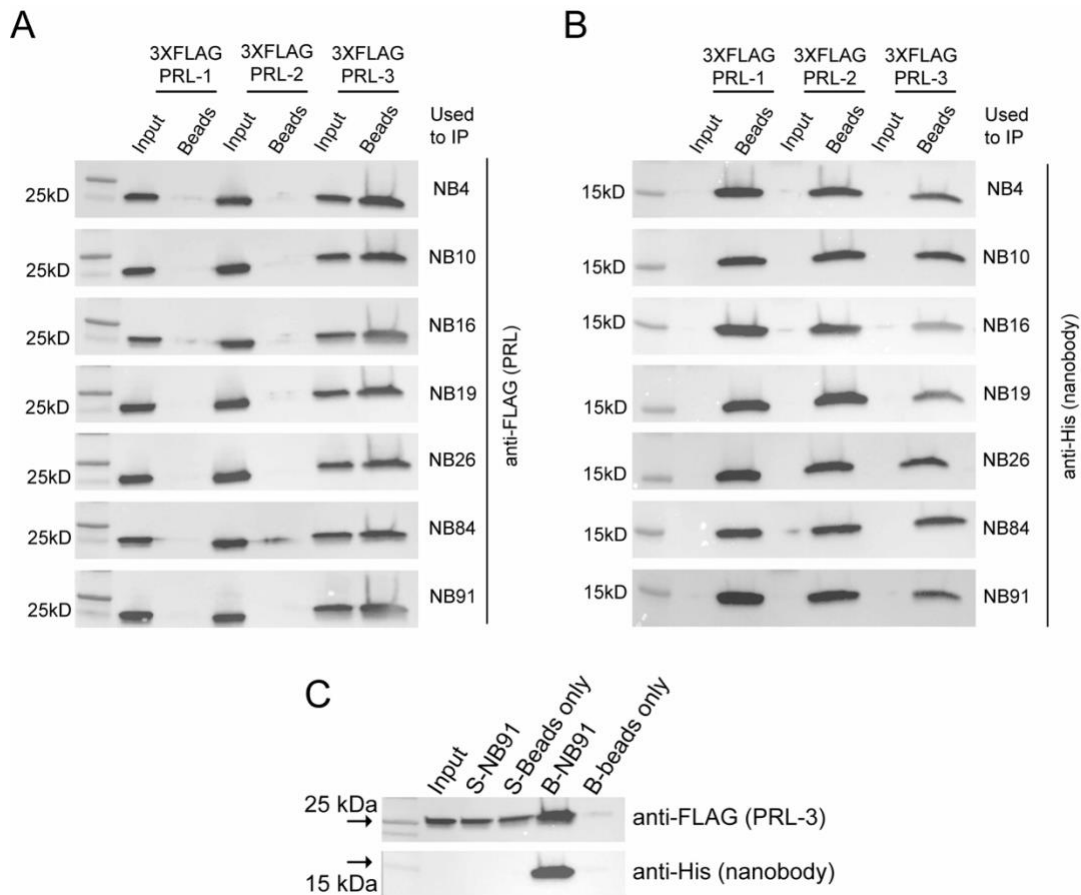


**Figure 4.3. Nanobodies selectively immunoprecipitate PRL-3 from HEK293T cell lysate.** PRL-3 specific nanobodies coupled to superparamagnetic Dynabeads® M-270 Epoxy beads were used in immunoprecipitation assays with lysates from HEK293T cells transduced with 3XFLAG-PRL-1, -2, or -3. (A) All nanobodies pulldown 3XFLAG-PRL-3 with minimal to no pulldown of 3XFLAG-PRL-1 or 3XFLAG-PRL-2. (B) Successful nanobody coupling to Dynabeads in all groups was verified using an antibody against the C-terminal 6XHis-tag on each nanobody. (C) Controls demonstrate that the Dynabeads® M-270 Epoxy beads do not readily bind 3XFLAG-PRL-3 without NB91. S – Supernatant from IP, B – Elution from NB91 or empty beads.

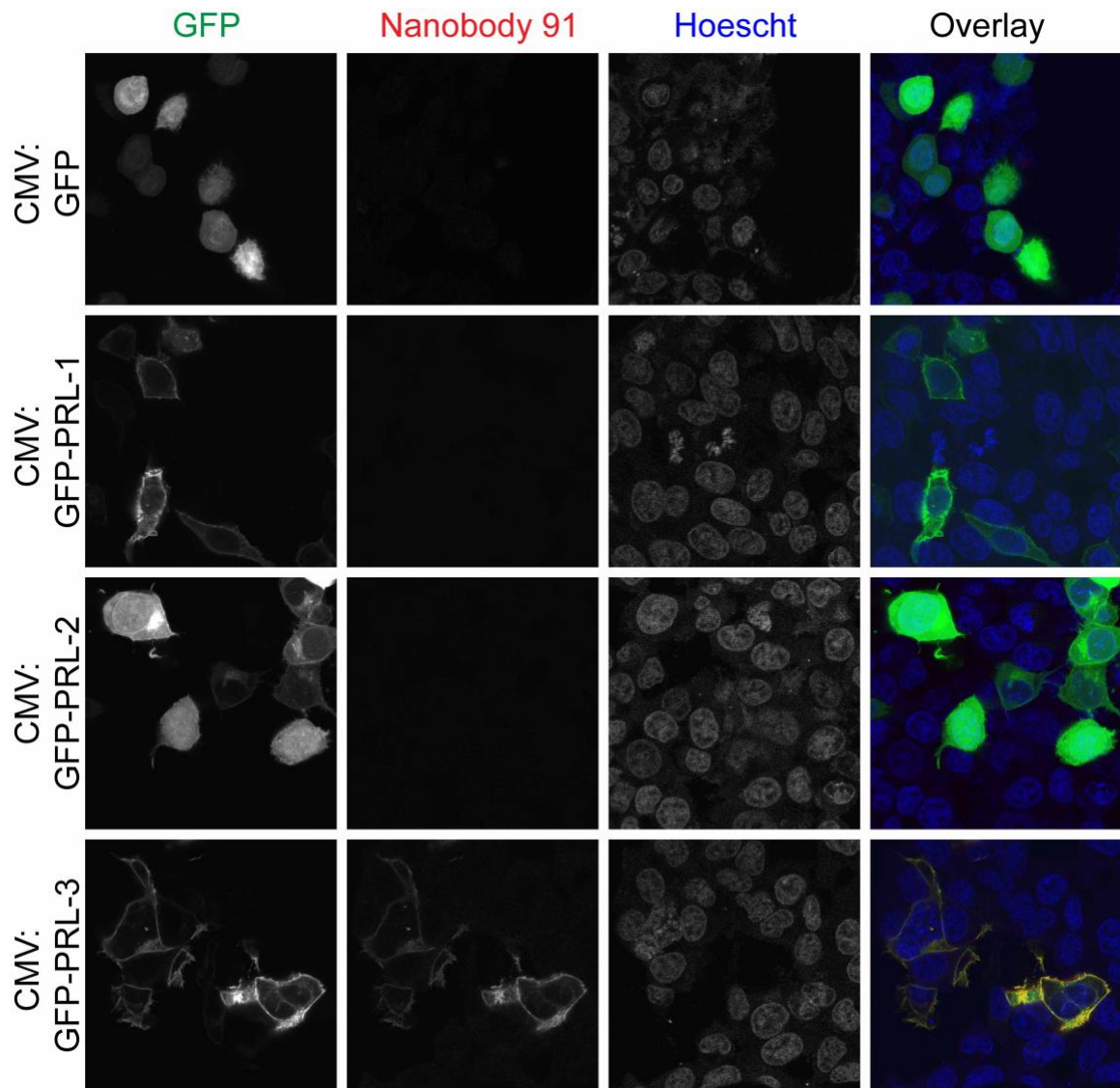


**Figure 4.4. Nanobody 91 is specific to PRL-3 in immunofluorescence assays.** HCT116 colorectal cancer cells were transfected with CMV:GFP, CMV:GFP-PRL-1, CMV:GFP-PRL-2, or CMV:GFP-PRL-3 for 24 hours before cell fixation and permeabilization. Immunofluorescence assays were completed with 1:100 1 mg/mL NB91 followed by 1:400 Alexa Fluor® 594-AffiniPure Goat Anti-Alpaca IgG, VHH domain, showing that nanobodies detect and co-localize with PRL-3 but not PRL-1 or PRL-2.

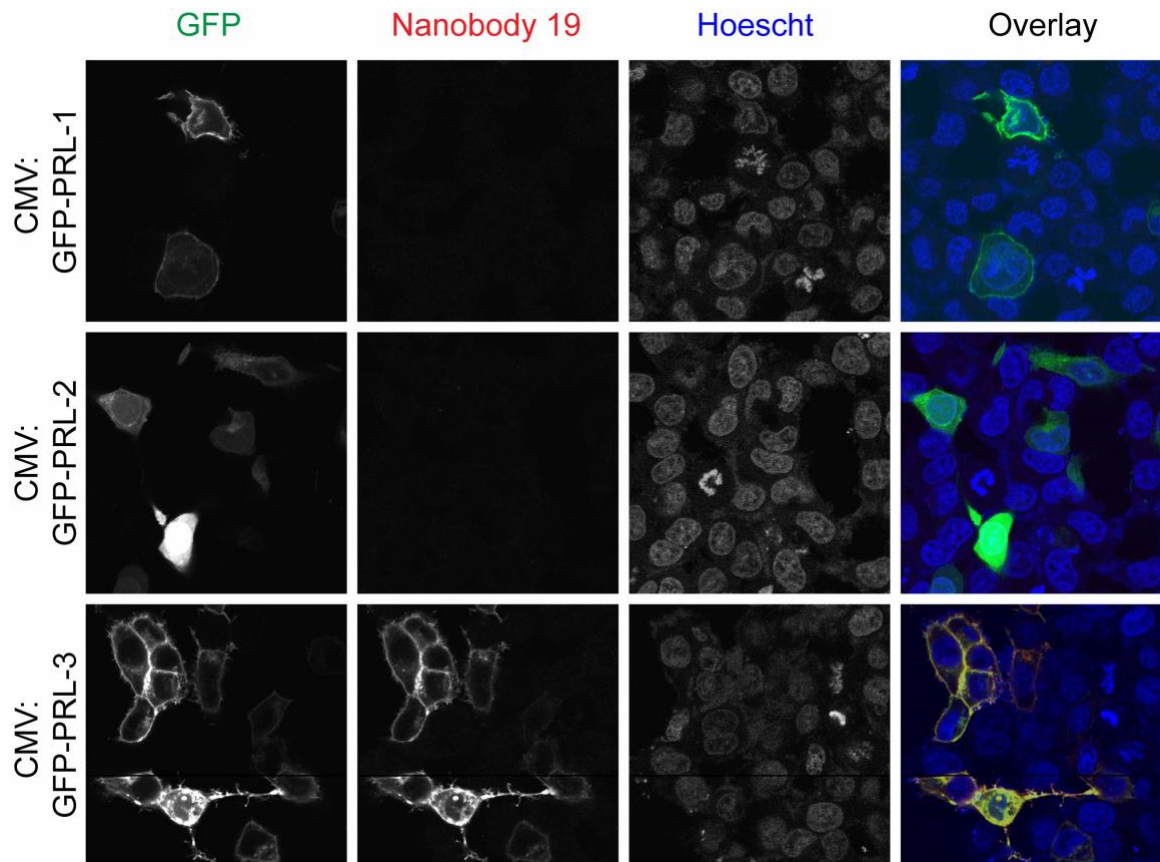


**Figure 4.5. Nanobody 19 is specific to PRL-3 in immunofluorescence assays.** HCT116 colorectal cancer cells were transfected with CMV:GFP-PRL-1, CMV:GFP-PRL-2, or CMV:GFP-PRL-3 for 24 hours before cell fixation and permeabilization. Immunofluorescence assays were completed with 1:100 1 mg/mL NB19 followed by 1:400 Alexa Fluor® 594-AffiniPure Goat Anti-Alpaca IgG, VHH domain, showing that nanobodies detect and co-localize with PRL-3 but not PRL-1 or PRL-2.

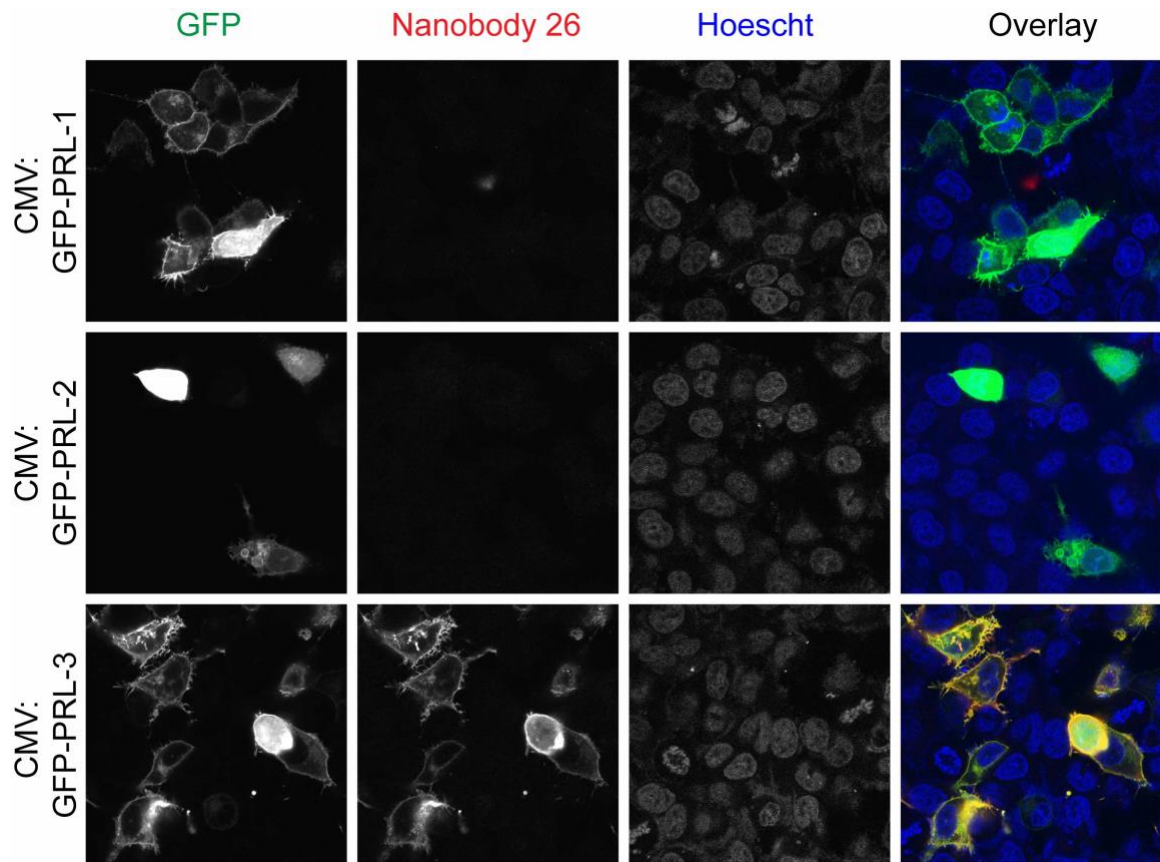


**Figure 4.6. Nanobody 26 is specific to PRL-3 in immunofluorescence assays.** HCT116 colorectal cancer cells were transfected with CMV:GFP-PRL-1, CMV:GFP-PRL-2, or CMV:GFP-PRL-3 for 24 hours before cell fixation and permeabilization. Immunofluorescence assays were completed with 1:100 1 mg/mL NB26 followed by 1:400 Alexa Fluor® 594-AffiniPure Goat Anti-Alpaca IgG, VHH domain, showing that nanobodies detect and co-localize with PRL-3 but not PRL-1 or PRL-2.

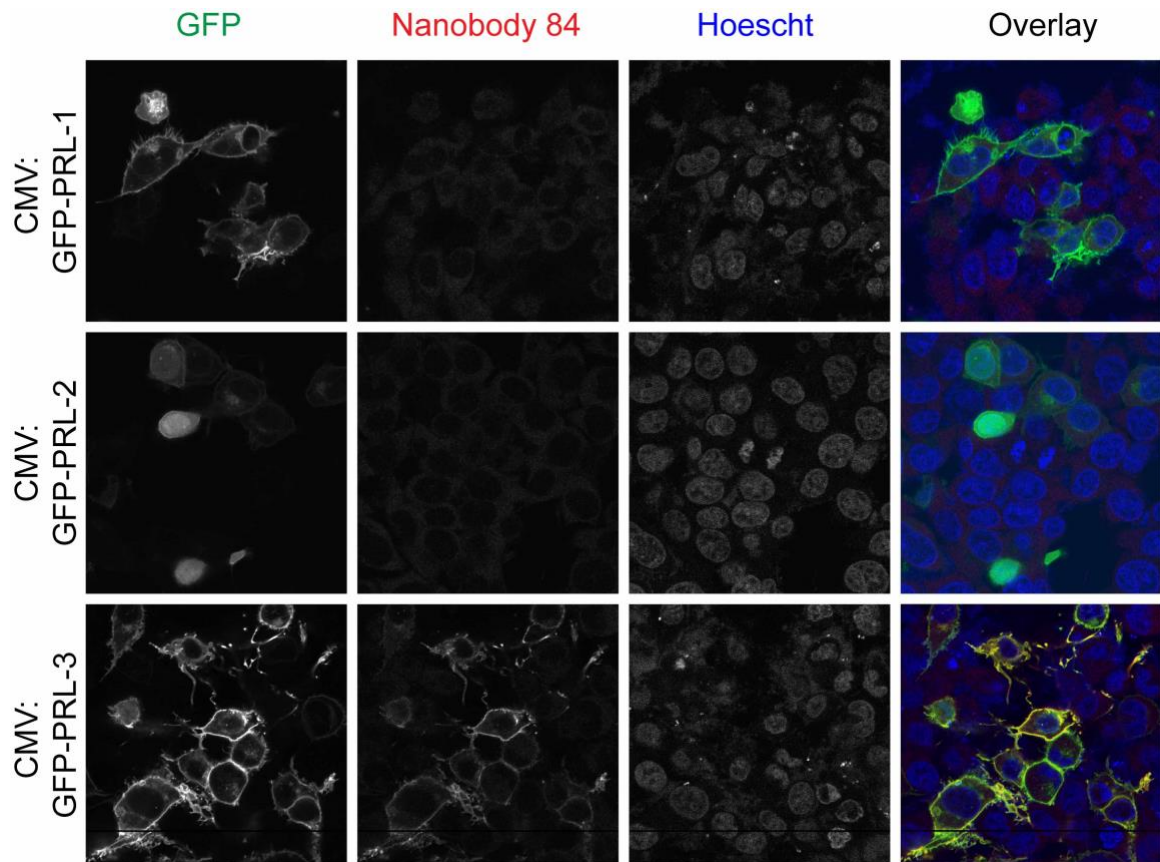


**Figure 4.7. Nanobody 84 is specific to PRL-3 in immunofluorescence assays.** HCT116 colorectal cancer cells were transfected with CMV:GFP-PRL-1, CMV:GFP-PRL-2, or CMV:GFP-PRL-3 for 24 hours before cell fixation and permeabilization. Immunofluorescence assays were completed with 1:100 1 mg/mL NB84 followed by 1:400 Alexa Fluor® 594-AffiniPure Goat Anti-Alpaca IgG, VHH domain, showing that nanobodies detect and co-localize with PRL-3 but not PRL-1 or PRL-2.

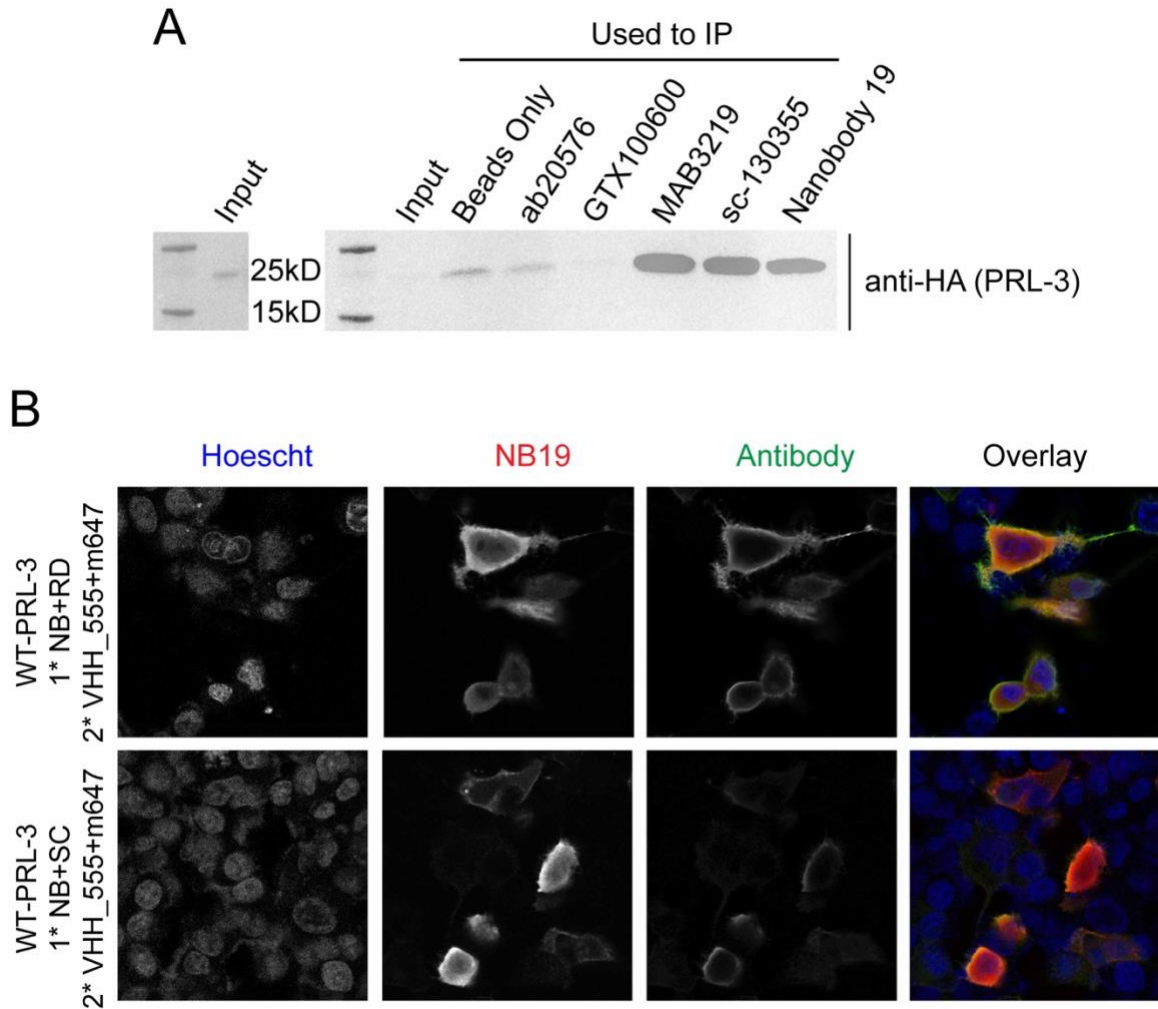


**Figure 4.8. Nanobody 19 binds more specifically to PRL-3 than commercial antibodies, MAB3219, and sc-130355.** (A) Nanobody 19 was coupled to superparamagnetic Dynabeads® M-270 Epoxy beads; commercial antibodies were coupled to Protein A and G beads. All were used in immunoprecipitation assays with lysates from HCT116 cells transfected with HA-PRL -3. Nanobody 19 pulls down HA-PRL-3 more efficiently than ab20576 and GTX100600, and equally compared to MAB3219 and sc-130355. (B) Immunofluorescence of HCT116 cells transfected with CMV:HA-PRL-3. Cells were stained with primary: anti-PRL-3 nanobody 19 (NB) and MAB3219 (top panel, RD) or sc-130355 (bottom panel, SC). This was followed by secondary staining with an anti-alpaca VHH coupled to Alexa594 (VHH\_555) and anti-mouse IgG coupled to Alexa647 (m647) for visualization. Each channel was pseudocolored as: Hoescht (blue), nanobody (red), MAB3219, and sc-130355 (green).



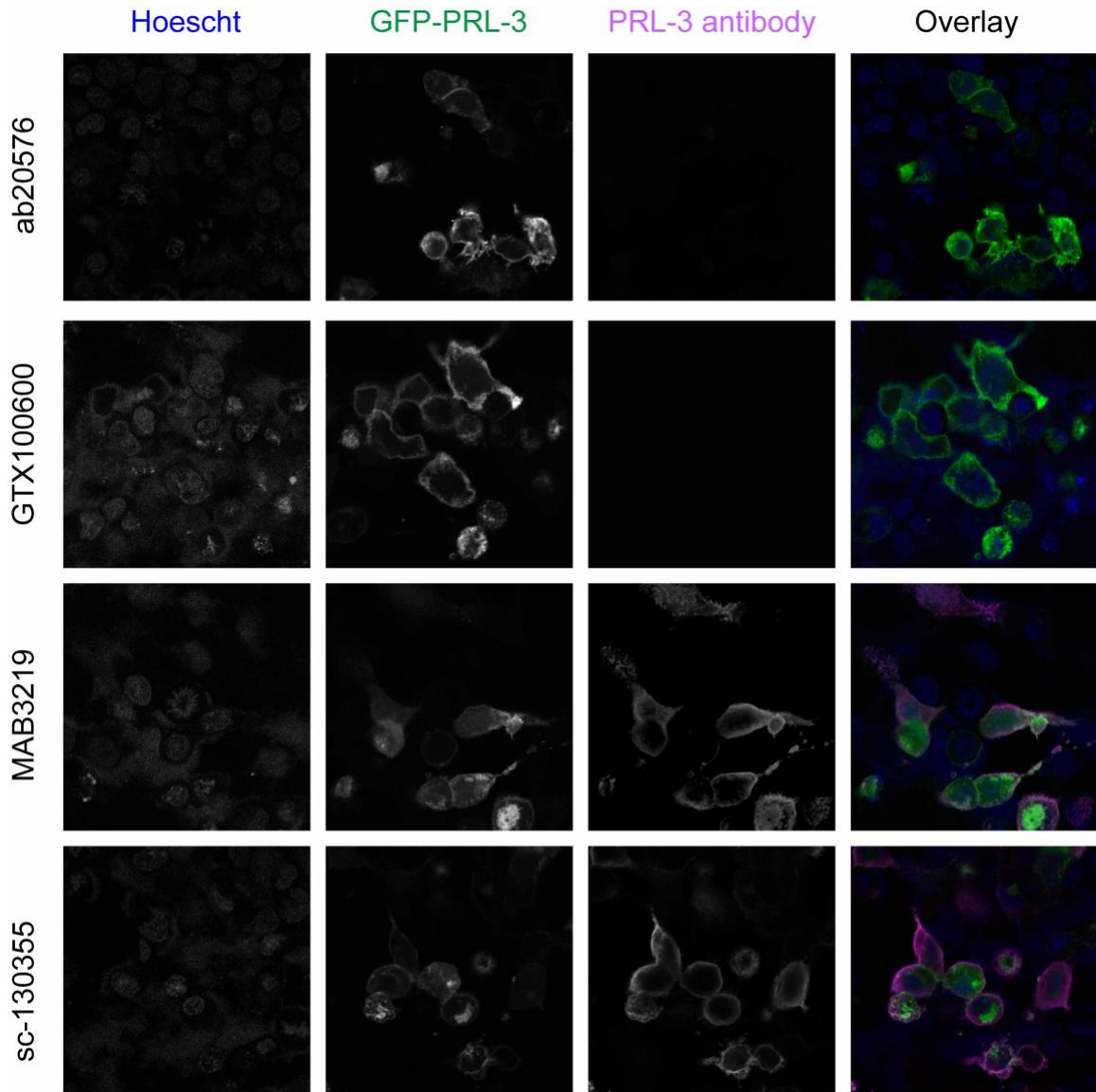


**Figure 4.9. Commercial antibodies MAB3219, and sc-130355 bind GFP-PRL-3 while ab20576 and GTX100600 do not.** Immunofluorescence of HCT116 cells transfected with CMV:GFP-PRL-3. Cells were stained with primary: ab20576, GTX100600, MAB3219 or sc-130355. This was followed by secondary staining with an anti-rabbit IgG coupled to Alexa647 (ab20576 and GTX100600) or an anti-mouse IgG coupled to Alexa647 (MAB3219 and sc-130355) for visualization. Each channel was pseudocolored as: Hoescht (blue), GFP-PRL-3 (green), commercial antibody (purple).

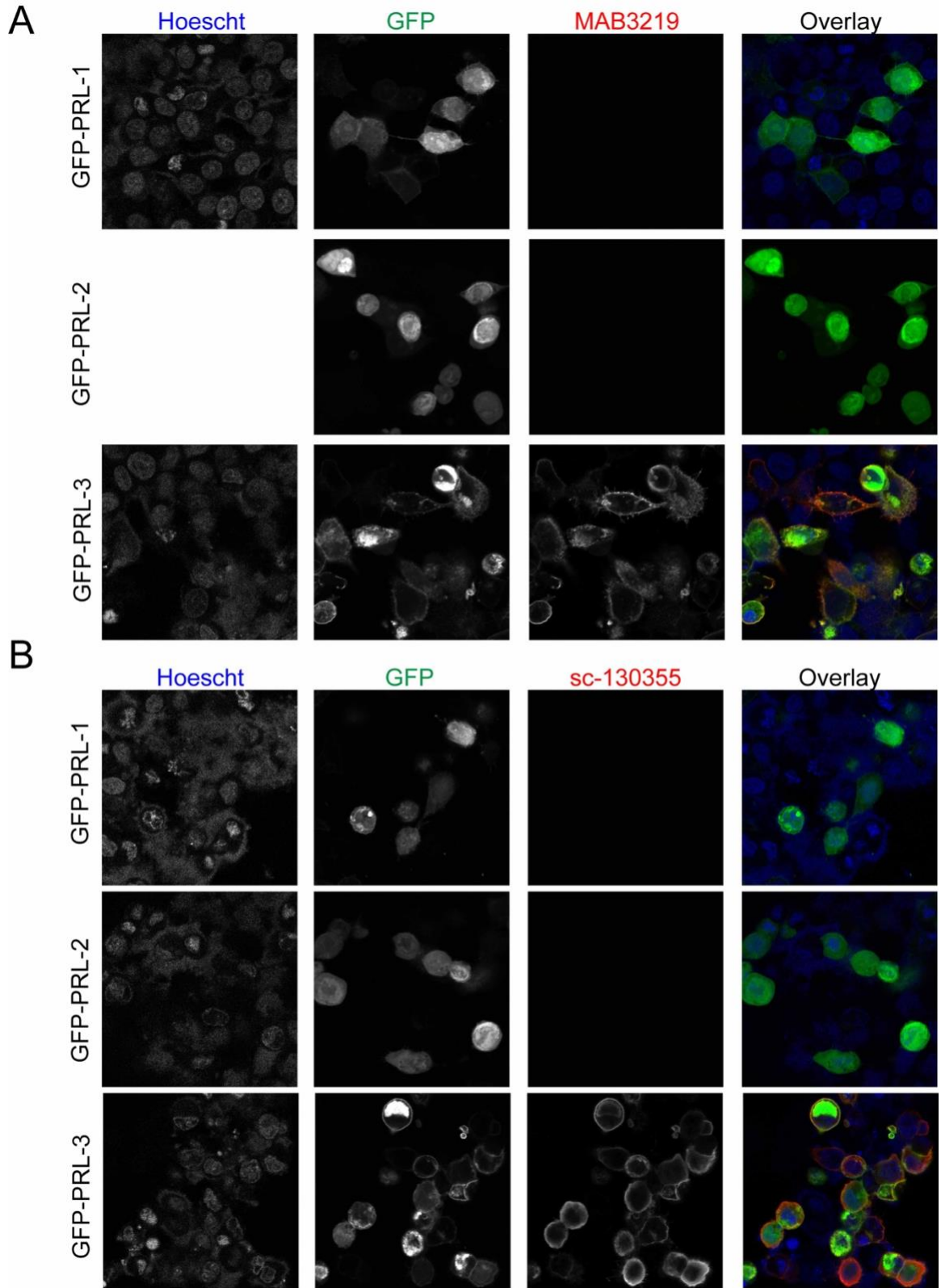


**Figure 4.10. Commercial antibodies MAB3219 and sc-130355 are specific for PRL-3 over PRL-1 and PRL-2.** HCT116 colorectal cancer cells were transfected with CMV:GFP-PRL-1, CMV:GFP-PRL-2, or CMV:GFP-PRL-3 for 24 hours before cell fixation and permeabilization. Immunofluorescence assays were completed with (A) MAB3219 or (B) sc-130355 primary staining followed by secondary staining with an anti-mouse IgG coupled to Alexa647 for visualization. Each channel was pseudocolored as: Hoescht (blue), GFP-PRL (green), commercial antibody (red). Hoescht staining for PRL-2 in (A) was skipped during experimentation and therefore could not be documented.

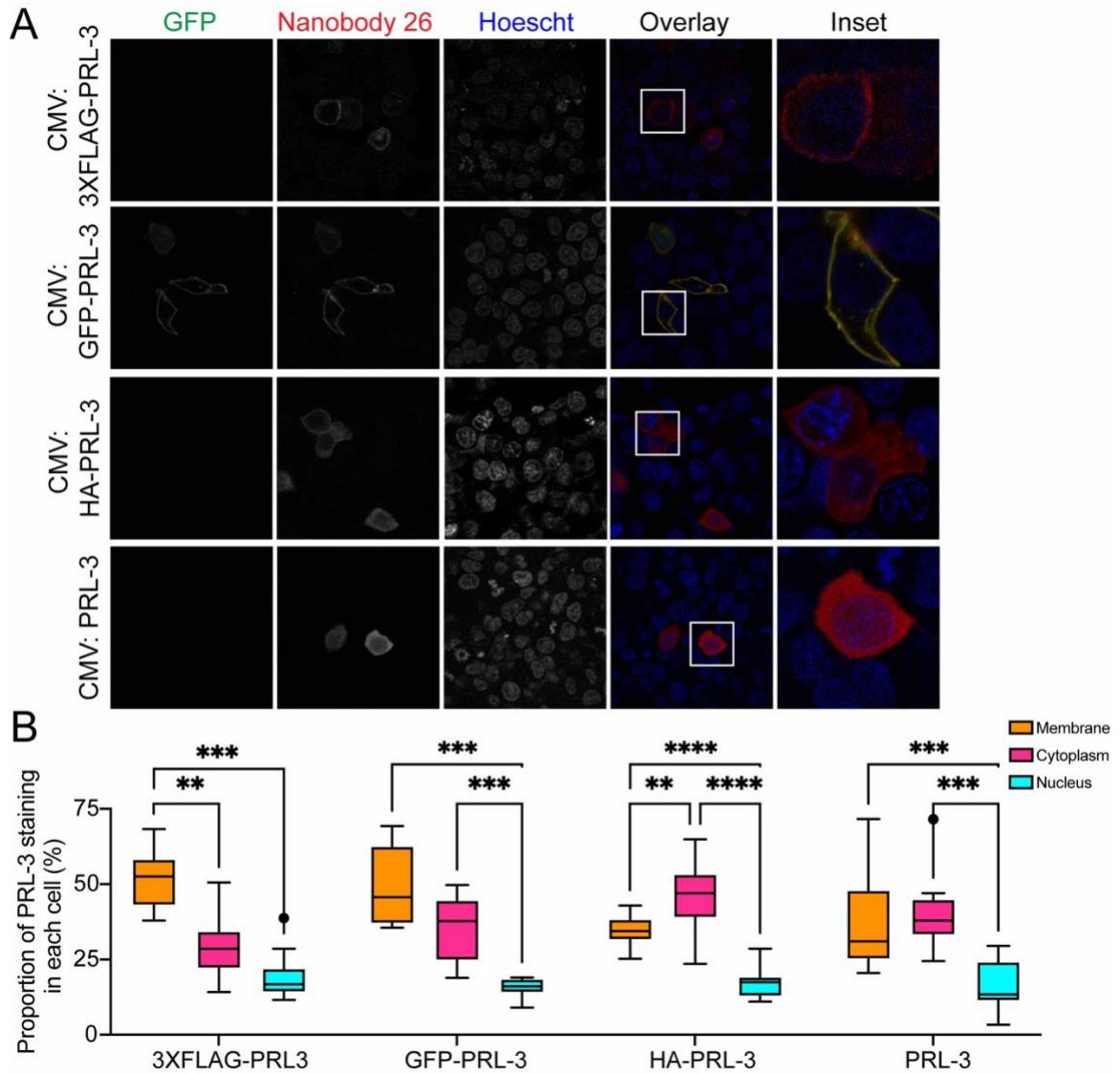


**Figure 4.11. PRL-3 localization assessed by Nanobody 26 and 19 is altered by N-terminal 3XFLAG and GFP tags.** (A) Immunofluorescence of HCT116 cells transfected with CMV:3XFLAG-PRL-3, CMV:GFP-PRL-3, CMV:HA-PRL-3, or CMV-PRL-3, as indicated. Cells were stained with anti-PRL-3 nanobody 26 or 19 (HA) followed by an anti-alpaca VHH coupled to Alexa594 secondary antibody for visualization. (B) ImageJ quantification of nanobody/PRL-3 staining. Groups were compared using a Mixed-effects analysis with Tukey's Multiple Comparisons Test where \*\* $p < 0.01$ , \*\*\* $p < 0.001$ , \*\*\*\* $p < 0.0001$ .

## **Chapter 5. Anti-PRL-3 nanobodies block the CNNM/PRL-3 interaction that contributes to tumorigenesis.**

### 5.1. Introduction.

After clearly defining that the alpaca-derived anti-PRL-3 nanobodies bind to PRL-3 with high specificity and can bind to cellular PRL-3, it was necessary to continue exploring how these nanobodies could help in studying PRL-3 biology. This process begins with determining these nanobodies' affinity for PRL-3 and where they bind to the protein. It is crucial to assess the binding relationship if the goal is to develop nanobodies as PRL-3 inhibitors. In addition, we need structural studies to examine where the nanobodies bind to PRL-3 to define better their functional effects on PRL-3 and how we can use them to design better tools to target PRL-3. The goal of this chapter is to demonstrate nanobody binding on PRL-3 and their potential for being adapted as PRL-3 inhibitors. The work in this chapter, specifically 5.2.2. was done in collaboration with Daniel Deredge and Kyle Kihn at the University of Maryland School of Pharmacy.

### 5.2. Results.

#### *5.2.1. Nanobody affinity for PRL-3 is comparable to the affinity of FDA-approved antibodies for their targets and partially inhibits PRL-3 activity.*

We determined the affinity of nanobodies 19, 26, 84, and 91 for PRL-3 using Biolayer Interferometry (BLI). The BLI technology used by the BLItz system provides real-time data on protein interactions. The BLItz system emits white light down the biosensor, then collects any reflected light. A spectrometer captures the reflected light and reports results in relative intensity units (nm). Any change in the number of molecules bound to the biosensor causes a shift in this interference pattern or reflected light measured in real-time. BLI allowed us to measure the association constant ( $k_a$ ) and dissociation constant ( $k_d$ ) of each nanobody at increasing concentrations of PRL-3 to calculate the equilibrium dissociation constant ( $K_D$ ) for each nanobody tested. For example, Figure 5.1 represents the readout for BLI of nanobody 26 binding to six concentrations of PRL-3.

A smaller  $K_D$  correlates to a higher  $K_A$  and indicates a stronger interaction between PRL-3 and nanobody. The BLItz analysis software calculated a local  $K_D$  for each concentration of PRL-3 loaded onto each nanobody (Table 5.1). Raw data for these calculations are shown in Supplemental Table 1. From here, it then calculated the global  $K_D$  of each nanobody, accounting for all local measurements (Table 5.2). Nanobodies 19 and 26 have the highest affinity for PRL-3, at 98.4 nM and 28.9 nM, respectively (Table 5.3). Nanobodies 84 and 91 had similar associations at 101.4 nM and 202.8 nM, respectively. On average, commercially available and FDA-approved antibodies have affinities ranging from  $10^{-5}$  to  $10^{-11}$  M for their targets; our anti-PRL-3 nanobodies are well within this range for binding to PRL-3.

With the nanobodies having this strong affinity for PRL-3, the next question we needed to answer is how they impact PRL-3 function. As outlined in Chapter 1, the field is debating the role of PRL-3 in general and cancer. Yet, following the discovery of PRL-3, scientists determined that PRL-3 has a phosphatase domain in its structure. Therefore, we began by testing the impact of nanobody presence on PRL-3's ability to dephosphorylate a generic substrate. When 6,8-Difluoro-4-Methylumbelliferyl Phosphate (DiFMUP) has its phosphate group removed by a phosphatase, the reaction product (DiFMU) has excitation/emission maxima of  $\sim 358/450$  nm, allowing us to quantify the amount of product made using a GFP filter cube (Fig 5.2A). We performed experiments with an excess substrate, and initially, we tested each nanobody's effect on PRL-3 at a single concentration of nanobody. We discovered that nanobodies 26 and 84 could reduce the phosphatase activity of PRL-3 (Fig 5.2B). Nanobody 19 caused no change in PRL-3 phosphatase activity, but nanobody 91 seemed to enact an increase in phosphatase activity (Fig 5.2B) which could be due to human error or an impurity in the nanobody 91 protein sample. Therefore, we took this a step further and examined the effect that nanobody 91 may have on PRL-3 phosphatase activity in a concentration-dependent manner. Nanobody 91 significantly decreased PRL-3's ability to dephosphorylate DiFMUP (Fig 5.2C), beginning at  $0.5 \mu\text{M}$  of nanobody. These results demonstrate that the findings for nanobody 91 in Figure 5.2B were most-likely due to an error in experimentation, and further research demonstrates nanobody 91 can inhibit phosphatase activity in a similar manner as nanobody 26 and 84.

While these results are exciting and could significantly impact PRL-3 inhibitor development, there are outstanding questions in the field, and we need to contribute to finding answers to advance our nanobodies as inhibitors. First, generally in a phosphatase assay, a reducing agent ensures that the active site can dephosphorylate the substrate. Unfortunately, we could not include a reducing agent in our studies, as it would also reduce the critical disulfide bond necessary for nanobody structure. Therefore, a second assay representing fully reduced PRL-3 is required to determine how intensely phosphatase activity is affected by nanobody presence. This could potentially be done by reducing PRL-3 protein prior to the phosphatase assay. Tris (2-carboxyethyl) phosphine (TCEP) is a reducing agent whose reaction is irreversible. Therefore, we could reduce PRL-3 in solution, and remove TCEP from the protein sample by dialysis or immobilization on magnetic beads (151). When the reduced PRL-3 is mixed with nanobody, the nanobody will not be reduced. Secondly, the nanobodies' ability to alter PRL-3 phosphatase activity does not mean that the nanobodies bind to the active site; they could interact elsewhere on the protein. Determining nanobody localization on PRL-3 would allow us to hypothesize better how these nanobodies reduce phosphatase activity. Therefore, we set out to determine if the effects of the nanobody on PRL-3's phosphatase activity are due to the nanobody physically blocking the active site or a potential shift in PRL-3's structure upon nanobody binding occurring elsewhere on the protein, allowing the nanobodies to work allosterically.

#### *5.2.2. Nanobodies partially bind the PRL-3 active site.*

To study the binding sites of nanobodies 19, 26, and 91 on PRL-3, we used Hydrogen Deuterium Exchange Mass Spectrometry (HDX-MS). HDX-MS probes the structure of a protein complex by monitoring the exchange of backbone amide hydrogen atoms with solvent deuterium atoms upon exposure to deuterated solvent. We compared the deuterium uptake of apo-PRL-3 to PRL-3 complexed with either nanobody 19, 26, or 91. Following deuterium exchange, apo-PRL-3 or the PRL-3/nanobody complex was subjected to trypsin digestion, and peptides were measured using mass spectrometry, as outlined in 3.10. The peptides where deuterium exchange did not occur due to complex

formation were compared to the same apo-PRL-3 deuterated peptides to examine potential nanobody binding sites on PRL-3. These experiments were performed in collaboration with Kyle Kihn and Dr. Daniel Deredge at the University of Maryland School of Pharmacy.

Through this form of epitope mapping, we found that nanobody interaction with PRL-3 protected PRL-3 from deuteration in two regions, shown in blue for nanobody 19 (Fig 5.3), nanobody 26 (Fig 5.4), and nanobody 91 (Fig 5.5). In addition, we unexpectedly found an increase in deuteration, or deprotection of PRL-3, of up to 30% in one region of PRL-3 after nanobody binding (shown in red), which may indicate a slight conformational change in PRL-3 caused by nanobody binding, compared to apo-PRL-3. One caveat to this experiment was our inability to determine some structural interactions at portions of the PRL-3 active site between amino acids 80 to 104 due to a lack of sequence coverage. This lack of coverage includes the catalytic cysteine of PRL-3, C104, involved in phosphatase activity. We currently cannot know if these nanobodies interact with this catalytic site based on these data. Nanobody 91 deprotected PRL-3 from residues 13-19 and protected at amino acids 56-79 and 132-146 (Fig 5.5B). One of the fundamental aspects of phosphatase catalysis is the WFPDD-loop, described in Chapter 1. The PRL-3 WFPDD-loop encapsulates residues 68-72, which is protected by Nanobody 91. If nanobodies bind near the WFPDD-loop, this may contribute to the decreased phosphatase activity in 5.2.1. Nanobody 19 and 26 had similar deuterium uptake alterations compared to nanobody 91, where nanobody 26 also shows protection of the WFPDD loop (Fig 5.3B and 5.4B). Through this pattern of protection and deprotection, we conclude that all three nanobodies bind very similar regions of PRL-3 and would likely have similar effects on overall protein structure, stability, and activity on the WFPDD-loop during a catalytic event.

### *5.2.3. Nanobodies disrupt interaction with known PRL-3 binding partner, CNNM3.*

As specified in Chapter 1, the magnesium transporter CNNM3 is a well-established PRL-3 binding partner in the field and is involved in PRL-3's oncogenic pseudo-phosphatase activity (152). Therefore, after first exploring how these nanobodies impact the phosphatase activity of PRL-3 and determining that they bind to amino acids essential for protein catalysis, we then needed to decide how to use these nanobodies to study the



other hypothesis in the field, that PRL-3 acts as a pseudo-phosphatase by binding CNNM proteins at the cellular membrane. Fortunately, other groups are studying the interface between the CNNM and PRL proteins and determined that the Bateman domain (CBS) of CNNM3 interacts with the active site of PRL-3, published by Kozlov et al. in an x-ray crystal structure of the complex, PDB:5TSR (51).

In Fig 5.6A, we display the 5TSR CBS:PRL-3 interaction in a space-filling structure, along with the amino acid footprint of Nanobody 91, where the nanobody protects PRL-3, as determined by HDX-MS epitope mapping. Based on this structural representation, these nanobodies may block or disrupt CBS binding in its resident binding pocket, as shown by the overlapping CBS (orange) and nanobody binding region (dark blue) on PRL-3 (cyan). To test this hypothesis, we designed multiple competition assays for the binding of each protein to PRL-3. For this, we utilized recombinantly expressed protein and purified the CNNM3 CBS domain fused to a hemagglutinin (HA) tag (CBS-HA) and a 3XFLAG-tagged PRL-3 (Fig 3.4) from *E. coli*, described in 3.11. The following experiment aimed to examine the impact of nanobody binding on the PRL-3:CBS complex.

To do this, we set up a series of competition immunoprecipitation assays outlined in 3.12 utilizing recombinant 3XFLAG-PRL-3, HA-tagged CBS domain, and the 6X-His-tagged nanobody 26. We used nanobody 26 in these studies as it has a strong affinity for PRL-3 (Table 5.2), inhibits PRL-3 phosphatase activity upon binding (Fig 5.2B), and binds the PRL-3 WFPDD-loop (Fig 5.3B). In this series of assays, we used 1:1.1 molar ratios of PRL-3:nanobody and PRL-3: CBS, with nanobody:CBS being 1:1. Therefore every molecule should only be bound to one nanobody or one CBS domain; there was excess nanobody and CBS to cause them to compete for the PRL-3 binding site. Fig 5.6B shows experimental controls, where FLAG Dynabeads pull down only 3XFLAG-PRL-3, and the CBS and nanobodies are not. Fig 5.6C demonstrates that individually, both anti-PRL-3 nanobody 26 and the CBS domain co-IP with FLAG-PRL-3, once PRL-3 is bound to FLAG Dynabeads. We then set up three different immunoprecipitation assays, as diagramed in Fig 5.6D. Assays 1 and 2 added either nanobody 26 or CBS to PRL-3 bound beads for one hour, then added the opposing protein for one hour to determine if one could block the other's binding to PRL-3. However, results shown in Fig 5.6D show that no matter the order of addition, both proteins can bind to PRL-3 simultaneously. These data

demonstrate that the binding sites of the CNNM3 CBS domain and our anti-PRL-3 nanobodies do not fully overlap.

In assay 3, we found that adding nanobody 26 and CBS-HA to PRL-3 simultaneously decreased the ability of both proteins to immunoprecipitate with PRL-3 (Fig 5.6D), compared to assays 1 and 2. These data suggest that the nanobody and CBS may compete for some of the same occupancies in the PRL-3 active site. In addition, these data indicate that anti-PRL-3 nanobodies bind near the active site of PRL-3 and impact the ability of protein substrates to interact while limiting catalytic phosphatase activity on those substrates. Further studies described in Chapter 6 will determine if these nanobodies can block the PRL-3 active site in such a way as to act as an inhibitor in scientific research and clinical studies.

**Table 5.1. Local  $K_D$  of nanobodies binding to six concentrations of PRL-3.**

<b>NANOBODY 19</b>					
PRL-3 (nM)	$K_D$ (M)	$k_a$ (1/Ms)	$k_a$ Error	$k_d$ (1/s)	$k_d$ Error
113.6	$1.00 \times 10^{-12}$	$3.49 \times 10^6$	$6.87 \times 10^8$	$1.00 \times 10^{-7}$	0
227.3	$1.00 \times 10^{-12}$	$2.68 \times 10^4$	$8.64 \times 10^3$	$1.00 \times 10^{-7}$	0
454.4	$2.46 \times 10^{-7}$	$1.05 \times 10^4$	$2.89 \times 10^3$	$2.58 \times 10^{-3}$	$1.47 \times 10^{-4}$
1136	$5.52 \times 10^{-8}$	$1.77 \times 10^4$	$5.95 \times 10^3$	$9.76 \times 10^{-4}$	$2.92 \times 10^{-4}$
2273	$4.03 \times 10^{-8}$	$7.58 \times 10^3$	6.917	$3.05 \times 10^{-4}$	$2.50 \times 10^{-6}$
4545	$2.15 \times 10^{-8}$	$4.74 \times 10^3$	4.179	$1.02 \times 10^{-4}$	$1.85 \times 10^{-6}$
<b>NANOBODY 26</b>					
PRL-3 (nM)	$K_D$ (M)	$k_a$ (1/Ms)	$k_a$ Error	$k_d$ (1/s)	$k_d$ Error
113.6	$1.00 \times 10^{-7}$	$1.00 \times 10^{-4}$	0	$1.00 \times 10^{-3}$	0
227.3	$1.63 \times 10^{-7}$	$1.56 \times 10^6$	$3.48 \times 10^6$	$2.54 \times 10^{-1}$	$1.50 \times 10^{-1}$
454.4	$6.37 \times 10^{-9}$	$6.82 \times 10^4$	$2.52 \times 10^4$	$4.34 \times 10^{-4}$	$2.53 \times 10^{-4}$
1136	$1.67 \times 10^{-8}$	$2.37 \times 10^4$	$8.56 \times 10^3$	$3.97 \times 10^{-4}$	$1.93 \times 10^{-4}$
2273	$1.00 \times 10^{-12}$	$6.45 \times 10^3$	$1.22 \times 10^1$	$1.00 \times 10^{-7}$	0
4545	$1.00 \times 10^{-12}$	$4.41 \times 10^3$	3.25	$1.00 \times 10^{-7}$	0
<b>NANOBODY 84</b>					
PRL-3 (nM)	$K_D$ (M)	$k_a$ (1/Ms)	$k_a$ Error	$k_d$ (1/s)	$k_d$ Error
113.6	$1.00 \times 10^{-7}$	$1.00 \times 10^4$	0	$1.00 \times 10^{-3}$	0
227.3	$1.00 \times 10^{-7}$	$1.00 \times 10^4$	0	$1.00 \times 10^{-3}$	0
454.4	$1.00 \times 10^{-12}$	$7.37 \times 10^2$	$8.30 \times 10^4$	$1.00 \times 10^{-7}$	0
1136	$5.64 \times 10^{-8}$	$8.34 \times 10^3$	$9.31 \times 10^1$	$4.71 \times 10^{-4}$	$1.31 \times 10^{-5}$
2273	$1.00 \times 10^{-12}$	$6.89 \times 10^3$	$2.16 \times 10^1$	$1.00 \times 10^{-7}$	0
4545	$3.42 \times 10^{-8}$	$4.56 \times 10^3$	3.26	$1.56 \times 10^{-4}$	$1.54 \times 10^{-6}$
<b>NANOBODY 91</b>					
PRL-3 (nM)	$K_D$ (M)	$k_a$ (1/Ms)	$k_a$ Error	$k_d$ (1/s)	$k_d$ Error
113.6	$1.00 \times 10^{-7}$	$1.00 \times 10^4$	0	$1.00 \times 10^{-3}$	0
227.3	$1.00 \times 10^{-7}$	$1.00 \times 10^4$	0	$1.00 \times 10^{-3}$	0
454.4	$1.00 \times 10^{-7}$	$1.00 \times 10^4$	0	$1.00 \times 10^{-3}$	0
1136	$2.77 \times 10^{-7}$	$4.87 \times 10^3$	$7.39 \times 10^2$	$1.35 \times 10^{-3}$	$6.41 \times 10^{-5}$
2273	$1.31 \times 10^{-7}$	$6.63 \times 10^3$	$3.77 \times 10^2$	$7.49 \times 10^{-4}$	$2.64 \times 10^{-5}$
4545	$2.95 \times 10^{-7}$	$6.28 \times 10^3$	$7.85 \times 10^1$	$1.85 \times 10^{-3}$	$2.31 \times 10^{-5}$

$K_D$ : equilibrium dissociation constant,  $k_a/k_d$

$k_a$ : association constant

$k_d$ : dissociation constant

Run Time per reaction: 510 s

Shaker Speed per reaction: 2200 rpm

Integration per reaction: 1.6 ms

**Table 5.2. Global  $K_D$  of nanobodies binding to PRL-3.**

Nanobody	$K_D$ (M)	$k_a$ (1/Ms)	$k_a$ Error	$k_d$ (1/s)	$k_d$ Error
NB 19	$9.84 \times 10^{-8}$	$3.922 \times 10^3$	$5.284 \times 10^1$	$3.860 \times 10^{-4}$	$1.399 \times 10^{-5}$
NB 26	$2.89 \times 10^{-8}$	$4.383 \times 10^3$	$2.742 \times 10^1$	$1.267 \times 10^{-4}$	$8.223 \times 10^{-6}$
NB 84	$1.014 \times 10^{-7}$	$3.277 \times 10^3$	$8.773 \times 10^1$	$3.324 \times 10^{-4}$	$1.547 \times 10^{-5}$
NB 91	$2.028 \times 10^{-7}$	$6.878 \times 10^3$	$1.358 \times 10^2$	$1.395 \times 10^{-3}$	$7.692 \times 10^{-5}$

$K_D$ : equilibrium dissociation constant,  $k_a/k_d$

$k_a$ : association constant

$k_d$ : dissociation constant

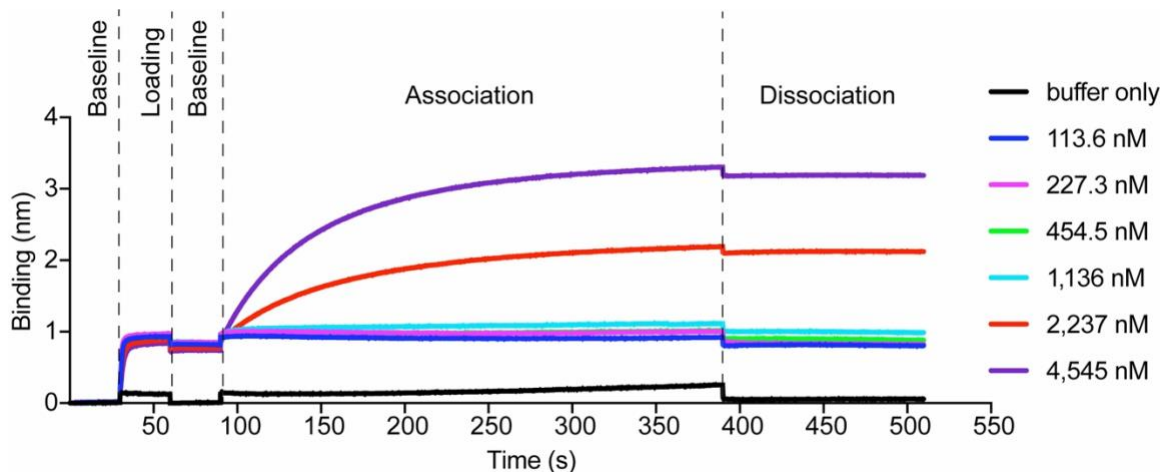


**Figure 5.1. Biolayer Interferometry Analysis (BLITZ) to denote KD of Nanobody 26 for PRL-3.** Sequential loading of five steps for Biolayer Interferometry Analysis of Nanobody 26 (626.57 nM) at six concentrations of PRL-3. Baseline – 30 seconds of BLI buffer to equilibrate the biosensor; Loading – 30 seconds of nanobody incubation with biosensor; Association – 300-second binding of recombinant PRL-3 at varying concentrations to measure association constant with nanobody 26; Dissociation – 120 seconds of incubation with BLI buffer to determine dissociation constant from PRL-3 at varying concentrations.

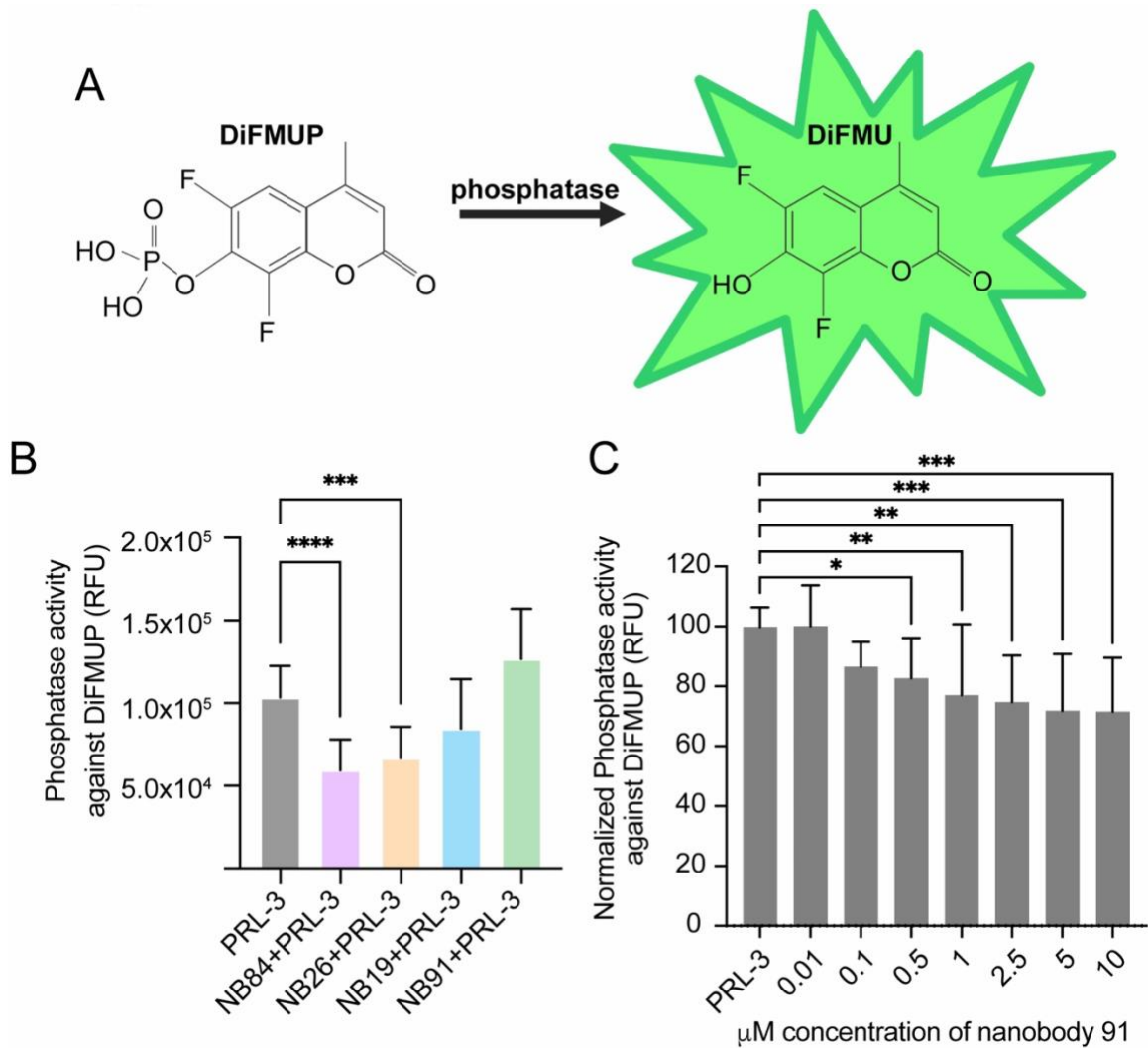


**Figure 5.2. Anti-PRL-3 nanobodies inhibit PRL-3 phosphatase activity in a dose-dependent manner.** (A) Schematic demonstrates that upon removing the phosphate group on DiFMUP, the DiFMU product fluoresces at excitation/emission maxima of ~358/450 nm. (B) Phosphatase activity of PRL-3 alone or in complex with one of four nanobodies against a generic diFMUP substrate. The graph shows relative fluorescence units,  $n=12 \pm$  standard deviation. (C) Phosphatase activity of PRL-3 alone or in complex with increasing nanobody 91 against a generic diFMUP substrate. The graph shows normalized fluorescence to PRL-3 alone,  $n=12 \pm$  standard deviation. Assays were completed with six technical replicates and repeated in two biological replicates. Error bars represent standard deviation. ns = not significant,  $**p < 0.01$ ,  $***p < 0.001$   $****p < 0.0001$  by two-way ANOVA with Dunnett's multiple comparisons tests.

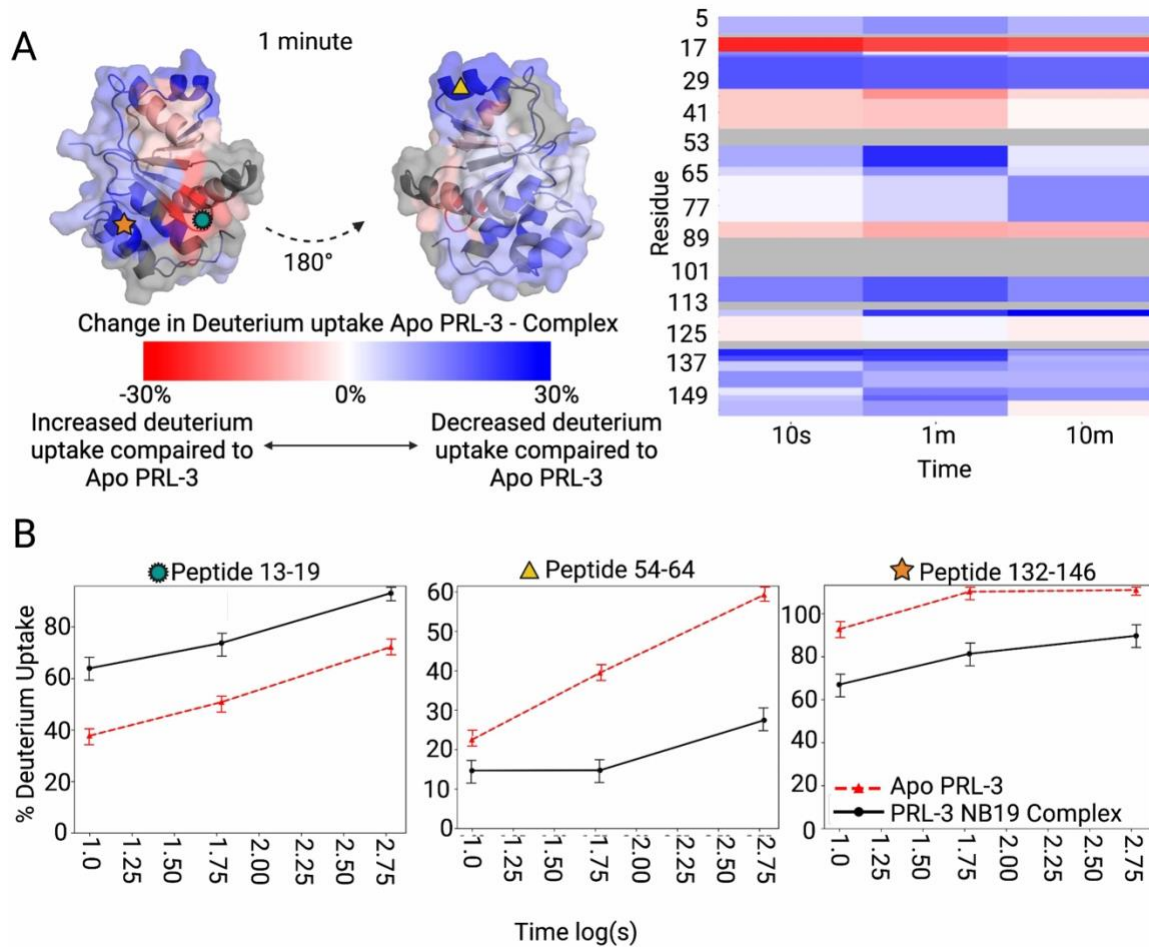


**Figure 5.3. Hydrogen Deuterium Exchange Mass Spectrometry (HDX-MS) defines Nanobody 19 binding sites with PRL-3.** (A) PRL-3 in complex with Nanobody 19 shows regions of increased (red) and decreased (blue) deuterium uptake compared to apo-PRL-3. Heatmap indicates approximately 70% sequence coverage by mass spectrometry; gray areas represent portions of PRL-3 where deuterium exchange was not recovered. (B) Peptide 13-19 showed PRL-3 deprotected following nanobody binding, while peptides 54-64 and 132-146 showed decreases in deuterium uptake, reflecting more protection by nanobody 19 on PRL-3 in these regions. This figure was developed through collaboration with Daniel Deredge and Kyle Kihn at the University of Maryland School of Pharmacy.

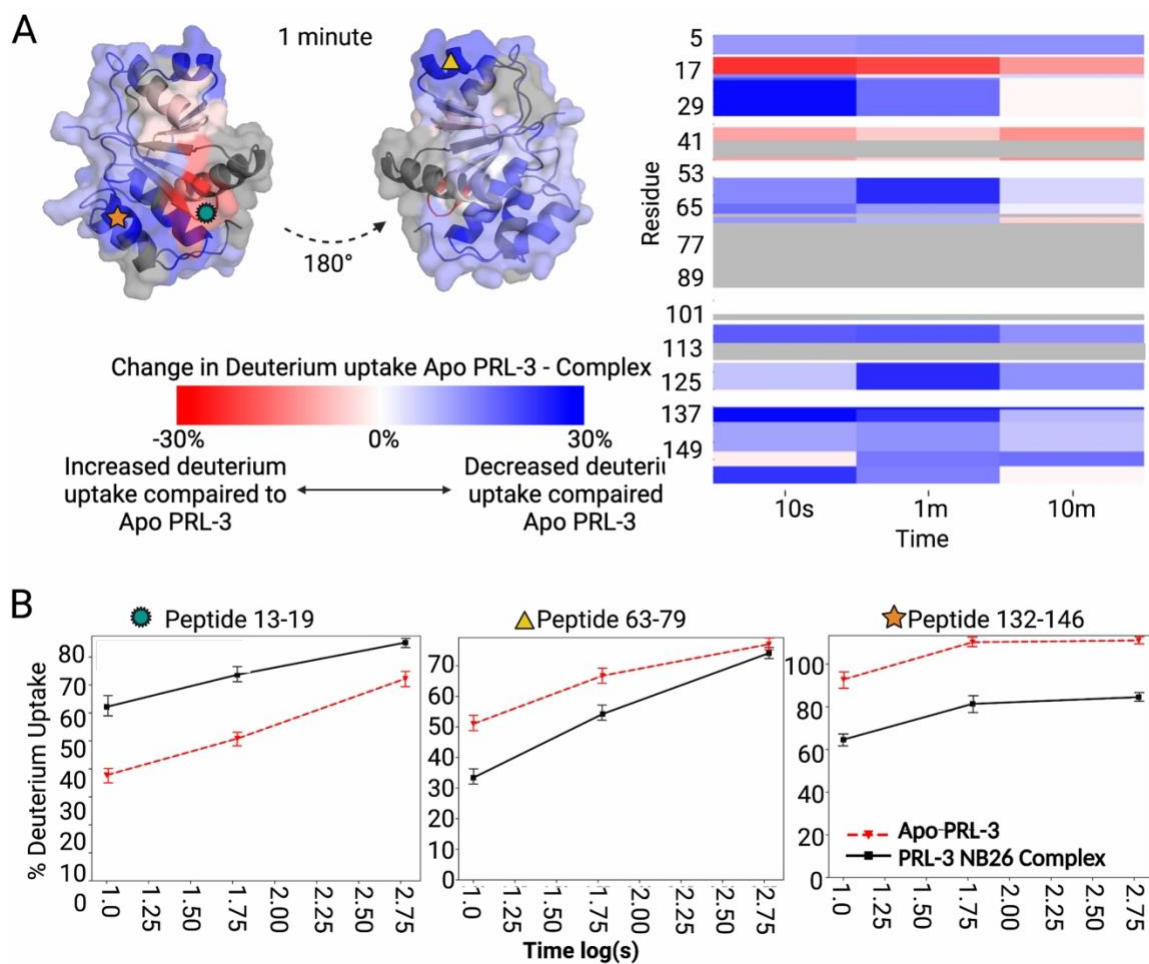


**Figure 5.4. Hydrogen Deuterium Exchange Mass Spectrometry (HDX-MS) defines Nanobody 26 binding sites with PRL-3.** (A) PRL-3 in complex with Nanobody 26 shows regions of increased (red) and decreased (blue) deuterium uptake compared to apo-PRL-3. Heatmap indicates approximately 70% sequence coverage by mass spectrometry; gray areas represent portions of PRL-3 where data for deuterium exchange was not recovered. (B) Peptide 13-19 showed PRL-3 deprotected following nanobody binding, while peptides 63-79 and 132-146 showed decreases in deuterium uptake, reflecting more protection by nanobody 26 and PRL-3 on these regions. This figure was developed through collaboration with Daniel Deredge and Kyle Kihn at the University of Maryland School of Pharmacy.



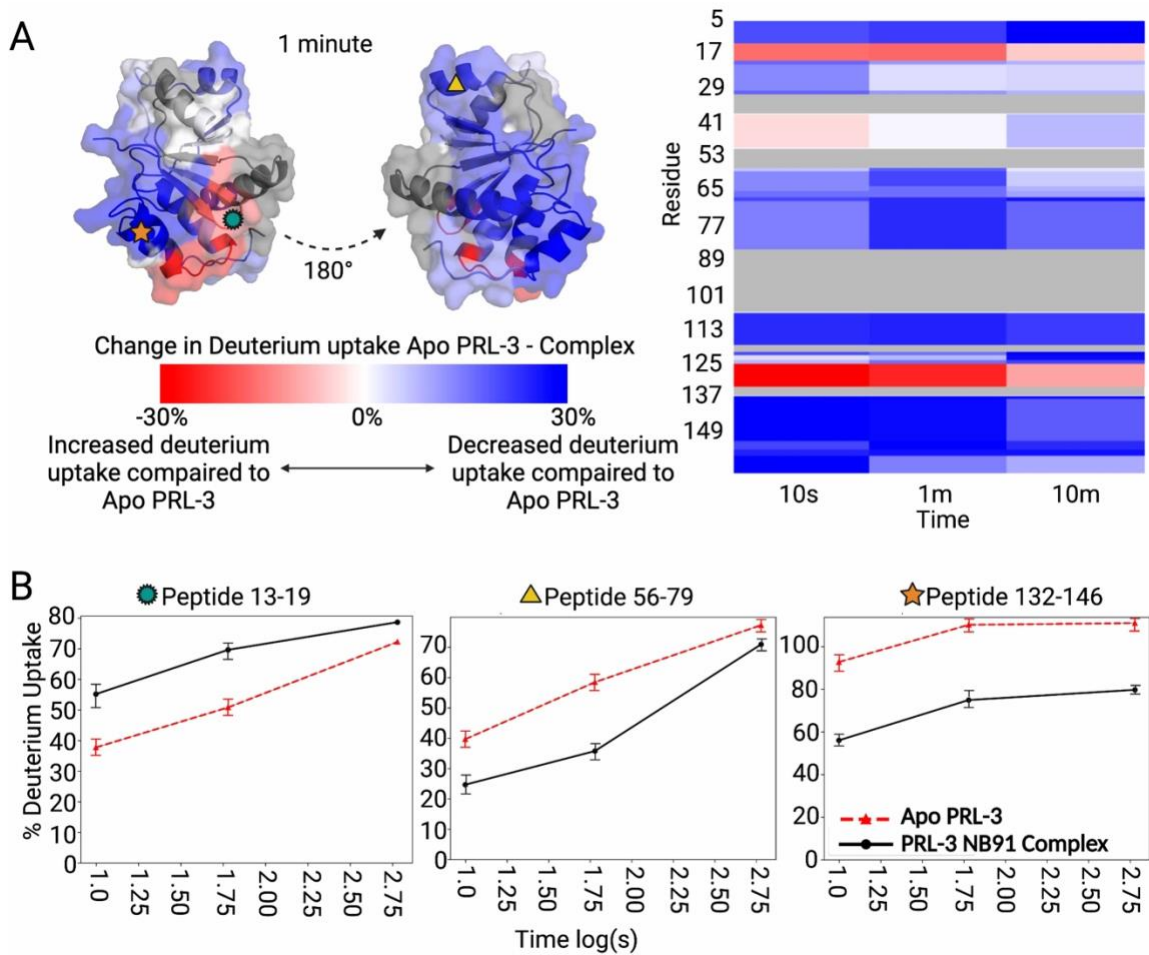


**Figure 5.5. Hydrogen Deuterium Exchange Mass Spectrometry (HDX-MS) defines Nanobody 91 binding sites with PRL-3.** (A) PRL-3 in complex with nanobody 91 shows regions of increased (red) and decreased (blue) deuterium uptake, compared to apo-PRL-3. Heatmap indicates approximately 70% sequence coverage by mass spectrometry; gray areas represent portions of PRL-3 where data for deuterium exchange was not recovered. (B) Peptides 13-19 on PRL-3 were deprotected following nanobody binding, while peptides 56-79 and 132-146 showed decreases in deuterium uptake, reflecting more protection by nanobody 91 on PRL-3 in these regions. This figure was developed through collaboration with Daniel Deredge and Kyle Kihn at the University of Maryland School of Pharmacy.

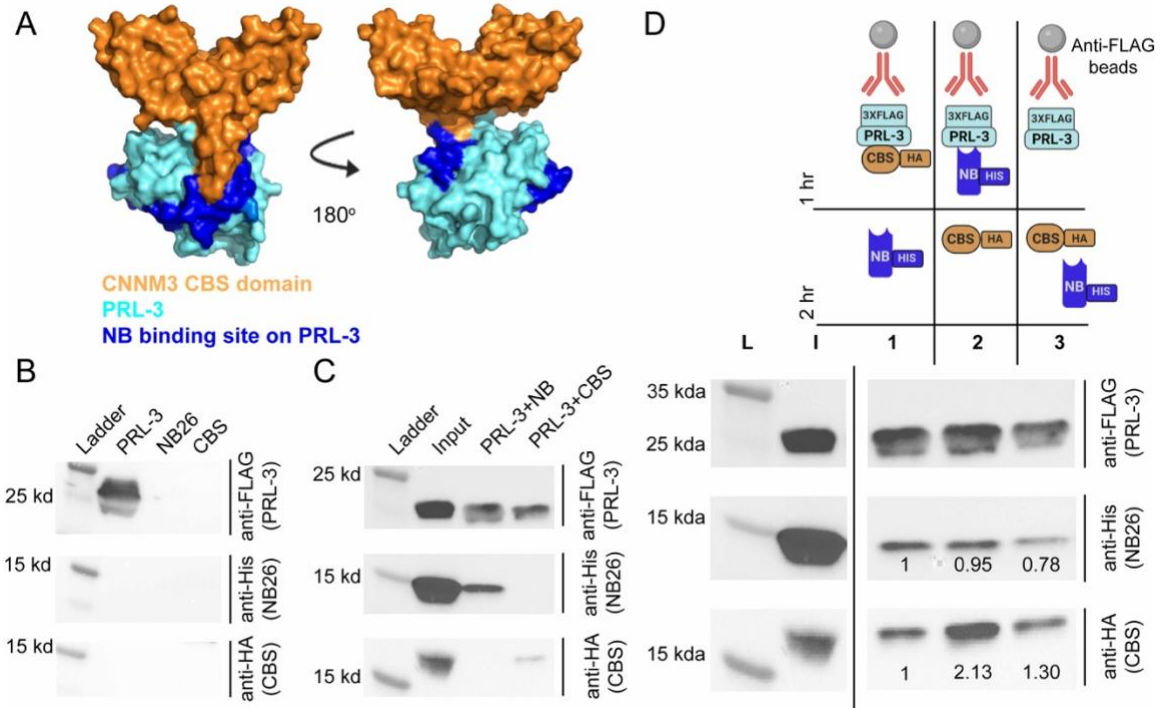


**Figure 5.6. Anti-PRL-3 nanobodies partially interact with the PRL-3 active site and site of CNNM3 CBS-domain binding.** (A) PDB:5TSR, where the CNNM3 CBS domain is colored in orange and PRL-3 in blue. Specifically, dark blue is the footprint for Nanobody 91 binding (Fig 5.5), and cyan is the rest of the PRL-3 surface filling structure. This figure was developed in Pymol after downloading the 5TSR PDB file from the Protein Data Bank (B) Recombinant 3XFLAG-PRL-3 readily binds ANTI-M2 FLAG beads, while recombinant nanobody 26 and CBS do not, eliminating background binding. (C) Recombinant His-tagged nanobody 26 and HA-tagged CBS readily bind 3XFLAG-PRL-3 bound to ANTI-M2 FLAG beads. (D) Immunoprecipitation competition assays 1-3. 3XFLAG-tagged PRL-3 was complexed with anti-FLAG beads and either the HA-tagged CBS domain of CNNM3 (1), histidine-tagged Nanobody 26 (2), or neither for 1 hour. After 1 hr incubation, NB26-His (1), CBS-HA (2), or both proteins (3) were added to the complex for the second hour. L, ladder; I, input. Antibodies used for western blot are shown. The Quantification of CBS-HA and NB26-His pulldown is normalized to 3XFLAG-PRL-3 immunoprecipitation lane by ImageLab normalization analysis.

## Chapter 6. Discussion

### 6.1. Strengths and weaknesses of anti-PRL-3 nanobodies in their current iteration.

The work of this dissertation aimed to demonstrate and develop a new tool to study the oncogenic phosphatase PRL-3. This finding was displayed by developing an alpaca-derived anti-PRL-3 nanobody, as these tools are highly specific for their antigens. The results of this dissertation demonstrate their necessity to the field and potential in future cancer research through numerous approaches. The results in Chapter 4 describe the development and characterization of the first novel PRL-3 nanobodies. These anti-PRL-3 nanobodies are useful in biochemical assays such as ELISA, immunofluorescence, and immunoprecipitation, where they interact with PRL-3 without binding to PRL-1 or PRL-2. Chapter 4 also compared currently available commercial resources to study PRL-3 to this set of PRL-3 nanobodies. In addition, the results of Chapter 4 show that nanobodies help study protein substrate interactions through co-immunoprecipitation studies. Finally, Chapter 4 demonstrates that tagged versions of PRL-3, tools used to define PRL-3 localization and trafficking in the literature, mis-localize the protein compared to the wild-type protein. With the help of these PRL-3 nanobodies, we can adequately assess PRL-3 localization. Chapter 5 investigates how these nanobodies can be useful in targeting PRL-3 in scientific research and cancer. Chapter 5 shows that the binding affinity between nanobodies and PRL-3 is in the nanomolar range, similar to many antibody-based therapeutics (153).

Furthermore, epitope mapping using HDX-MS demonstrates that the PRL-3 nanobodies partially disrupt the protein active site, ultimately limiting the protein's phosphatase activity and binding with a known partner, the CBS domain of the CNNM3 magnesium transporter. There are two main drawbacks to these nanobodies. First, we have been unable to detect endogenous PRL-3 expression with these nanobodies in immunoprecipitation and immunofluorescence. All experiments in this dissertation utilized recombinantly purified PRL-3 protein or ectopically expressed PRL-3 in human cell lines. We are in the process of optimizing the detection of endogenous PRL-3 with this new tool. Our current data suggest that these nanobodies and CNNM proteins compete for the same binding area on PRL-3, but they do not fully inhibit CBS binding, the second drawback. If

most or all endogenous PRL-3 is bound to CNNM proteins, the amount of free PRL-3 available for nanobody binding may be too low to detect in our current cell models. Our efforts are currently focused on optimizing conditions and mutations to move PRL-3 away from the CNNMs and the cell membrane to demonstrate the utility of the nanobodies in recognizing CNNM-free PRL-3 and identifying nanobodies with alternative PRL-3 binding sites.

The work in this dissertation indicates that PRL-3 nanobodies will be helpful in further research to understand PRL-3's role in cancer and will act as an initial framework for developing specific PRL-3 inhibitors. These anti-PRL-3 nanobodies will help define the standard and oncogenic functions of PRL-3 and will aid in developing therapeutics to target this protein.

## 6.2. Impact on the field – understanding PRL-3 function.

The PRL family of proteins has emerged as important in cancer progression, with PRL-3 now recognized as a bona fide oncogene. However, the mechanisms by which PRL-3 promotes tumor growth and spread are largely unknown and essential to define before introducing PRL-3 inhibitors in the clinic. A significant roadblock in understanding the role of PRL-3 in general and in cancer is the lack of tools to study this protein. While PRL antibodies and inhibitors exist for research, they often come with caveats.

For example, the allosteric PRL-3 inhibitor JMS-053 equally targets the entire PRL family and other phosphatases through oxidation (REF), making it impossible to reduce PRL-3 activity alone to measure cellular effects. In addition, while there are two antibodies in the literature that detect PRL-3 specifically in western blot and IP (R&D Systems MAB3219 and SantaCruz Biotechnology sc-130355) based on our data, they do not detect PRL-3 localized outside of the plasma membrane in immunofluorescence studies. Finally, while PRL-3-zumab specifically targets PRL-3, it requires an *in vivo* microenvironment for its anti-cancer activity and has not been made widely available. Therefore, the development and characterization of PRL-3 nanobodies were necessary to examine PRL-3 function at the cellular level.

Because of the lack of tools available to distinguish PRL-3 from the rest of its family members and other protein tyrosine phosphatases, it was crucial to show PRL-3 specificity in multiple assays. Secondly, many of the nanobodies developed in the literature and those in clinical trial target extracellular proteins, meaning they do not face the same challenges of entering the cell. Therefore, this dissertation demonstrated the high specificity of PRL-3 in a variety of ways to illustrate just how specific these nanobodies are for PRL-3 and to designate their potential as intracellular tracers of PRL-3 localization and for their use in clinical settings.

Multiple assays displayed nanobody specificity for recombinant PRL-3, including the in-direct ELISA approach and immunoprecipitation and immunofluorescence approaches. The immunofluorescence experiments demonstrate that these nanobodies can detect PRL-3 independent of post-translational modifications when expressed in human cell culture. Post-translational modifications (PTMs) are rapidly and constantly evolving and changing within the cell. These nanobodies can detect PRL-3 with these constant alterations in modifications, making them a potential candidate tool to define PRL-3 PTMs better. Currently, there are only two PTM sites on PRL-3 described in the literature, a phosphorylation event at Y53 and Y126, while there are over nine predicted sites of phosphorylation, ubiquitination, and sumoylation (154). Defining PTMs of PRL-3 faces the same challenges as the other functional studies of PRL-3 described in Chapter 1, a need for more tools. Suppose these nanobodies can detect PRL-3 independent of PTMs. In that case, they will act as an excellent resource for immunoprecipitation of the wild-type protein rather than the tagged protein, followed by mass spectrometry experiments to better define the PTMs of PRL-3.

Furthermore, the studies examining tagged-PRL-3 versus the wild-type protein in immunofluorescence demonstrate the need for these nanobodies in localization studies. The majority of PRL-3 literature revolves around tagged versions of this protein. Localization studies widely use GFP-PRL-3, and substrate studies continue to exploit 3XFLAG-PRL-3. The results of this dissertation demonstrate that to find accurate PRL-3 trafficking patterns and binding partners, researchers need to switch to studying PRL-3 using HA-PRL-3 or the wild-type protein. Our goal is to distribute this tool throughout the field, with the help of the University of Kentucky Office of Technology

Commercialization. These nanobodies will greatly impact the PRL-3 field as they provide the opportunity to study untagged PRL-3 specifically in cell models so we can better understand how localization and trafficking impact function, finally determine and validate PRL-3 binding partners in immunoprecipitation studies and ultimately continue to find approaches to determine the role that PRL-3 plays in cancer to work toward defining targeting mechanisms to treat this disease.

### 6.3. Impact on the field – new ways to target PRL-3.

Beyond studying PRL-3 biology, these nanobodies offer multiple avenues for researching and targeting PRL-3's role in cancer. First, these nanobodies disrupt PRL-3 phosphatase activity. Hopefully, utilizing immunoprecipitation techniques will allow the field to determine substrates of PRL-3 phosphatase activity in cancer, and the mechanisms associated. Once that occurs, we will have the privilege of determining if our nanobodies can disrupt the dephosphorylation of PRL-3 substrates, pushing this research beyond generic substrates like DiFMUP. The ultimate goal will be to examine if PRL-3 phosphatase activity plays a role in cancer progression and spread and utilize nanobodies to inhibit those processes.

Furthermore, the field has demonstrated that the CNNM proteins are a binding partner of PRL-3. However, they are not dephosphorylated by PRL-3. When PRL-3 interacts with CNNM3, CNNM-dependent magnesium transport is prevented and contributes to cell metabolism leading to tumor progression (52, 56). When that CNNM/PRL-3 interaction is interrupted, metastasis is no longer promoted in mouse models (155). This dissertation displays the potential of these nanobodies to partially block CNNM3 CBS domain binding. However, the CNNM3 protein is much larger than the CBS domain alone, and interaction dynamics may differ when examining nanobody versus CNNM3 binding. The next step is determining if our nanobodies, when delivered to cells, will block CNNM binding to PRL-3 and can be used as an inhibitor. Finally, if the nanobodies alone cannot enter cells and remain stable in the cytosol's reducing environment, other approaches are outlined in 6.4 to enhance the nanobodies' ability to

block CNNM3 binding. If these studies are possible, we will utilize similar techniques to target other PRL-3 binding partners following substrate studies.

Ultimately, these nanobodies impact the field of targeting PRL-3 with their high specificity and affinity for the protein, along with their ability to reduce activity and binding to CNNM3. Future studies must focus on reducing PRL-3 protein expression to potentially reduce cancer phenotypes as well as blocking interactions with cancer-associated substrates, in order to halt tumorigenesis.

#### 6.4. Future Directions.

As described in Chapter 2, there are various avenues where nanobodies are developing better research and therapeutic tools. The next course of action for this work is to implore our nanobodies in many of these actions, a large body of work we have started exploring.

##### *6.4.1. Analysis of PRL-3 trafficking.*

One of the most important characteristics of the PRL proteins is their C-terminal CAAX motif. Previous literature has continued to describe that PRL-3 localizes to the plasma membrane via this motif, demonstrated using GFP- and Myc-tagged PRL-3. The results of this dissertation show that untagged PRL-3 localizes in the cytoplasm and nucleus and is not exclusive to cellular membranes. It is very important to define and understand how PRL-3 is trafficked because trafficking mechanisms may be involved in tumorigenesis. For example, if PRL-3 is localized to the nucleus, it may impact the transcription of genes associated with tumorigenic pathways. We can use these nanobodies to study PRL-3 trafficking and if PRL-3 trafficking mechanisms are involved with cancer, we can also use these nanobodies to target those trafficking mechanisms.

There are two avenues we are currently exploring to better examine PRL-3 localization and trafficking. First is developing PRL-3 intrabodies and chromobodies. Intrabodies would allow for the expression of fluorescently tagged PRL-3 in cancer cell lines, followed by live-cell confocal microscopy. These experiments would expand

knowledge in the field by showcasing PRL-3 trafficking in real time. We hypothesize that PRL-3 traffics back and forth between the plasma membrane and nucleus through the cytoplasm for cancer-associated function, and monitoring live-cell trafficking would test this hypothesis. The primary challenge we are currently facing is that when developing intrabodies, one must be aware of how the reducing environment of the cytosol may impact the formation of the disulfide bonds needed for nanobody folding. In our previous attempts, the cellular expression has negatively impacted nanobody-reporter gene folding and the ability of the intrabody to recognize PRL-3, leading to aggregation in the cytosol. We are currently assessing multiple screening methods to develop function PRL-3 nanobodies. By developing PRL-3 intrabodies, we could not only study wild-type PRL-3 trafficking but also manipulate the PRL-3 CAAX motif to determine how lipidation events affect PRL-3 trafficking. If PRL-3 trafficking is involved in tumorigenesis, this would be an excellent avenue to explore blocking this cellular mechanism.

Due to the challenges faced with PRL-3 intrabodies, we have also focused on developing PRL-3 chromobodies by conjugating nanobody 19 to an AlexaFluor 555. We are currently in the process of determining how to best transport these chromobodies into cancer cell lines. Unfortunately, nanobodies do not readily cross the membrane, so we must utilize different transfection methods. In the field, multiple protein transfection methods are used, including liposome packaging and electroporation (156). Our goal is to transfect fluorescently labeled nanobodies into PRL-3-expressing cells as another way to examine PRL-3 trafficking mechanisms.

#### *6.4.2. Targeted degradation of PRL-3.*

We are also examining techniques to knock down or halt PRL-3 protein expression in multiple models. While other research groups have used RNA silencing or CRISPR techniques to knock down PRL-3 expression, many have not simultaneously removed PRL-1 and PRL-2 expression. One of the main functional aspects of this protein family that has yet to be fully explored is whether they can compensate for one another functionally. Therefore, our goal is to assess PRL-3 function and its role in cancer without the expression of the other PRLs. The Blackburn lab has recently developed a pan-PRL



knock-out zebrafish model currently being characterized phenotypically. This knock-out was performed using a multi-guide CRISPR approach, with three guide RNAs per PRL, followed by numerous rounds of genotyping. Most importantly, we can utilize this tool to study specific PRL-3 knock-down. We can exogenously over-express PRL-3 in these models, and target the protein in multiple assays described below, to determine which tools degrade PRL-3 effectively, and the phenotypes associated following knock-down.

Currently, we are designing PRL-3 immunotoxins fused to a portion of the PE38 bacterial toxin. Our first round of NB-PE38 purification yielded low amounts of protein. Therefore we are currently assessing how to construct the protein at the cDNA level and alternative purification methods. Secondly, we are examining how to degrade PRL-3 in zebrafish and cell models instantly. We have acquired the zGrad plasmid from Yamaguchi et al. and plan to test its capability to degrade GFP-tagged proteins following temperature changes. Following quality control experiments, we will replace the GFP nanobody in this system by cloning in one of our PRL-3 specific plasmids. We will explore similar strategies when degrading PRL-3 in cell lines, including proteolysis-targeting chimeras (PROTACS) (157), which would link a PRL-3 nanobody to an E3 ligase ligand, recruiting PRL-3 to the proteasome for degradation.

Ultimately these degradation tools will benefit the PRL field in two ways. First, we can utilize immunotoxins, zGrad, and PROTACs to initiate timely degradation of PRL-3 to study its function in early development along with early and late-stage tumor models. Secondly, if they efficiently degrade PRL-3 in cellular and zebrafish models, they will spearhead discovery into potential models that may be useful for PRL-3 inhibition in clinical studies.

#### *6.4.3. Advancing PRL-3 crystal structures.*

A primary goal in the PRL field is to complete in-depth, high-resolution structural studies of PRL-3, especially in complexes with current inhibitors or substrates. This information could give insight into designing better small molecules to target PRL-3 and identify novel sites to target the protein. However, PRL-3 has been challenging to crystallize without a substrate-bound in its active site, as it can move between open and closed

conformation (9). Current PRL-3 antibodies are not practical to stabilize PRL-3 for crystallization, as they are large, glycosylated, multi-domain proteins unsuitable for applications such as X-ray crystallography. The small size, high stability, and high specificity of nanobodies lend them well to acting as chaperones in structural studies (130). Our data demonstrate that anti-PRL-3 nanobodies interact with PRL-3 in solution and partially bind with a high affinity within PRL-3's active site, based on HDX-MS parameters. Therefore, the nanobodies may help stabilize PRL-3 in a single conformation for crystallization studies. A high-resolution crystal structure of PRL-3 with an unbound active site would be useful in *in-silico* drug design and substrate identification.

#### 6.4.4. Other PRL nanobodies.

Finally, we plan to continue this ground-breaking work by developing and characterizing PRI-1 and PRI-2 nanobodies. During PRL-3 nanobody production, we also had recombinant PRL-1 and PRL-2 injected into separate alpacas to reduce compensation. In doing so, the Protein Core at the University of Kentucky constructed cDNA libraries of potential PRL-1 and -2 nanobodies. This dissertation has developed a pipeline that we can follow to construct and characterize nanobodies against PRL-1 and PRL-2. Thus far, no conventional antibodies on the market can specifically identify these proteins. Furthermore, this will act as a pipeline for others to develop novel tools to study proteins of interest in the field where tool development is lacking.

#### 6.5. Final conclusions.

In summary, we have developed the first alpaca-derived single domain antibodies against PRL-3 and showed that they could specificity detect PRL-3 in multiple *in vitro* assays, in human cell lysates overexpressing PRL-3, and *in situ* in fixed cancer cells. At the same time, they interfere with PRL-3 phosphatase activity and CNNM CBS-domain interactions. These nanobodies have pushed the field forward by beginning to fill an important gap in the tools needed to study PRL-3 function in normal physiology and cancer and have the potential to provide valuable insight into PRL-3 substrates, trafficking,

structure, and inhibition. Furthermore, their potential to act as inhibitors of cancer progression is directly in line with our overall goal of continuing to impact patient lives, improving quality of life and prognosis.

## References

1. Ardito, F., Giuliani, M., Perrone, D., Troiano, G., and Lo Muzio, L. (2017) The crucial role of protein phosphorylation in cell signaling and its use as targeted therapy (Review) *Int J Mol Med* **40**, 271-280 10.3892/ijmm.2017.3036
2. Turdo, A., D'Accardo, C., Glaviano, A., Porcelli, G., Colarossi, C., Colarossi, L. *et al.* (2021) Targeting Phosphatases and Kinases: How to Checkmate Cancer *Front Cell Dev Biol* **9**, 690306 10.3389/fcell.2021.690306
3. Chen, C. Y., Chen, J., He, L., and Stiles, B. L. (2018) PTEN: Tumor Suppressor and Metabolic Regulator *Front Endocrinol (Lausanne)* **9**, 338 10.3389/fendo.2018.00338
4. Wang, X., Cao, X., Sun, R., Tang, C., Tzankov, A., Zhang, J. *et al.* (2018) Clinical Significance of PTEN Deletion, Mutation, and Loss of PTEN Expression in De Novo Diffuse Large B-Cell Lymphoma Neoplasia **20**, 574-593 10.1016/j.neo.2018.03.002
5. Wang, J., Kang, G., Yuan, H., Cao, X., Huang, H., and de Marco, A. (2021) Research Progress and Applications of Multivalent, Multispecific and Modified Nanobodies for Disease Treatment *Front Immunol* **12**, 838082 10.3389/fimmu.2021.838082
6. Mohi, M. G., and Neel, B. G. (2007) The role of Shp2 (PTPN11) in cancer *Curr Opin Genet Dev* **17**, 23-30 10.1016/j.gde.2006.12.011
7. Sivaganesh, V., Sivaganesh, V., Scanlon, C., Iskander, A., Maher, S., Le, T. *et al.* (2021) Protein Tyrosine Phosphatases: Mechanisms in Cancer *Int J Mol Sci* **22**, 10.3390/ijms222312865
8. Mohn, K. L., Laz, T. M., Hsu, J. C., Melby, A. E., Bravo, R., and Taub, R. (1991) The immediate-early growth response in regenerating liver and insulin-stimulated H-35 cells: comparison with serum-stimulated 3T3 cells and identification of 41 novel immediate-early genes *Mol Cell Biol* **11**, 381-390 10.1128/mcb.11.1.381-390.1991
9. Wei, M., Korotkov, K. V., and Blackburn, J. S. (2018) Targeting phosphatases of regenerating liver (PRLs) in cancer *Pharmacol Ther* **190**, 128-138 10.1016/j.pharmthera.2018.05.014
10. Diamond, R. H., Cressman, D. E., Laz, T. M., Abrams, C. S., and Taub, R. (1994) PRL-1, a unique nuclear protein tyrosine phosphatase, affects cell growth *Mol Cell Biol* **14**, 3752-3762 10.1128/mcb.14.6.3752-3762.1994
11. Zeng, Q., Hong, W., and Tan, Y. H. (1998) Mouse PRL-2 and PRL-3, two potentially prenylated protein tyrosine phosphatases homologous to PRL-1 *Biochem Biophys Res Commun* **244**, 421-427 10.1006/bbrc.1998.8291
12. Zhou, H., Gallina, M., Mao, H., Nietlispach, D., Betz, S. F., Fetrow, J. S. *et al.* (2003) <sup>1</sup>H, <sup>13</sup>C and <sup>15</sup>N resonance assignments and secondary structure of the human protein tyrosine phosphatase, PRL-2 *J Biomol NMR* **27**, 397-398 10.1023/a:1025875618084
13. Tautz, L., Critton, D. A., and Grotegut, S. (2013) Protein tyrosine phosphatases: structure, function, and implication in human disease *Methods Mol Biol* **1053**, 179-221 10.1007/978-1-62703-562-0\_13

14. Hardy, S., Kostantin, E., Hatzihristidis, T., Zolotarov, Y., Uetani, N., and Tremblay, M. L. (2018) Physiological and oncogenic roles of the PRL phosphatases FEBS J **285**, 3886-3908 10.1111/febs.14503
15. Zeng, Q., Si, X., Horstmann, H., Xu, Y., Hong, W., and Pallen, C. J. (2000) Prenylation-dependent association of protein-tyrosine phosphatases PRL-1, -2, and -3 with the plasma membrane and the early endosome J Biol Chem **275**, 21444-21452 10.1074/jbc.M000453200
16. Kozlov, G., Cheng, J., Ziomek, E., Banville, D., Gehring, K., and Ekiel, I. (2004) Structural insights into molecular function of the metastasis-associated phosphatase PRL-3 J Biol Chem **279**, 11882-11889 10.1074/jbc.M312905200
17. Tonks, N. K. (2006) Protein tyrosine phosphatases: from genes, to function, to disease Nat Rev Mol Cell Biol **7**, 833-846 10.1038/nrm2039
18. Bai, Y., Zhou, H. M., Zhang, L., Dong, Y., Zeng, Q., Shou, W. *et al.* (2016) Role of phosphatase of regenerating liver 1 (PRL1) in spermatogenesis Sci Rep **6**, 34211 10.1038/srep34211
19. Yan, H., Kong, D., Ge, X., Gao, X., and Han, X. (2011) Generation of conditional knockout alleles for PRL-3 J Biomed Res **25**, 438-443 10.1016/S1674-8301(11)60058-4
20. Zimmerman, M. W., Homanics, G. E., and Lazo, J. S. (2013) Targeted deletion of the metastasis-associated phosphatase Ptp4a3 (PRL-3) suppresses murine colon cancer PLoS One **8**, e58300 10.1371/journal.pone.0058300
21. Johansson, J. A., Marie, K. L., Lu, Y., Brombin, A., Santoriello, C., Zeng, Z. *et al.* (2020) PRL3-DDX21 Transcriptional Control of Endolysosomal Genes Restricts Melanocyte Stem Cell Differentiation Dev Cell **54**, 317-332 e319 10.1016/j.devcel.2020.06.013
22. Saha, S., Bardelli, A., Buckhaults, P., Velculescu, V. E., Rago, C., St Croix, B. *et al.* (2001) A phosphatase associated with metastasis of colorectal cancer Science **294**, 1343-1346 10.1126/science.1065817
23. Wang, Q., Holmes, D. I., Powell, S. M., Lu, Q. L., and Waxman, J. (2002) Analysis of stromal-epithelial interactions in prostate cancer identifies PTPCAAX2 as a potential oncogene Cancer Lett **175**, 63-69 10.1016/s0304-3835(01)00703-0
24. Kato, H., Semba, S., Miskad, U. A., Seo, Y., Kasuga, M., and Yokozaki, H. (2004) High expression of PRL-3 promotes cancer cell motility and liver metastasis in human colorectal cancer: a predictive molecular marker of metachronous liver and lung metastases Clin Cancer Res **10**, 7318-7328 10.1158/1078-0432.CCR-04-0485
25. Xing, X., Peng, L., Qu, L., Ren, T., Dong, B., Su, X. *et al.* (2009) Prognostic value of PRL-3 overexpression in early stages of colonic cancer Histopathology **54**, 309-318 10.1111/j.1365-2559.2009.03226.x
26. Mollevi, D. G., Aytes, A., Padulles, L., Martinez-Iniesta, M., Baixeras, N., Salazar, R. *et al.* (2008) PRL-3 is essentially overexpressed in primary colorectal tumours and associates with tumour aggressiveness Br J Cancer **99**, 1718-1725 10.1038/sj.bjc.6604747
27. Tonks, N. K. (2013) Protein tyrosine phosphatases--from housekeeping enzymes to master regulators of signal transduction FEBS J **280**, 346-378 10.1111/febs.12077

28. Dai, N., Lu, A. P., Shou, C. C., and Li, J. Y. (2009) Expression of phosphatase regenerating liver 3 is an independent prognostic indicator for gastric cancer *World J Gastroenterol* **15**, 1499-1505 10.3748/wjg.15.1499
29. Ren, T., Jiang, B., Xing, X., Dong, B., Peng, L., Meng, L. *et al.* (2009) Prognostic significance of phosphatase of regenerating liver-3 expression in ovarian cancer *Pathol Oncol Res* **15**, 555-560 10.1007/s12253-009-9153-1
30. Yeh, H. C., Li, C. C., Huang, C. N., Hour, T. C., Yeh, B. W., Li, W. M. *et al.* (2015) PTP4A3 Independently Predicts Metastasis and Survival in Upper Tract Urothelial Carcinoma Treated with Radical Nephroureterectomy *J Urol* **194**, 1449-1455 10.1016/j.juro.2015.05.101
31. Yeh, H. C., Huang, C. N., Li, C. C., Chang, L. L., Lin, H. H., Ke, H. L. *et al.* (2016) Overexpression of PTP4A3 is associated with metastasis and unfavorable prognosis in bladder cancer *World J Urol* **34**, 835-846 10.1007/s00345-015-1698-x
32. Ming, J., Liu, N., Gu, Y., Qiu, X., and Wang, E. H. (2009) PRL-3 facilitates angiogenesis and metastasis by increasing ERK phosphorylation and up-regulating the levels and activities of Rho-A/C in lung cancer *Pathology* **41**, 118-126 10.1080/00313020802579268
33. den Hollander, P., Rawls, K., Tsimelzon, A., Shepherd, J., Mazumdar, A., Hill, J. *et al.* (2016) Phosphatase PTP4A3 Promotes Triple-Negative Breast Cancer Growth and Predicts Poor Patient Survival *Cancer Res* **76**, 1942-1953 10.1158/0008-5472.CAN-14-0673
34. Wang, L., Liu, J., Zhong, Z., Gong, X., Liu, W., Shi, L. *et al.* (2016) PTP4A3 is a target for inhibition of cell proliferation, migration and invasion through Akt/mTOR signaling pathway in glioblastoma under the regulation of miR-137 *Brain Res* **1646**, 441-450 10.1016/j.brainres.2016.06.026
35. Vandsemb, E. N., Bertilsson, H., Abdollahi, P., Storkersen, O., Vatsveen, T. K., Rye, M. B. *et al.* (2016) Phosphatase of regenerating liver 3 (PRL-3) is overexpressed in human prostate cancer tissue and promotes growth and migration *J Transl Med* **14**, 71 10.1186/s12967-016-0830-z
36. Fang, X. Y., Song, R., Chen, W., Yang, Y. Y., Gu, Y. H., Shu, Y. Q. *et al.* (2015) PRL-3 Promotes the Malignant Progression of Melanoma via Triggering Dephosphorylation and Cytoplasmic Localization of NHERF1 *J Invest Dermatol* **135**, 2273-2282 10.1038/jid.2015.154
37. Wei, M., Haney, M. G., Rivas, D. R., and Blackburn, J. S. (2020) Protein tyrosine phosphatase 4A3 (PTP4A3/PRL-3) drives migration and progression of T-cell acute lymphoblastic leukemia in vitro and in vivo *Oncogenesis* **9**, 6 10.1038/s41389-020-0192-5
38. Zhou, J., Chong, P. S., Lu, X., Cheong, L. L., Bi, C., Liu, S. C. *et al.* (2014) Phosphatase of regenerating liver-3 is regulated by signal transducer and activator of transcription 3 in acute myeloid leukemia *Exp Hematol* **42**, 1041-1052 e1041-1042 10.1016/j.exphem.2014.08.001
39. Al-Aidaros, A. Q., Yuen, H. F., Guo, K., Zhang, S. D., Chung, T. H., Chng, W. J. *et al.* (2013) Metastasis-associated PRL-3 induces EGFR activation and addiction in cancer cells *J Clin Invest* **123**, 3459-3471 10.1172/JCI66824

40. Peng, L., Xing, X., Li, W., Qu, L., Meng, L., Lian, S. *et al.* (2009) PRL-3 promotes the motility, invasion, and metastasis of LoVo colon cancer cells through PRL-3-integrin beta1-ERK1/2 and-MMP2 signaling *Mol Cancer* **8**, 110 10.1186/1476-4598-8-110
41. Radke, I., Gotte, M., Smollich, M., Scharle, N., Kiesel, L., andWulfing, P. (2017) Expression of PRL-3 regulates proliferation and invasion of breast cancer cells in vitro *Arch Gynecol Obstet* **296**, 1153-1160 10.1007/s00404-017-4542-2
42. McParland, V., Varsano, G., Li, X., Thornton, J., Baby, J., Aravind, A. *et al.* (2011) The metastasis-promoting phosphatase PRL-3 shows activity toward phosphoinositides *Biochemistry* **50**, 7579-7590 10.1021/bi201095z
43. Forte, E., Orsatti, L., Talamo, F., Barbato, G., De Francesco, R., andTomei, L. (2008) Ezrin is a specific and direct target of protein tyrosine phosphatase PRL-3 *Biochim Biophys Acta* **1783**, 334-344 10.1016/j.bbamcr.2007.11.004
44. Mizuuchi, E., Semba, S., Kodama, Y., andYokozaki, H. (2009) Down-modulation of keratin 8 phosphorylation levels by PRL-3 contributes to colorectal carcinoma progression *Int J Cancer* **124**, 1802-1810 10.1002/ijc.24111
45. Peng, L., Jin, G., Wang, L., Guo, J., Meng, L., andShou, C. (2006) Identification of integrin alpha1 as an interacting protein of protein tyrosine phosphatase PRL-3 *Biochem Biophys Res Commun* **342**, 179-183 10.1016/j.bbrc.2006.01.102
46. Orsatti, L., Forte, E., Tomei, L., Caterino, M., Pessi, A., andTalamo, F. (2009) 2-D Difference in gel electrophoresis combined with Pro-Q Diamond staining: a successful approach for the identification of kinase/phosphatase targets *Electrophoresis* **30**, 2469-2476 10.1002/elps.200800780
47. Semba, S., Mizuuchi, E., andYokozaki, H. (2010) Requirement of phosphatase of regenerating liver-3 for the nucleolar localization of nucleolin during the progression of colorectal carcinoma *Cancer Sci* **101**, 2254-2261 10.1111/j.1349-7006.2010.01651.x
48. Wang, H., Quah, S. Y., Dong, J. M., Manser, E., Tang, J. P., andZeng, Q. (2007) PRL-3 down-regulates PTEN expression and signals through PI3K to promote epithelial-mesenchymal transition *Cancer Res* **67**, 2922-2926 10.1158/0008-5472.CAN-06-3598
49. Xiong, J., Li, Z., Zhang, Y., Li, D., Zhang, G., Luo, X. *et al.* (2016) PRL-3 promotes the peritoneal metastasis of gastric cancer through the PI3K/Akt signaling pathway by regulating PTEN *Oncol Rep* **36**, 1819-1828 10.3892/or.2016.5030
50. Liang, F., Liang, J., Wang, W. Q., Sun, J. P., Udho, E., andZhang, Z. Y. (2007) PRL3 promotes cell invasion and proliferation by down-regulation of Csk leading to Src activation *J Biol Chem* **282**, 5413-5419 10.1074/jbc.M608940200
51. Gimenez-Mascarell, P., Gonzalez-Recio, I., Fernandez-Rodriguez, C., Oyenarte, I., Muller, D., Martinez-Chantar, M. L. *et al.* (2019) Current Structural Knowledge on the CNNM Family of Magnesium Transport Mediators *Int J Mol Sci* **20**, 10.3390/ijms20051135
52. Hardy, S., Uetani, N., Wong, N., Kostantin, E., Labbe, D. P., Begin, L. R. *et al.* (2015) The protein tyrosine phosphatase PRL-2 interacts with the magnesium transporter CNNM3 to promote oncogenesis *Oncogene* **34**, 986-995 10.1038/onc.2014.33

53. Gimenez-Mascarell, P., Oyenarte, I., Hardy, S., Breiderhoff, T., Stuiver, M., Kostantin, E. *et al.* (2017) Structural Basis of the Oncogenic Interaction of Phosphatase PRL-1 with the Magnesium Transporter CNNM2 *J Biol Chem* **292**, 786-801 10.1074/jbc.M116.759944
54. Gulerez, I., Funato, Y., Wu, H., Yang, M., Kozlov, G., Miki, H. *et al.* (2016) Phosphocysteine in the PRL-CNNM pathway mediates magnesium homeostasis *EMBO Rep* **17**, 1890-1900 10.15252/embr.201643393
55. Zhang, H., Kozlov, G., Li, X., Wu, H., Gulerez, I., and Gehring, K. (2017) PRL3 phosphatase active site is required for binding the putative magnesium transporter CNNM3 *Scientific Reports* **7**, 10.1038/s41598-017-00147-2
56. Funato, Y., Yamazaki, D., Mizukami, S., Du, L., Kikuchi, K., and Miki, H. (2014) Membrane protein CNNM4-dependent Mg<sup>2+</sup> efflux suppresses tumor progression *J Clin Invest* **124**, 5398-5410 10.1172/JCI76614
57. Kozlov, G., Funato, Y., Chen, Y. S., Zhang, Z., Illes, K., Miki, H. *et al.* (2020) PRL3 pseudophosphatase activity is necessary and sufficient to promote metastatic growth *J Biol Chem* **295**, 11682-11692 10.1074/jbc.RA120.014464
58. Xie, H., and Wang, H. (2018) PRL-3 promotes breast cancer progression by downregulating p14(ARF)-mediated p53 expression *Oncol Lett* **15**, 2795-2800 10.3892/ol.2017.7639
59. Zhou, Q., Zhou, Q., Liu, Q., He, Z., Yan, Y., Lin, J. *et al.* (2020) PRL-3 facilitates Hepatocellular Carcinoma progression by co-amplifying with and activating FAK *Theranostics* **10**, 10345-10359 10.7150/thno.42069
60. Edwards, D. R., Moroz, K., Zhang, H., Mulholland, D., Abdel-Mageed, A. B., and Mondal, D. (2018) PRL-3 increases the aggressive phenotype of prostate cancer cells in vitro and its expression correlates with high-grade prostate tumors in patients *Int J Oncol* **52**, 402-412 10.3892/ijo.2017.4208
61. Zhang, Y., Li, Z., Fan, X., Xiong, J., Zhang, G., Luo, X. *et al.* (2018) PRL-3 promotes gastric cancer peritoneal metastasis via the PI3K/AKT signaling pathway in vitro and in vivo *Oncol Lett* **15**, 9069-9074 10.3892/ol.2018.8467
62. Li, L., Shi, H., Zhang, M., Guo, X., Tong, F., Zhang, W. *et al.* (2016) Upregulation of metastasis-associated PRL-3 initiates chordoma in zebrafish *Int J Oncol* **48**, 1541-1552 10.3892/ijo.2016.3363
63. Haney, M. G. (2021) Therapeutic Targeting of Leukemia Stem Cells to Prevent T-Cell Acute Lymphoblastic Leukemia Relapse, University of Kentucky
64. Trenkmann, M., Brock, M., Gay, R. E., Michel, B. A., Gay, S., and Huber, L. C. (2013) Tumor necrosis factor alpha-induced microRNA-18a activates rheumatoid arthritis synovial fibroblasts through a feedback loop in NF-kappaB signaling *Arthritis Rheum* **65**, 916-927 10.1002/art.37834
65. Ooki, A., Yamashita, K., Kikuchi, S., Sakuramoto, S., Katada, N., and Watanabe, M. (2010) Phosphatase of regenerating liver-3 as a convergent therapeutic target for lymph node metastasis in esophageal squamous cell carcinoma *Int J Cancer* **127**, 543-554 10.1002/ijc.25082
66. Daouti, S., Li, W. H., Qian, H., Huang, K. S., Holmgren, J., Levin, W. *et al.* (2008) A selective phosphatase of regenerating liver phosphatase inhibitor suppresses tumor cell anchorage-independent growth by a novel mechanism involving p130Cas cleavage *Cancer Res* **68**, 1162-1169 10.1158/0008-5472.CAN-07-2349



67. Wang, Z., He, Y. L., Cai, S. R., Zhan, W. H., Li, Z. R., Zhu, B. H. *et al.* (2008) Expression and prognostic impact of PRL-3 in lymph node metastasis of gastric cancer: Its molecular mechanism was investigated using artificial microRNA interference *International Journal of Cancer* **123**, 1439-1447 10.1002/ijc.23643
68. Rivas, D. R., Dela Cerna, M. V. C., Smith, C. N., Sampathi, S., Patty, B. G., Lee, D. *et al.* (2021) A screen of FDA-approved drugs identifies inhibitors of protein tyrosine phosphatase 4A3 (PTP4A3 or PRL-3) *Sci Rep* **11**, 10302 10.1038/s41598-021-89668-5
69. Abdollahi, P., Vandsemb, E. N., Elsaadi, S., Rost, L. M., Yang, R., Hjort, M. A. *et al.* (2021) Phosphatase of regenerating liver-3 regulates cancer cell metabolism in multiple myeloma *FASEB J* **35**, e21344 10.1096/fj.202001920RR
70. Shi, Y., Xu, S., Ngoi, N. Y. L., Zeng, Q., and Ye, Z. (2021) PRL-3 dephosphorylates p38 MAPK to promote cell survival under stress *Free Radic Biol Med* **177**, 72-87 10.1016/j.freeradbiomed.2021.10.015
71. Vandsemb, E. N., Rye, M. B., Steiro, I. J., Elsaadi, S., Ro, T. B., Slordahl, T. S. *et al.* (2021) PRL-3 induces a positive signaling circuit between glycolysis and activation of STAT1/2 *FEBS J* **288**, 6700-6715 10.1111/febs.16058
72. Duciel, L., Anezo, O., Mandal, K., Laurent, C., Planque, N., Coquelle, F. M. *et al.* (2019) Protein tyrosine phosphatase 4A3 (PTP4A3/PRL-3) promotes the aggressiveness of human uveal melanoma through dephosphorylation of CRMP2 *Sci Rep* **9**, 2990 10.1038/s41598-019-39643-y
73. Yoshida, A., Funato, Y., and Miki, H. (2018) Phosphatase of regenerating liver maintains cellular magnesium homeostasis *Biochem J* **475**, 1129-1139 10.1042/BCJ20170756
74. Sun, F., Li, W., Wang, L., and Jiao, C. (2017) Expression of phosphatase of regenerating liver-3 is associated with prognosis of Wilms' tumor *Onco Targets Ther* **10**, 311-317 10.2147/OTT.S107076
75. Abdollahi, P., Vandsemb, E. N., Hjort, M. A., Misund, K., Holien, T., Sponaas, A. M. *et al.* (2017) Src Family Kinases Are Regulated in Multiple Myeloma Cells by Phosphatase of Regenerating Liver-3 *Mol Cancer Res* **15**, 69-77 10.1158/1541-7786.MCR-16-0212
76. Zhang, C., Tian, W., Meng, L., Qu, L., and Shou, C. (2016) PRL-3 promotes gastric cancer migration and invasion through a NF-kappaB-HIF-1alpha-miR-210 axis *J Mol Med (Berl)* **94**, 401-415 10.1007/s00109-015-1350-7
77. Jiang, Y., Liu, X. Q., Rajput, A., Geng, L., Ongchin, M., Zeng, Q. *et al.* (2011) Phosphatase PRL-3 is a direct regulatory target of TGFbeta in colon cancer metastasis *Cancer Res* **71**, 234-244 10.1158/0008-5472.CAN-10-1487
78. Zimmerman, M. W., McQueeney, K. E., Isenberg, J. S., Pitt, B. R., Wasserloos, K. A., Homanics, G. E. *et al.* (2014) Protein-tyrosine phosphatase 4A3 (PTP4A3) promotes vascular endothelial growth factor signaling and enables endothelial cell motility *J Biol Chem* **289**, 5904-5913 10.1074/jbc.M113.480038
79. Hjort, M. A., Hov, H., Abdollahi, P., Vandsemb, E. N., Fagerli, U. M., Lund, B. *et al.* (2018) Phosphatase of regenerating liver-3 (PRL-3) is overexpressed in classical Hodgkin lymphoma and promotes survival and migration *Exp Hematol Oncol* **7**, 8 10.1186/s40164-018-0100-2

80. Hjort, M. A., Abdollahi, P., Vandsemb, E. N., Fenstad, M. H., Lund, B., Slordahl, T. S. *et al.* (2018) Phosphatase of regenerating liver-3 is expressed in acute lymphoblastic leukemia and mediates leukemic cell adhesion, migration and drug resistance *Oncotarget* **9**, 3549-3561 10.18632/oncotarget.23186
81. Peng, L., Li, Y., Meng, L., and Shou, C. (2004) Preparation and characterization of monoclonal antibody against protein tyrosine phosphatase PRL-3 Hybrid *Hybridomics* **23**, 23-27 10.1089/153685904322771999
82. Thura, M., Al-Aidaros, A. Q. O., Yong, W. P., Kono, K., Gupta, A., Lin, Y. B. *et al.* (2016) PRL3-zumab, a first-in-class humanized antibody for cancer therapy *JCI Insight* **1**, e87607 10.1172/jci.insight.87607
83. Thura, M., Al-Aidaros, A. Q., Gupta, A., Chee, C. E., Lee, S. C., Hui, K. M. *et al.* (2019) PRL3-zumab as an immunotherapy to inhibit tumors expressing PRL3 oncoprotein *Nat Commun* **10**, 2484 10.1038/s41467-019-10127-x
84. Pathak, M. K., Dhawan, D., Lindner, D. J., Borden, E.C., Farver, C., Yi, T. (2002) Pentamidine is an inhibitor of PRL phosphatases with anticancer activity *Molecular Cancer Therapy* **1**, 1255-1264,
85. Wang, L., Shen, Y., Song, R., Sun, Y., Xu, J., and Xu, Q. (2009) An anticancer effect of curcumin mediated by down-regulating phosphatase of regenerating liver-3 expression on highly metastatic melanoma cells *Mol Pharmacol* **76**, 1238-1245 10.1124/mol.109.059105
86. Ahn, J. H., Kim, S. J., Park, W. S., Cho, S. Y., Ha, J. D., Kim, S. S. *et al.* (2006) Synthesis and biological evaluation of rhodanine derivatives as PRL-3 inhibitors *Bioorg Med Chem Lett* **16**, 2996-2999 10.1016/j.bmcl.2006.02.060
87. Hoeger, B., Diether, M., Ballester, P. J., and Kohn, M. (2014) Biochemical evaluation of virtual screening methods reveals a cell-active inhibitor of the cancer-promoting phosphatases of regenerating liver *Eur J Med Chem* **88**, 89-100 10.1016/j.ejmech.2014.08.060
88. Min, G., Lee, S. K., Kim, H. N., Han, Y. M., Lee, R. H., Jeong, D. G. *et al.* (2013) Rhodanine-based PRL-3 inhibitors blocked the migration and invasion of metastatic cancer cells *Bioorg Med Chem Lett* **23**, 3769-3774 10.1016/j.bmcl.2013.04.092
89. McQueeney, K. E., Salamoun, J. M., Burnett, J. C., Barabutis, N., Pekic, P., Lewandowski, S. L. *et al.* (2018) Targeting ovarian cancer and endothelium with an allosteric PTP4A3 phosphatase inhibitor *Oncotarget* **9**, 8223-8240 10.18632/oncotarget.23787
90. McQueeney, K. E., Salamoun, J. M., Ahn, J. G., Pekic, P., Blanco, I. K., Struckman, H. L. *et al.* (2018) A chemical genetics approach identifies PTP4A3 as a regulator of colon cancer cell adhesion *FASEB J* **32**, 5661-5673 10.1096/fj.201701446R
91. Lazo, J. S., Sharlow, E. R., Cornelison, R., Hart, D. J., Llana, D. C., Mendelson, A. J. *et al.* (2021) Credentialing and Pharmacologically Targeting PTP4A3 Phosphatase as a Molecular Target for Ovarian Cancer *Biomolecules* **11**, 10.3390/biom11070969
92. Zhang, Z., Kozlov, G., Chen, Y. S., and Gehring, K. (2019) Mechanism of thienopyridone and iminothienopyridinedione inhibition of protein phosphatases *Medchemcomm* **10**, 791-799 10.1039/c9md00175a

93. Pascaru, M., Tanase, C., Vacaru, A. M., Boeti, P., Neagu, E., Popescu, I. *et al.* (2009) Analysis of molecular determinants of PRL-3 J Cell Mol Med **13**, 3141-3150 10.1111/j.1582-4934.2008.00591.x
94. Xing, X., Lian, S., Hu, Y., Li, Z., Zhang, L., Wen, X. *et al.* (2013) Phosphatase of regenerating liver-3 (PRL-3) is associated with metastasis and poor prognosis in gastric carcinoma J Transl Med **11**, 309 10.1186/1479-5876-11-309
95. Song, R., Qian, F., Li, Y. P., Sheng, X., Cao, S. X., and Xu, Q. (2009) Phosphatase of regenerating liver-3 localizes to cyto-membrane and is required for B16F1 melanoma cell metastasis in vitro and in vivo PLoS One **4**, e4450 10.1371/journal.pone.0004450
96. Lian, S., Meng, L., Yang, Y., Ma, T., Xing, X., Feng, Q. *et al.* (2017) PRL-3 promotes telomere deprotection and chromosomal instability Nucleic Acids Res **45**, 6546-6571 10.1093/nar/gkx392
97. Hamers-Casterman, C., Atarhouch, T., Muyldermans, S., Robinson, G., Hamers, C., Songa, E. B. *et al.* (1993) Naturally occurring antibodies devoid of light chains Nature **363**, 446-448 10.1038/363446a0
98. Greenberg, A. S., Avila, D., Hughes, M., Hughes, A., McKinney, E. C., and Flajnik, M. F. (1995) A new antigen receptor gene family that undergoes rearrangement and extensive somatic diversification in sharks Nature **374**, 168-173 10.1038/374168a0
99. Muyldermans, S., Atarhouch, T., Saldanha, J., Barbosa, J. A., and Hamers, R. (1994) Sequence and structure of VH domain from naturally occurring camel heavy chain immunoglobulins lacking light chains Protein Eng **7**, 1129-1135 10.1093/protein/7.9.1129
100. Lauwereys, M., Arbabi Ghahroudi, M., Desmyter, A., Kinne, J., Holzer, W., De Genst, E. *et al.* (1998) Potent enzyme inhibitors derived from dromedary heavy-chain antibodies EMBO J **17**, 3512-3520 10.1093/emboj/17.13.3512
101. Hoogenboom, H. R., de Bruine, A. P., Hufton, S. E., Hoet, R. M., Arends, J. W., and Roovers, R. C. (1998) Antibody phage display technology and its applications Immunotechnology **4**, 1-20 10.1016/s1380-2933(98)00007-4
102. Muyldermans, S. (2001) Single domain camel antibodies: current status J Biotechnol **74**, 277-302 10.1016/s1389-0352(01)00021-6
103. Skerra, A. (1993) Bacterial expression of immunoglobulin fragments Curr Opin Immunol **5**, 256-262 10.1016/0952-7915(93)90014-j
104. Arbabi Ghahroudi, M., Desmyter, A., Wyns, L., Hamers, R., and Muyldermans, S. (1997) Selection and identification of single domain antibody fragments from camel heavy-chain antibodies FEBS Lett **414**, 521-526 10.1016/s0014-5793(97)01062-4
105. Bao, G., Tang, M., Zhao, J., and Zhu, X. (2021) Nanobody: a promising toolkit for molecular imaging and disease therapy EJM Res **11**, 6 10.1186/s13550-021-00750-5
106. Muyldermans, S., and Lauwereys, M. (1999) Unique single-domain antigen binding fragments derived from naturally occurring camel heavy-chain antibodies Journal of Molecular Recognition **12**, 131-140 10.1002/(sici)1099-1352(199903/04)12:2<131::Aid-jmr454>3.0.Co;2-m
107. Muyldermans, S. (2021) A guide to: generation and design of nanobodies FEBS J **288**, 2084-2102 10.1111/febs.15515

108. Revets, H., De Baetselier, P., and Muyltermans, S. (2005) Nanobodies as novel agents for cancer therapy *Expert Opin Biol Ther* **5**, 111-124 10.1517/14712598.5.1.111
109. Aguilar, G., Matsuda, S., Vigano, M. A., and Affolter, M. (2019) Using Nanobodies to Study Protein Function in Developing Organisms *Antibodies (Basel)* **8**, 10.3390/antib8010016
110. de Beer, M. A., and Giepmans, B. N. G. (2020) Nanobody-Based Probes for Subcellular Protein Identification and Visualization *Front Cell Neurosci* **14**, 573278 10.3389/fncel.2020.573278
111. Pleiner, T., Bates, M., Trakhanov, S., Lee, C. T., Schliep, J. E., Chug, H. *et al.* (2015) Nanobodies: site-specific labeling for super-resolution imaging, rapid epitope-mapping and native protein complex isolation *Elife* **4**, e11349 10.7554/eLife.11349
112. De Meyer, T., Muyltermans, S., and Depicker, A. (2014) Nanobody-based products as research and diagnostic tools *Trends Biotechnol* **32**, 263-270 10.1016/j.tibtech.2014.03.001
113. Roder, R., Helma, J., Preiss, T., Radler, J. O., Leonhardt, H., and Wagner, E. (2017) Intracellular Delivery of Nanobodies for Imaging of Target Proteins in Live Cells *Pharm Res* **34**, 161-174 10.1007/s11095-016-2052-8
114. Oba, M., and Tanaka, M. (2012) Intracellular internalization mechanism of protein transfection reagents *Biol Pharm Bull* **35**, 1064-1068 10.1248/bpb.b12-00001
115. Virant, D., Traenkle, B., Maier, J., Kaiser, P. D., Bodenhofer, M., Schmees, C. *et al.* (2018) A peptide tag-specific nanobody enables high-quality labeling for dSTORM imaging *Nat Commun* **9**, 930 10.1038/s41467-018-03191-2
116. Stewart, M. P., Lorenz, A., Dahlman, J., and Sahay, G. (2016) Challenges in carrier-mediated intracellular delivery: moving beyond endosomal barriers *Wiley Interdiscip Rev Nanomed Nanobiotechnol* **8**, 465-478 10.1002/wnan.1377
117. Herce, H. D., Schumacher, D., Schneider, A. F. L., Ludwig, A. K., Mann, F. A., Fillies, M. *et al.* (2017) Cell-permeable nanobodies for targeted immunolabelling and antigen manipulation in living cells *Nat Chem* **9**, 762-771 10.1038/nchem.2811
118. Nischan, N., Herce, H. D., Natale, F., Bohlke, N., Budisa, N., Cardoso, M. C. *et al.* (2015) Covalent attachment of cyclic TAT peptides to GFP results in protein delivery into live cells with immediate bioavailability *Angew Chem Int Ed Engl* **54**, 1950-1953 10.1002/anie.201410006
119. Wagner, T. R., and Rothbauer, U. (2020) Nanobodies Right in the Middle: Intrabodies as Toolbox to Visualize and Modulate Antigens in the Living Cell *Biomolecules* **10**, 10.3390/biom10121701
120. Hu, Y., Romão, E., Vincke, C., Brys, L., Elkrım, Y., Vandevenne, M. *et al.* (2021) Intrabody Targeting HIF-1  $\alpha$  Mediates Transcriptional Downregulation of Target Genes Related to Solid Tumors *International Journal of Molecular Sciences* **22**, 10.3390/ijms222212335
121. Zhang, W., Shan, H., Jiang, K., Huang, W., and Li, S. (2021) A novel intracellular nanobody against HPV16 E6 oncoprotein *Clin Immunol* **225**, 108684 10.1016/j.clim.2021.108684

122. Cetin, M., Evenson, W. E., Gross, G. G., Jalali-Yazdi, F., Krieger, D., Arnold, D. *et al.* (2017) RasIns: Genetically Encoded Intrabodies of Activated Ras Proteins *J Mol Biol* **429**, 562-573 10.1016/j.jmb.2016.11.008
123. Woods, J. (2019) Selection of Functional Intracellular Nanobodies *SLAS Discov* **24**, 703-713 10.1177/2472555219853235
124. Fields, S., and Song, O. (1989) A novel genetic system to detect protein-protein interactions *Nature* **340**, 245-246 10.1038/340245a0
125. Katoh, Y., Nakamura, K., and Nakayama, K. (2018) Visible Immunoprecipitation (VIP) Assay: a Simple and Versatile Method for Visual Detection of Protein-protein Interactions *Bio Protoc* **8**, e2687 10.21769/BioProtoc.2687
126. Nguyen-Duc, T., Peeters, E., Muyldermans, S., Charlier, D., and Hassanzadeh-Ghassabeh, G. (2013) Nanobody(R)-based chromatin immunoprecipitation/microarray analysis for genome-wide identification of transcription factor DNA binding sites *Nucleic Acids Res* **41**, e59 10.1093/nar/gks1342
127. Caussin, E., and Affolter, M. (2016) deGradFP: A System to Knockdown GFP-Tagged Proteins *Methods Mol Biol* **1478**, 177-187 10.1007/978-1-4939-6371-3\_9
128. Caussin, E., Kanca, O., and Affolter, M. (2011) Fluorescent fusion protein knockout mediated by anti-GFP nanobody *Nat Struct Mol Biol* **19**, 117-121 10.1038/nsmb.2180
129. Yamaguchi, N., Colak-Champollion, T., and Knaut, H. (2019) zGrad is a nanobody-based degron system that inactivates proteins in zebrafish *Elife* **8**, 10.7554/eLife.43125
130. Chow, K. M., Whiteheart, S. W., Smiley, J. R., Sharma, S., Boaz, K., Coleman, M. J. *et al.* (2019) Immunization of Alpacas (*Lama pacos*) with Protein Antigens and Production of Antigen-specific Single Domain Antibodies *J Vis Exp* 10.3791/58471
131. Uchanski, T., Pardon, E., and Steyaert, J. (2020) Nanobodies to study protein conformational states *Curr Opin Struct Biol* **60**, 117-123 10.1016/j.sbi.2020.01.003
132. Zavrtnik, U., Lukan, J., Loris, R., Lah, J., and Hadzi, S. (2018) Structural Basis of Epitope Recognition by Heavy-Chain Camelid Antibodies *J Mol Biol* **430**, 4369-4386 10.1016/j.jmb.2018.09.002
133. Erreni, M., Schorn, T., D'Autilia, F., and Doni, A. (2020) Nanobodies as Versatile Tool for Multiscale Imaging Modalities *Biomolecules* **10**, 10.3390/biom10121695
134. Hrynchak, I., Santos, L., Falcao, A., Gomes, C. M., and Abrunhosa, A. J. (2021) Nanobody-Based Theranostic Agents for HER2-Positive Breast Cancer: Radiolabeling Strategies *Int J Mol Sci* **22**, 10.3390/ijms221910745
135. Yandrapalli S, P. Y. (2022) *SPECT Imaging*, StatPearls Publishing LLC, Treasure Island, FL
136. Xavier, C., Vaneycken, I., D'Huyvetter, M., Heemskerk, J., Keyaerts, M., Vincke, C. *et al.* (2013) Synthesis, preclinical validation, dosimetry, and toxicity of <sup>68</sup>Ga-NOTA-anti-HER2 Nanobodies for iPET imaging of HER2 receptor expression in cancer *J Nucl Med* **54**, 776-784 10.2967/jnumed.112.111021
137. Puttemans, J., Dekempeneer, Y., Eersels, J. L., Hanssens, H., Debie, P., Keyaerts, M. *et al.* (2020) Preclinical Targeted alpha- and beta(-)-Radionuclide Therapy in HER2-Positive Brain Metastasis Using Camelid Single-Domain Antibodies *Cancers (Basel)* **12**, 10.3390/cancers12041017

138. Anderson, N. M., and Simon, M. C. (2020) The tumor microenvironment *Curr Biol* **30**, R921-R925 10.1016/j.cub.2020.06.081
139. Kong, D. H., Kim, Y. K., Kim, M. R., Jang, J. H., and Lee, S. (2018) Emerging Roles of Vascular Cell Adhesion Molecule-1 (VCAM-1) in Immunological Disorders and Cancer *Int J Mol Sci* **19**, 10.3390/ijms19041057
140. Hernot, S., Unnikrishnan, S., Du, Z., Shevchenko, T., Cosyns, B., Broisat, A. *et al.* (2012) Nanobody-coupled microbubbles as novel molecular tracer *J Control Release* **158**, 346-353 10.1016/j.jconrel.2011.12.007
141. D'Huyvetter, M., Vincke, C., Xavier, C., Aerts, A., Impens, N., Baatout, S. *et al.* (2014) Targeted radionuclide therapy with A 177Lu-labeled anti-HER2 nanobody *Theranostics* **4**, 708-720 10.7150/thno.8156
142. Kijanka, M., Dorresteyn, B., Oliveira, S., and van Bergen en Henegouwen, P. M. (2015) Nanobody-based cancer therapy of solid tumors *Nanomedicine (Lond)* **10**, 161-174 10.2217/nmm.14.178
143. Van Audenhove, I., and Gettemans, J. (2016) Nanobodies as Versatile Tools to Understand, Diagnose, Visualize and Treat Cancer *EBioMedicine* **8**, 40-48 10.1016/j.ebiom.2016.04.028
144. Khireghesh, M. R., Sharifi, J., Safari, F., and Akbari, B. (2021) Immunotoxins and nanobody-based immunotoxins: review and update *J Drug Target* **29**, 848-862 10.1080/1061186X.2021.1894435
145. Behdani, M., Zeinali, S., Karimipour, M., Khanahmad, H., Schoonooghe, S., Aslemarz, A. *et al.* (2013) Development of VEGFR2-specific Nanobody Pseudomonas exotoxin A conjugated to provide efficient inhibition of tumor cell growth *N Biotechnol* **30**, 205-209 10.1016/j.nbt.2012.09.002
146. Oliveira, S., Schiffelers, R. M., van der Veeken, J., van der Meel, R., Vongpromek, R., van Bergen En Henegouwen, P. M. *et al.* (2010) Downregulation of EGFR by a novel multivalent nanobody-liposome platform *J Control Release* **145**, 165-175 10.1016/j.jconrel.2010.03.020
147. Naidoo, D. B., and Chuturgoon, A. A. (2021) Nanobodies Enhancing Cancer Visualization, Diagnosis and Therapeutics *Int J Mol Sci* **22**, 10.3390/ijms22189778
148. Leem, J., Dunbar, J., Georges, G., Shi, J., and Deane, C. M. (2016) A BodyBuilder: Automated antibody structure prediction with data-driven accuracy estimation *MAbs* **8**, 1259-1268 10.1080/19420862.2016.1205773
149. Bannas, P., Hambach, J., and Koch-Nolte, F. (2017) Nanobodies and Nanobody-Based Human Heavy Chain Antibodies As Antitumor Therapeutics *Front Immunol* **8**, 1603 10.3389/fimmu.2017.01603
150. Macek, B., Forchhammer, K., Hardouin, J., Weber-Ban, E., Grangeasse, C., and Mijakovic, I. (2019) Protein post-translational modifications in bacteria *Nat Rev Microbiol* **17**, 651-664 10.1038/s41579-019-0243-0
151. Zwysig, A., Schneider, E. M., Zeltner, M., Rebmann, B., Zlateski, V., Grass, R. N. *et al.* (2017) Protein Reduction and Dialysis-Free Work-Up through Phosphines Immobilized on a Magnetic Support: TCEP-Functionalized Carbon-Coated Cobalt Nanoparticles *Chemistry* **23**, 8585-8589 10.1002/chem.201701162
152. Zhang, H., Kozlov, G., Li, X., Wu, H., Gulerez, I., and Gehring, K. (2017) PRL3 phosphatase active site is required for binding the putative magnesium transporter *CNNM3 Sci Rep* **7**, 48 10.1038/s41598-017-00147-2

153. Sliwkowski, M. X., and Mellman, I. (2013) Antibody therapeutics in cancer Science **341**, 1192-1198 10.1126/science.1241145
154. Rubio, T., and Kohn, M. (2016) Regulatory mechanisms of phosphatase of regenerating liver (PRL)-3 Biochem Soc Trans **44**, 1305-1312 10.1042/BST20160146
155. Gehring, K., and Miki, H. (2021) Phosphatase, pseudo-phosphatase, or both? Understanding PRL oncogenicity Br J Cancer **124**, 1035-1036 10.1038/s41416-020-01194-9
156. Alex, A., Piano, V., Polley, S., Stuiver, M., Voss, S., Ciossani, G. *et al.* (2019) Electroporated recombinant proteins as tools for in vivo functional complementation, imaging and chemical biology Elife **8**, 10.7554/eLife.48287
157. Zhang, H., Han, Y., Yang, Y., Lin, F., Li, K., Kong, L. *et al.* (2021) Covalently Engineered Nanobody Chimeras for Targeted Membrane Protein Degradation J Am Chem Soc **143**, 16377-16382 10.1021/jacs.1c08521

## Vita

### Caroline N. Smith

#### EDUCATION

- 2017 - present      Doctor of Philosophy (Biochemistry), University of Kentucky,  
Lexington, KY  
*Research Advisor: Jessica S. Blackburn, Ph.D.*  
GPA: 4.0
- 2013 - 2017        B.Sc. (Biology) Minor (Biochemistry), Bellarmine University,  
Louisville, KY  
*Research Advisor: Mary O. Huff, Ph.D.*  
GPA: 3.95

#### RESEARCH EXPERIENCE

- 2017 - present      Graduate Research Assistant, College of Medicine, Molecular and  
Cellular Biochemistry Department, University of Kentucky,  
Lexington, KY  
*Research Advisor: Jessica S. Blackburn, Ph.D.*
- 2016 - 2017        Honors Undergraduate Research Student, Department of Biology,  
Bellarmine University, Louisville, KY  
*Research Advisor: Mary O. Huff, Ph.D.*
- May - Jul 2016      NSF Research Experience for Undergraduates, College of  
Medicine, Molecular and Cellular Biochemistry Department,  
University of Kentucky, Lexington, KY  
*Research Advisor: Yvonne Fondufe-Mittendorf, Ph.D.*

#### OTHER GRADUATE WORK EXPERIENCE

- Aug 2021 - present      Foundation and Corporate Philanthropy Paid Intern, University of  
Kentucky



## PUBLICATIONS

(# Denotes Co-authorship)

1. **Smith, C.N.**, Kihn, K., Williamson, Z.A., Chow, K.M., Hersh, L.B., Korotkov, K.V., Deredge, D., Blackburn, J.S. (2022). Development and characterization of nanobodies that specifically target the oncogenic Phosphatase of Regenerating Liver-3 (PRL-3) and partially block its interaction with a known binding partner, CNNM3. bioRxiv; DOI: 10.1101/2020.10.02.311787 (In Revision at *PLoSOne*)
2. **Smith, C.N.**, & Blackburn, J. S. (2021). PRL-3 promotes a positive feedback loop between STAT1/2-induced gene expression and glycolysis in multiple myeloma. *The FEBS journal*, 10.1111/febs.16120.
3. Rivas, D.R.#, Dela Cerna, M.V.C. #, **Smith, C.N.**, Sampathi, S., Patty, B.G., Lee, D., Blackburn, J.S. (2020). A screen of FDA-approved drugs identifies inhibitors of protein tyrosine phosphatase 4A3 (PTP4A3 or PRL-3). *Sci Rep* 11, 10302. DOI: <https://doi.org/10.1038/s41598-021-89668-5>
4. **Smith, C.N.** (2017). Determining the protective effects of quercetin against cadmium toxicity in human embryonic kidney cells. *ScholarWorks@Bellarmine. Undergraduate Theses.21.* (ScholarWorks Link: [https://scholarworks.bellarmino.edu/ugrad\\_theses/21/](https://scholarworks.bellarmino.edu/ugrad_theses/21/))
5. Rea, M., Eckstein, M., Eleazer, R., **Smith, C.**, Fondufe-Mittendorf, Y.N. (2017). Genome-wide DNA methylation reprogramming in response to inorganic arsenic links inhibition of CTCF binding, DNMT expression and cellular transformation. *Sci Rep.*, 7, 41474. DOI: 10.1038/srep41474

## HONORS AND AWARDS

2023	Presidential Management Fellowship Finalist (U.S. Office of Personnel Management)
2022	Most Outstanding Graduate Student Award (University of Kentucky College of Medicine)
2022	P.E.O. Scholar Award (Philanthropic Educational Organization)
2022	Office of Biomedical Education Travel Award (University of Kentucky)
2022	GMaP Region 1 North Travel Award (National Cancer Institute)
2021	Max Steckler Fellowship Award (University of Kentucky)
2021	Markey Cancer Center Trainee Mentorship Award (University of Kentucky)
2021	Markey Cancer Center Scientist in Training Travel Award (University of Kentucky)
2020	GMaP Region 1 North Stimulus Award (National Cancer Institute)
2019	Women's Club Endowed Fellowship (University of Kentucky)
2019 - 2022	AACR Associate Member Council (American Association for Cancer Research)
2019	ASBMB 2019 Annual Meeting Graduate Student and Postdoctoral Researcher Travel Award Recipient (American Society for Biochemistry and Molecular Biology)

- 2019 - 2021 Student Invited Speaker Host (University of Kentucky, Molecular and Cellular Biochemistry Department)
- 2019 - 2020 Women in Medicine and Science Rising Star Award Finalist
- 2017 - 2019 Dean's List (University of Kentucky)

#### ACADEMIC LEADERSHIP

- 2021 - 2022 Markey STRONG Summer Research Program Guest Speaker
- 2020 - present Council to the Chair on Diversity and Inclusion, University of Kentucky Department of Molecular and Cellular Biochemistry
- 2019 - present Biomedical Graduate Student Organization Buddies Mentorship Program
- 2019 - present Markey Cancer Center Trainee Advisory Council
- 2019 - present Markey Cancer Center Career Enhancement Club Member
- 2019 - 2021 Appalachian Career Training in Oncology (ACTION) High School Program (Special Topics and Cancer Workshop Instructor)
- 2019 - 2021 Biomedical Graduate Student Organization Board Member (Director of IT)
- 2019 - 2021 Women in Medicine and Science Professional Development Certificate
- 2018 - 2019 Biomedical Graduate Student Organization Board Member
- 2018 NSF Research Experience for Undergraduates, University of Kentucky (Graduate Student Program Liaison)
- 2017 - present Biomedical Graduate Student Organization Social Committee Member
- 2017 - present Biomedical Graduate Student Organization Outreach Committee Member
- 2017 - present Office of Biomedical Education, Integrated Biomedical Science Ph.D. Student Recruitment Volunteer